

Numerical investigation of bioinspired flexible protective systems using the discrete element method

by

Ali Shafiei

Department of Mechanical Engineering McGill University

Montreal, Quebec, Canada

April 2021

A thesis submitted to McGill University in partial fulfillment of the requirements for a doctoral degree

© Ali Shafiei, 2021

Table of Contents

List of figures	iv
Abstract	ix
Résumé	xi
Acknowledgment	xiii
Contributions of the Author	xiv
Chapter 1: Introduction	9
1.1 flexible protective systems in nature	9
1.2 Modeling fish-skin-like systems	11
1.3 Thesis objectives	12
1.4 Thesis organization	12
1.5 References	14
Chapter 2: The very hard and the very soft: Modeling bio-inspired scaled skins using discrete element method	_
2.1 Abstract	
2.2 Introduction	
2.3 Discrete element method (DEM) for scales: formulation and validation	
2.4 Parametric study and exploration of geometry-puncture resistance relationships	
2.5 Hard scales on a soft membrane: flexural compliance	35
2.6 Optimum mechanical performance	39
2.7 Summary	42
2.8 Acknowledgments	44
2.9 References	44
Link between the chapter 2 and chapter 3	47
Chapter 3: Bioinspired buckling of scaled skins	49
3.1 Abstract	49
3.2 Introduction	50
3.3 DEM model setup and validation	52
3.4 Post-buckling response	59
3.5 Buckling of symmetrically scaled membranes	64
3.6 Summary	67
3.7 Acknowledgments	68

3.8 References	69
Link between chapter 3 and chapter 4	72
Chapter 4: 3D mechanics of scaled membranes	74
4.1 Abstract	74
4.2 Introduction	75
4.3 Modeling and validation	76
4.4 Puncture resistance of isolated 3D scales	81
4.5 Puncture resistance of arrays of scales	83
4.6 Effects of slant angles in arrays of scales	87
4.7 Flexural response	90
4.8 Summary	93
4.9 Acknowledgements	95
4.10 References	96
Chapter 5: Conclusions	99
5.1 Summary of findings	99
5.2 Original thesis contributions and accomplishment	
5.3 Possible future directions	100
5.4 Publications	

List of figures

Figure 1-1: The three main failure modes in a fish-skin-like system (adapted from [21]) 10
Figure 2-1: Examples of animals with armors made of combinations of segmented hard elements and soft materials together: (a)-(b) alligator gar (<i>Atractosteus spatula</i> , adapted from [18]); (c)-(d Armadillo (<i>Dasypus novemcinctus</i> , adapted from [19, 20]); (e)-(f) Northern pine snake (<i>Pituophi melanoleucus</i> , adapted from [21])
Figure 2-2: (a) The system of hard scales attached to a soft substrate, The DEM model in which the substrate is replaced by spring elements in the x - and y -directions, and torsional spring elements; The distribution of the shear load $q(x)$ and the normal load $p(x)$ for the models with (b a horizontal displacement boundary condition (the surfaces at the sides are fixed, and the middle one is displaced); (c) a vertical displacement boundary condition (the surfaces at the sides are fixed, and the middle one is displaced); (d) applying a rotation boundary condition (the surfaces at the sides are fixed, and the middle one is rotated) which makes both the shear and normal loads on the surfaces $(q(x) + p(x))$; (e) Intersection of two scales with a triangle shape which makes a force along the line of action (the red line), or with a four sided shape which makes two separate forces along their line of actions (the red lines).
Figure 2-3: (a) Experimental and DEM puncture tests on a pair of ABS blocks on a polyurethand substrate; (b) Force-displacement curve showing a good agreement between the experimental and DEM results.
Figure 2-4: Models with different combinations of scale gaps (d/t) , aspect ratios (L/t) and slan angles (α)
Figure 2-5: Diagrams showing three examples on how to compute ts and λ =ts/t: (a) Example with no scale overall and no coverage (λ = 0); (b) Example with two scales overlapping, leading to intermediate λ ; (c) Example with three scales overlapping, leading to high λ
Figure 2-6: Deformation of three systems of scales at $u/t=0.7$ on a soft substrate in a puncture test and the related force-displacement curves: for (a) and (b) a fixed aspect ratio of $L/t=1$ and a gap size of $d/t=0.1$, (c) and (d) a fixed gap size of $d/t=0.1$ and a slant angle of $\alpha=45^{\circ}$, (e) and (f) a fixed aspect ratio of $L/t=0.5$ and a slant angle of $\alpha=45^{\circ}$.

Figure 2-7: (a) Reaching the critical angle causes the needle to slide off the scale surface; (b) the
effect of the slant angle (α) , the aspect ratio (L/t) and the gap (d/t) on the critical force of the system.
The critical force is denoted as F_c and is normalized by $F_c^* = F_c (1-v^2)/E_sLt$
Figure 2-8: The relation between the normalized stiffness and the critical force for different
combinations of slant angle (α) , aspect ratio (L/t) and gap (d/t) . The stiffness and critical force are
denoted as K and F_c , and are normalized by $K^* = K/E_s t$, and $F_c^* = F_c (1-v^2)/E_s L t$, respectively 33
Figure 2-9: Force distribution over the models with different slant angles in a puncture test 34
Figure 2-10: (a) Schematic for the DEM flexural model; (b) Bending moment-curvature curves
showing good agreement between the experiment and DEM results; (c) Evolution of strain energy
from axial stresses and strain energy form bending stresses during loading, computed from the
DEM simulations. (d) Comparison between a DEM simulation and an experiment on 3D printed
blocks on elastomer strip
Figure 2-11: Deformation of three systems of scales on a soft membrane under pure bending, and
the related moment - curvature curves: for (a) and (b) a fixed aspect ratio of $L/t=1$ and a gap size
of $d/t=0.1$, (c) and (d) a fixed gap size of $d/t=0.1$ and a slant angle of $\alpha=75^{\circ}$, and (e) and (f) a fixed
aspect ratio of $L/t=0.5$ and a slant angle of $\alpha=75^{\circ}$.
Figure 2-12: The effect of the gap size, aspect ratio and slant angle on the flexural compliance of
a series of scales on a soft membrane. The flexural compliance is denoted as C_f and normalized by
$C_f *= C_f E_m I_m. 39$
Figure 2-13: The quaternary plot showing the best designs for the fitness indices of $m=1$, $n=1$, $k=1$
and $l=1$ (the four corners of the plot). Also the best balanced design is shown for the case with
(m=0.25, n=0.25, k=0.25, l=0.25). 41
Figure 3-1: (a) Buckling / folding / flexure of skin at the palm of a hand allows for high compliance;
(b) However hard ceramic scales at the palm of a Kevlar glove suppress these mechanisms: The
scales jam and significant stiffening is felt when the hand is closed. Nature demonstrates that the
buckling / folding of scaled skins is possible: (c) Emerald tree boa snake (Corallus caninus, the
photo taken by William Warby [25]); (d) Christmas Island chained gecko (Lepidodactylus listeri,
adapted from [26])

Figure 3-2: (a) Snapshots and schematics of a buckling experiment on a bare polyurethane
membrane with fixed-ends conditions (no rotation); (b) Corresponding longitudinal force -
longitudinal displacement curves
Figure 3-3: (a) DEM model of a system of hard scales bonded onto a soft membrane with fixed ends conditions; Schematic showing the penetration of two scales for the case of (b) a "sharp' contact and (c) a "flat" contact. For both cases the lines of action of the contact forces are shown in red; (d) The normalized resultant contact as a function of the normalized penetration for the models with different incidence angles, which was used to obtain the constants C_1 and C_2 56
Figure 3-4: Experimental and DEM buckling test on a scaled polyurethene strip where the system buckles into (a) mode I-extrados and (b) mode I-intrados; (c) longitudinal force-longitudinal displacement curves showing a good agreement between the experimental and DEM results; (d) Curvature of the membrane as a function of the position along the membrane in the mode I extrados and mode I-intrados configurations at loading point δ_L =6mm
Figure 3-5: Buckling results from DEM on a bare membrane: (a) Buckling profiles, (b) force landscape and (c) strain energy landscape. To generate this plot a transverse displacement is applied to the mid-point of the membrane.
Figure 3-6: Buckling energy landscape for a bare membrane and a membrane uniformly covered by three, five and six scales with fixed sizes of $t/L_m = 0.05$ and $L/L_m = 0.15$
Figure 3-7: Buckling energy landscape for three different scaled membranes: (a) Varying scale thickness with a fixed gap distance of d/L_m =0.05 and scale number of N_s =3; (b) Varying numbe (and length) of the scales for a fixed gap distance of d/L_m =0.01 and scale thickness of t/L_m =0.05. The energy of the bare membrane is also shown for comparison
Figure 3-8: DEM and experimental results on scaled membranes in jammed configurations: with (a) t/L_m =0.1, N_s =3, d/L_m =0.01 and (b) t/L_m =0.1, N_s =6, d/L_m =0.01
Figure 3-10: (a) Buckling energy landscape for two models symmetric from one another; (b) the two designs are combined to create a stable mode II
Figure 3-11: Buckling energy landscape for membranes covered with scales on both sides: (a varying scale thickness for fixed gap distance of d/L_m =0.05 and scale number of N_s =3; (b) varying scale spacing for fixed scale thickness of t/L_m =0.04 and scale number of N_s =3; (c) varying number

(and therefore length) of scales for fixed gap distance of d/L_m =0.03 and scale thickness of t/L_m =0.04
Figure 4-1: Typical system considered in this study: 5 x5 Array of hard scales bonded to a soft substrate and subjected to puncture. Key dimensions for individual scales are shown
Figure 4-2: Setup of linear springs captures the interactions of individual scales with the substrate, and also the interactions between neighboring scales through the substrate
Figure 4-3: (a) Snapshots of experiments and models for a puncture test on four different designs; (b) Corresponding puncture force-displacement curves showing a good agreement between models and experiments.
Figure 4-4: Puncture resistance of isolated scales with five different base shapes as function of rotational stiffness. All the scales have an equal base area
Figure 4-5: Eight designs for the base shape and arrangements we considered in this study 83
Figure 4-6: (a) Puncture resistance for eight difference scale arrays normalized by the puncture resistance of an isolated scale with the same geometry. For each design, results with full interaction and only partial interaction through substrate or through direct contact are shown. The punctured scales are marked with red dots, and the effective neighboring scales are marked by orange dots;
(b) the displacement distribution in the complete model at the point where the punctured scale reached the critical tilting angle.
Figure 4-7: In-plane sliding of rows of scales may be (a) kinematically allowed by the shape and arrangement of the scales or (b) prevented because of interlocking
Figure 4-8: Starting from scales with straight faces, we considered 60 degree slant angles towards three different directions.
Figure 4-9: (a) Puncture resistance of arrays of scales. Within each design the effect of slant angle is also shown; (b) In-plane displacement maps for these designs. The red arrows show the direction of the slant angle.
Figure 4-10: Configuration for the three-point bending (experiments and models). We considered two orientations for the loading pin (load line): (a) parallel to <i>x</i> -direction and (b) parallel to <i>y</i> -direction

Figure 4-11: (a) Three-point flexural tests (diagrams and DEM results) on arrays of scales bonded
onto a soft membrane where the line load is parallel to x-direction and (b) corresponding force
deflection curves from experiments and DEM models, showing good agreements; (c) Same test
with the line load parallel to y-direction with (d) corresponding force deflection curves from
experiments and DEM models also showing good agreements
Figure 4-12: Flexural compliance of arrays of scales on soft membrane with different combinations
of base shapes, slant angles and arrangements and where the line load is applied (a) parallel to the
<i>x</i> -direction and (b) parallel to the <i>y</i> -direction
Figure 4-13: Ashby chart showing the normalized puncture resistance and the normalized flexura
compliance for different combinations of base shapes, slant angles and arrangements 95

Abstract

Natural protective systems have been a source of inspiration for scientists because of their highperformance and multifunctional properties. It is a challenge to design a material which provides simultaneously flexibility and puncture resistance which are mutually exclusive. Nature proposes a solution to this challenge, which is combining hard and soft materials together in specific ways. In natural flexible armors, the soft skin of the animals is covered by segmented hard plates which protect the animal against any external threats. The discrete hard plates also give a great flexibility to the skin and facilitate the mobility of the animal. To apply this idea into human-made structures, we first need to learn about the mechanics of such systems and the effect of the geometries and arrangement of the scales on the mechanical performance. To do so, we chose discrete element method (DEM) which is computationally more efficient than the conventional finite element method (FEM). We started with developing and validating 2D DEM models with two different configurations: hard scales attached onto a soft substrate to examine the puncture resistance, and hard scales bonded to a soft membrane to explore the flexural compliance. The time efficiency of DEM enabled us to study a large number of models (720 models) with various combinations of aspect ratio, slant angle and gap distance to optimize the geometrical parameters considering four design criteria: the tilting resistance, coverage, penetration resistance and flexural compliance. We learnt that the contact between the neighboring scales had a significant effect on the mechanical behavior of the system. The results showed that the presence of scales improved the puncture resistance of the system, but in the cost of low flexural compliance. Nature shows a unique strategy to increase the flexibility in armored skins, which is making wrinkles and folds in the skin. Inspired of nature, we used the DEM model of hard scales bonded onto a soft membrane to investigate the buckling behavior of a fish-skin-like structure and the effect of the scales on the stability of the buckled system. With examining the energetics of buckling in mode I and II configurations, we showed that the contact between the scales on the intrados side of the membrane was a source of stiffness in the system, which is not desirable in terms of flexibility. We also showed that we were able to induce a stable mode II to the system by using scales, which is necessary for forming wrinkles in the system. 2D discrete element models gave us helpful insights into the mechanics of scale-covered systems, however, had some limitations such as not being able to explore the effect of the base shape of the scales on the system. We therefore created a 3D discrete element model

using ABAQUS software to explore other aspects of scale-covered systems. We examined scales with different base shapes, arrangements and slant angles in different in-plane directions, and discussed the effect of the neighboring scales on the puncture resistance and the flexural compliance. We showed that by only choosing a right base shape for the scales we could highly improve the puncture resistance of the system. The results show that the interlocking mechanism between the rows of the scales plays an important role in stabilizing the punctured scale by engaging a large number of scales.

Résumé

Les systèmes de protection naturels sont une source d'inspiration pour les scientifiques en raison de leurs propriétés performantes et multifonctionnelles. C'est un défi de concevoir un matériau qui offre à la fois une flexibilité et une résistance à la perforation qui s'excluent mutuellement. La nature propose une solution à ce défi qui consiste à combiner des matériaux durs et mous de manière spécifique. Dans les armures souples naturelles, la peau flexible des animaux est recouverte de plaques dures segmentées qui protègent l'animal contre les menaces extérieures. Les plaques dures et discrètes confèrent également une grande souplesse à la peau et facilitent la mobilité de l'animal. Pour appliquer cette idée dans des structures synthetiques, nous devons d'abord nous familiariser avec la mécanique de ces systèmes et avec les effets des géométries et de la disposition des échelles sur les performances mécaniques. Pour ce faire, nous avons choisi la méthode des éléments discrets (DEM) qui est plus efficace que la méthode des éléments finis (FEM) conventionnelle. Nous avons commencé par développer et valider des modèles DEM 2D avec deux configurations différentes: des échelles dures fixées sur un substrat souple pour examiner la résistance à la perforation et des échelles dures liées à une membrane souple pour explorer la souplesse en flexion. L'efficacité temporelle du DEM nous a permis d'étudier un grand nombre de modèles (720 modèles) avec diverses combinaisons de rapport hauteur / largeur, d'angle d'inclinaison et de distance d'écart pour optimiser les paramètres géométriques. Ces modèles on pris en compte la résistance à l'inclinaison, la couverture, la résistance à la pénétration et la compliance en flexion. Nous avons appris que le contact entre les écailles voisines avait un effet significatif sur le comportement mécanique du système. Les résultats ont montré que la présence d'écailles améliore la résistance à la perforation du système, mais au détriment d'une moindre compliance en flexion. La nature montre une stratégie unique pour augmenter la flexibilité des peaux écaillées, qui crée des rides et des plis dans la peau. Nous avons utilisé la nature comme inspiration pour la création d'un modèle DEM dans lequel des écailles dures ont été collées sur une membrane souple. Cela permet d'étudier le comportement de flambement d'une structure ressemblant à une peau de poisson et l'effet des écailles sur la stabilité du système bouclé. En examinant l'énergétique du flambage dans les configurations mode I et II, nous avons montré que le contact entre les écailles du côté intrados de la membrane rigidifie le système ce qui n'est pas souhaitable dans les aspects de flexibilité. Nous avons également montré que nous pouvions

induire un mode II stable au système en utilisant des écailles, ce qui est nécessaire pour former des rides dans le système. Un modèle d'éléments discrets en 2D nous a donné des informations utiles sur la mécanique des systèmes à écailles couverte, mais présentait certaines limites telles que l'impossibilité d'explorer l'effet de la forme de base des écailles sur le système. Nous avons donc créé un modèle d'éléments discrets 3D à l'aide du logiciel ABAQUS pour explorer d'autres aspects des systèmes à écailles couverte. Nous avons examiné des écailles avec différentes formes de base, arrangements et angles d'inclinaison dans différentes directions, et discuté l'effet des écailles voisines sur la résistance à la perforation et la souplesse en flexion. Nous avons montré qu'en changeant uniquement la forme de base des écailles, nous pouvions grandement améliorer la résistance à la perforation du système. Les résultats montrent que le mécanisme de verrouillage entre les rangées d'écailles joue un rôle important dans la stabilisation de l'écaille perforée en engageant un grand nombre d'écailles.

Acknowledgment

First of all, I would like to thank my supervisor, Prof. Francois Barthelat, for giving me the

opportunity to join his research group and for all his supervisions, supports and kindness during

my study.

I would also like to thank my committee members Prof. Larry Lessard and Prof. Jovan Nedic for

their useful insights and suggestions. Special thanks to the Faculty of Engineering at McGill

University, the Natural Sciences and Engineering Research Council of Canada and the Canadian

Institutes of Health Research for their collaborative financial support for this project.

I would like to express my appreciation to Dr. John William Pro for his ever-ready support and

mentorship throughout my journey. I would also like to thank the former and current members of the

biomimetic laboratory at McGill: Dr. Florent Hannard, Dr. Mohammad Mirkhalaf, Ahmed Dalaq, Idris

Malik, Alireza Mirmohammadi, Najmul Hasan Abid, Sacha Cavelier, Zhen Yin, Aram Bahmani,

Abdulrahman Almessabi and Siyu Liu. They were great friends and a source of inspiration during the

past several years.

Last but not least, I would like to say my deepest thanks to my lovely family for their support, patience

and encouragement throughout my ongoing journey in education. To my girl, Taylor McNulty, who

always excitedly followed my work.

Ali Shafiei

Montreal, Canada

April 2021

xiii

Contributions of the Author

This is a manuscript-based thesis which mainly consists of three journal articles. The title of the articles, name of the authors, and their contributions are listed below:

1) The very hard and the very soft: Modeling bio-inspired scaled skins using the discrete element method

Ali Shafiei, J. William Pro, Roberto martini and Francois Barthelat

Published in the Journal of Mechanics and Physics of Solids, Volume 146, January 2021, 104176

Author contributions:

AS: Contributed in developing the discrete element model, ran the simulations, analyzed the data, and prepared the figures and the manuscript.

WP: Contributed in developing the discrete element model, gave technical and scientific advice and helped prepare the manuscript.

RM: Contributed in developing the discrete element model, gave technical and scientific advice.

FB: Supervised the research and review process, gave technical and scientific advice, edited the figures and the manuscripts.

2) Bioinspired buckling of scaled skins

Ali Shafiei, J. William Pro and François Barthelat

Accepted in the Journal of Bioinspiration & Biomimetics, March 2021

Author contributions:

AS: Contributed in developing the discrete element model, ran the simulations, analyzed the data, and prepared the figures and the manuscript.

WP: Contributed in developing the discrete element model, gave technical and scientific advice and helped prepare the manuscript.

FB: Supervised the research and review process, gave technical and scientific advice, edited the figures and the manuscripts.

2) 3D mechanics of scaled membranes

Ali Shafiei and Francois Barthelat

Submitted to the International Journal of Solids and Structures, April 2021

Author contributions:

AS: Contributed in developing the discrete element model, ran the simulations, analyzed the data, and prepared the figures and the manuscript.

FB: Supervised the research and review process, gave technical and scientific advice, edited the figures and the manuscripts.

Chapter 1

Introduction

Chapter 1: Introduction

1.1 flexible protective systems in nature

Current engineering technologies are focusing on creating materials with lighter, stronger, tougher and multifunctional properties. Monolithic materials have been used for a long time, but they are not able to address current functional requirements [1, 2]. A modern approach to create multifunctional materials is to form composites in which the materials that have mutually exclusive properties are combined together such as combining strong and tough materials [3-6]. A high performance can be achieved with controlling the microstructure and the distribution of different phases [3, 4, 7]. Engineers and builders have always been inspired by nature for making tools and structures, but recently the ingenuity of nature has attracted attentions of many scientists. Research on natural structures shows that nature is full of novel ideas for making multifunctional composites with remarkable mechanical performance [8, 9]. For instance, natural flexible armors are combined of hard and soft materials in a well-controlled and specific architecture, to simultaneously give protection and flexibility to the animals [10]. Over time, engineers have used different designs to fabricate protective clothing with flexibility and comfort such as Loricasegmentata which is one of the oldest designs (goes back to ancient Rome). This tessellated armor was composed of 30-40 metallic plates, which is similar to the one made by Samurai. Mail armor is another example where metallic rings were meshed together to make a protective and flexible web. More advanced armors are made of special textiles such as Kevlar or Spectra. These armors have down-sides including large weight, weakness against sharp penetration, and low flexibility and comfort. Recently, fishskin-like armors have attracted more attentions [11-13]. Dragon skin armor is a an example, which is made of overlapping ceramic disks [14]. This armor provides protection against ballistic loads but decreases the mobility of the users. The natural armors evolved during millions of years and perfectly function according to the needs of the animals. Fish skin is one of the well reputed natural protective systems which its extraordinary mechanical behavior is a function of the interaction of the scales with the underlying dermis layer and also with each other [10, 15, 16]. Besides having hydrodynamic properties [17], fish scales play a significant role in the protection of fish against predators [18, 19]. The skin beneath the scales is mainly made of fibrils of collagen type I which is considered as a very soft material compared to the scales [10]. In fish skin, the scales are

overlapped and embedded into the soft dermis layer. The interaction between the neighboring scales helps the locomotion by providing an exotendon-effect during swimming [15, 20]. Research on striped bass skin shows that each scale overlaps with six scales, also, with a particular arrangement any points on the skin is covered by three scales. Puncture tests on a half-striped bass shows that scales increase the puncture resistance of the skin by four to five times. The interaction of the scales together help distributing load over a large area, which prevents the local deformation of the skin, excessive strain and blunt damage in the dermis layer [15, 16]. The scales are about five orders of magnitude stiffer than the dermis layer, where this high contrast in the stiffness leads to three main failure modes in a fish-skin-like system (figure 1) [21, 22]. Depending on the stiffness and thickness ratios of the scales and the dermis layer, one of the three failure modes is dominant [21]: Conical cracks caused by contact stresses, radial cracks caused by flexural stresses and tilting of the indented scale resulting in a fast sliding of the indenter into the substrate. In the last failure mode, the scale itself is not damaged, but tilting of the scale exposes the vulnerable substrate to the tip of the indenter.

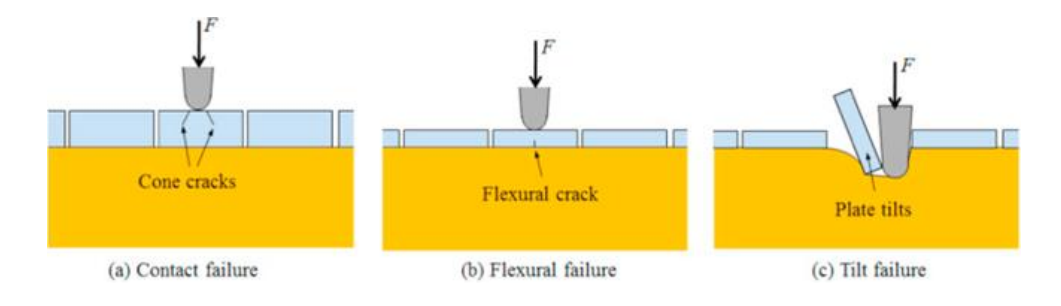


Figure 1-1: The three main failure modes in a fish-skin-like system (adapted from [21])

Osteoderm, "bony skin", is another example of natural armors which is found in armadillos and alligators. The structure of this material is similar to fish skin where hard scales are attached onto the animals' skin. Armadillos' carapace is composed of scales with two different morphologies (hexagon and triangle), which are covered by keratin [23, 24]. The neighboring scales are connected together by collagen fibers, also called Sharpney's fibers, which provide flexibility to the skin of the animal [25].

1.2 Modeling fish-skin-like systems

Experimental investigation on fish-skin-like systems provides insights into the mechanics of this particular type of structures [22, 26, 27]. Finite element method is another approach to study these systems such as a 2D simulation of blunt indentation into a scale-covered substrate [28], and a 3D flexural modeling of a scale-covered membrane [29]. Finite element method (FEM) however is suitable only for a limited number of scales. In the models with a large number of scales, it is hard to properly capture all the contact regions occurring concurrently and convergence is not ensured. Moreover, to model the underlying substrate a large number of elements is required which makes the FEM computationally inefficient. A different numerical method therefore needs to be considered to model large numbers of scales attached onto a thick substrate. Discrete element method (DEM) is used to model the motion of a large number of particles or building blocks. In this method, the building blocks are defined by nodes which are connected to the neighboring nodes with interaction laws such as Hooke's law, contact algorithm, friction etc. [30]. Discrete element method (DEM) is much more computationally efficient compared to FEM because it reduces the degrees of freedom in the model [31, 32]. DEM was initially developed by Cundall and Strack for granular materials [33] where the granular materials were modeled as rigid particles and the contact between them was defined by normal and shear stiffness. This method has been used to model various materials with a large number of rigid elements and complex interaction laws including granular materials [34, 35], topologically interlocked structures [31], fiber reinforced composites [36, 37], laminated composites [38] and porous materials [39]. This method has been found to be promising for modeling bio-inspired structures which are made of segmented hard materials connected together with a much softer material such as nacre and tooth enamel [7, 32, 40, 41]. In this work, modeling fish-skin-like systems with traditional approaches such as FEM proved to be computationally extremely expensive, with contact mechanics, large deformation and a large number of elements to model the substrate. We therefore used DEM as an alternative to investigate these systems.

1.3 Thesis objectives

The overall aim of this thesis was to use the discrete element method (DEM) to investigate the mechanics of scale-covered systems. The objectives were as following:

- Develop and validate DEM models to investigate the behavior of scale-covered substrates subjected to sharp puncture
- Develop and validate DEM models to explore the flexural response of scaled-covered membranes
- Use DEM modeling to study the effect of the geometries and the arrangement of the scales on the performance of the system
- Design synthetic scale-covered materials with a high mechanical performance including a high puncture resistance and a high flexural compliance

1.4 Thesis organization

This is a manuscript-based thesis composed of five chapters. The first chapter (current chapter) briefly introduces the general concepts in natural protective systems and the computational method we chose. This chapter also include the objectives and the structure of the thesis.

Chapter 2 describes and proposes the discrete element method (DEM) as an approach to model a system of segmented hard scales bonded onto a soft material. We developed 2D models with two different configurations: hard scales on a soft substrate to explore the puncture resistance, and hard scales on a soft membrane to explore the flexural compliance of the system. After validating the DEM models with experiments, we investigate the effect of the scale geometries (aspect ratio and slant angle) and the arrangement (gap distance) on the puncture and flexural response of the system. We study the role of contact between the scales in improving the mechanical performance including the puncture resistance and the flexural compliance. At the end, we define four design criteria and, using a quaternary plot, show the best designs based on the criteria.

Chapter 3 focuses on the flexural behavior of scale-covered systems. We use the DEM model which was developed in chapter 2 (hard scales on a soft membrane) to investigate the post-buckling stability of such systems in mode I and mode II. After validation of the numerical results with

experiments, we discuss the stability of buckled systems considering the strain energy stored in them. We then explore the effect of the scale geometries (aspect ratio) and arrangement (gap distance) on the post-buckling stability. First, we investigate the stability of the mode I configuration where the scales are placed on the intrados and extrados sides of the membrane. We then study the stability of mode II configuration and propose a design (bonding scales onto both sides of the membrane) to induce a stable mode II to the system.

Chapter 4 explores the 3D mechanics of scale-covered systems. We therefore made 3D DEM models of hard scales on a soft substrate and hard scales on a soft membrane in ABAQUS/CAE to investigate the puncture resistance and the flexural compliance of the system, respectively. After validating the models with experiments, we study the effect of the base shape and the arrangement of the scales on the mechanical performance of the system. We then discuss slant angle as another effective design parameter, and explore scales with different combinations of base shape, slant angle and arrangement. Specifically, we study the puncture resistance and the flexural compliance of such systems, and how to maximize them. The results give useful insights into designing scale-covered systems with a high mechanical performance (puncture resistance and flexural compliance).

Finally, chapter 5 highlights the main conclusions and the research contribution of this thesis, also gives a few guidelines for future works.

1.5 References

- 1. Ashby, M., *Designing architectured materials*. Scripta Materialia, 2013. **68**(1): p. 4-7.
- 2. Barthelat, F., *Architectured materials in engineering and biology: fabrication, structure, mechanics and performance.* International Materials Reviews, 2015. **60**(8): p. 413-430.
- 3. Ashby*, M.F., *Hybrids to fill holes in material property space*. Philosophical Magazine, 2005. **85**(26-27): p. 3235-3257.
- 4. Jones, R.M., *Mechanics of composite materials*. 1998: CRC press.
- 5. Shah, D.U., *Natural fibre composites: Comprehensive Ashby-type materials selection charts.* Materials & Design (1980-2015), 2014. **62**: p. 21-31.
- 6. Ritchie, R.O., *The conflicts between strength and toughness*. Nature materials, 2011. **10**(11): p. 817-822.
- 7. Abid, N., M. Mirkhalaf, and F. Barthelat, *Discrete-element modeling of nacre-like materials: Effects of random microstructures on strain localization and mechanical performance*. Journal of the Mechanics and Physics of Solids, 2018. **112**: p. 385-402.
- 8. Wegst, U.G.K., et al., *Bioinspired structural materials*. Nature Materials, 2014. **14**: p. 23.
- 9. Meyers, M.A., et al., *Biological materials: structure and mechanical properties*. Progress in Materials Science, 2008. **53**(1): p. 1-206.
- 10. Funk, N., et al., *Bioinspired Fabrication and Characterization of a Synthetic Fish Skin for the Protection of Soft Materials*. ACS Applied Materials & Interfaces, 2015. **7**(10): p. 5972-5983.
- 11. Neal, M.L. and A.D. Bain, *Method and apparatus for defeating high-velocity projectiles*. 2001, Google Patents.
- 12. Larsen, J. and C. Cross, *Composite segmented flexible armor*. 2007, Google Patents.
- 13. Zhu, D. and F. Barthelat, A Novel Biomimetic Material Duplicating the Structure and Mechanics of Natural Nacre, in Mechanics of Biological Systems and Materials, Volume 2: Proceedings of the 2011 Annual Conference on Experimental and Applied Mechanics, T. Proulx, Editor. 2011, Springer New York: New York, NY. p. 181-187.
- 14. Neal, M.L., *Encapsulated imbricated armor system*. 2003, Google Patents.
- 15. Vernerey, F.J. and F. Barthelat, *On the mechanics of fishscale structures*. International Journal of Solids and Structures, 2010. **47**(17): p. 2268-2275.
- 16. Zhu, D.J., et al., *Puncture resistance of the scaled skin from striped bass: Collective mechanisms and inspiration for new flexible armor designs.* Journal of the Mechanical Behavior of Biomedical Materials, 2013. **24**: p. 30-40.
- 17. Sudo, S., et al., *A Study on the Surface Shape of Fish Scales*. JSME International Journal Series C Mechanical Systems, Machine Elements and Manufacturing, 2002. **45**(4): p. 1100-1105.
- 18. Zhu, D., et al., *Structure and Mechanical Performance of a "Modern" Fish Scale*. Advanced Engineering Materials, 2012. **14**(4): p. B185-B194.
- 19. Lin, Y.S., et al., *Mechanical properties and the laminate structure of Arapaima gigas scales*. Journal of the Mechanical Behavior of Biomedical Materials, 2011. **4**(7): p. 1145-1156.
- 20. Vernerey, F.J. and F. Barthelat, *Skin and scales of teleost fish: Simple structure but high performance and multiple functions.* Journal of the Mechanics and Physics of Solids, 2014. **68**: p. 66-76.

- 21. Martini, R. and F. Barthelat, *Stability of hard plates on soft substrates and application to the design of bioinspired segmented armor*. Journal of the Mechanics and Physics of Solids, 2016. **92**: p. 195-209.
- 22. Chintapalli, R.K., et al., Fabrication, testing and modeling of a new flexible armor inspired from natural fish scales and osteoderms. Bioinspiration & Biomimetics, 2014. **9**(3): p. 036005.
- 23. Vickaryous, M.K. and B.K. Hall, Osteoderm morphology and development in the nine-banded armadillo, Dasypus novemcinctus (Mammalia, Xenarthra, Cingulata). Journal of Morphology, 2006. **267**(11): p. 1273-1283.
- 24. Chen, I.H., et al., *Armadillo armor: Mechanical testing and micro-structural evaluation.* Journal of the Mechanical Behavior of Biomedical Materials, 2011. **4**(5): p. 713-722.
- 25. Yang, W., et al., *Natural Flexible Dermal Armor*. Advanced Materials, 2013. **25**(1): p. 31-48.
- 26. Martini, R., Y. Balit, and F. Barthelat, *A comparative study of bio-inspired protective scales using 3D printing and mechanical testing*. Acta Biomaterialia, 2017. **55**: p. 360-372.
- 27. Connors, M., et al., *Bioinspired design of flexible armor based on chiton scales*. Nature Communications, 2019. **10**(1): p. 5413.
- 28. Browning, A., C. Ortiz, and M.C. Boyce, *Mechanics of composite elasmoid fish scale assemblies and their bioinspired analogues*. Journal of the Mechanical Behavior of Biomedical Materials, 2013. **19**: p. 75-86.
- 29. Vernerey, F.J., K. Musiket, and F. Barthelat, *Mechanics of fish skin: A computational approach for bio-inspired flexible composites*. International Journal of Solids and Structures, 2014. **51**(1): p. 274-283.
- 30. Rinaldi, A. and S. Mastilovic, *Two-Dimensional Discrete Damage Models: Lattice and Rational Models*, in *Handbook of Damage Mechanics: Nano to Macro Scale for Materials and Structures*, G.Z. Voyiadjis, Editor. 2015, Springer New York: New York, NY. p. 305-337.
- 31. Dugué, M., et al., *Indentation of interlocked assemblies: 3D discrete simulations and experiments.* Computational Materials Science, 2013. **79**: p. 591-598.
- 32. Abid, N., J.W. Pro, and F. Barthelat, *Fracture mechanics of nacre-like materials using discrete-element models: Effects of microstructure, interfaces and randomness.* Journal of the Mechanics and Physics of Solids, 2019. **124**: p. 350-365.
- 33. Cundall, P.A., *The measurement and analysis of accelerations in rock slopes.* 1971.
- 34. Kim, H., M.P. Wagoner, and W.G. Buttlar, Simulation of Fracture Behavior in Asphalt Concrete Using a Heterogeneous Cohesive Zone Discrete Element Model. Journal of Materials in Civil Engineering, 2008. **20**(8): p. 552-563.
- 35. Schöpfer, M.P.J., et al., *The impact of porosity and crack density on the elasticity, strength and friction of cohesive granular materials: Insights from DEM modelling.* International Journal of Rock Mechanics and Mining Sciences, 2009. **46**(2): p. 250-261.
- 36. Bažant, Z.P., et al., Random Particle Model for Fracture of Aggregate or Fiber Composites. Journal of Engineering Mechanics, 1990. **116**(8): p. 1686-1705.
- 37. Ismail, Y., et al., *Discrete element modelling of unidirectional fibre-reinforced polymers under transverse tension.* Composites Part B: Engineering, 2015. **73**: p. 118-125.
- 38. Sheng, Y., et al., *Microstructure effects on transverse cracking in composite laminae by DEM.* Composites Science and Technology, 2010. **70**(14): p. 2093-2101.

- 39. Morrison, C.N., et al., *A discrete lattice model of quasi-brittle fracture in porous graphite*. Materials Performance and Characterization, 2014. **3**(3): p. 414-428.
- 40. Pro, J.W. and F. Barthelat, *Discrete element models of fracture in tooth enamel: Failure mode competition and statistical effects.* Journal of the Mechanics and Physics of Solids, 2020. **137**: p. 103868.
- 41. Pro, J.W. and F. Barthelat, *Discrete element models of tooth enamel, a complex three-dimensional biological composite*. Acta Biomaterialia, 2019. **94**: p. 536-552.

Chapter 2

The very hard and the very soft: Modeling bio-inspired scaled skins using the discrete element method

Chapter 2: The very hard and the very soft: Modeling bioinspired scaled skins using the discrete element method

Ali Shafiei², J. William Pro², Roberto Martini² and François Barthelat^{1,2}*

¹ Department of Mechanical Engineering, University of Colorado, 427 UCB, 1111 Engineering Dr, Boulder, CO 80309, United States

² Department of Mechanical Engineering, McGill University, 817 Sherbrooke Street West, Montreal, QC H3A 2K6, Canada

* Correspondence to: francois.barthelat@colorado.edu

2.1 Abstract

Natural protective systems are attracting an increasing amount of attention for their ability to provide simultaneous flexibility and puncture resistance by combining hard and soft materials in mechanically efficient ways. In typical flexible natural armors, a continuous layer of soft material is either covered or embedded with segmented hard scales. The interaction between the hard scales and the softer surrounding materials give rise to unusual and attractive mechanisms which are not fully understood to this day. Here we propose and validate the discrete-element method (DEM) to capture the mechanics of stiff scales on soft substrates including scale-substrate elastic deformations, scale-scale interaction through the substrate, and direct scale-scale interaction by contact. We considered two configurations: (i) hard scales on soft substrates to capture scale tilting and penetration resistance, and (ii) hard scales on soft membranes to study flexural compliance. The computational efficiency of the DEM algorithm allowed for large parametric studies with many combinations of aspect ratio, slant angle, and gap size to identify the best designs in terms of resistance to unstable tilting, coverage, penetration resistance, and flexural compliance. DEM is a promising tool for the design and optimization of fish-skin-like protective structures, also providing new insights into the synergistic role of the hard scales and the soft substrate.

Keywords: Bioinspiration, discrete element method, segmented hard material, penetration resistance, flexural compliance

2.2 Introduction

Modern engineering applications are requiring lighter, stronger, tougher, and multifunctional materials. In this quest for better engineering materials, nature can provide outstanding models and inspiration for new designs. Natural materials have high mechanical performance, can produce seemingly mutually exclusive properties [1], and are inherently multifunctional [2]. A powerful paradigm in structural biological materials is the combination of hard and soft materials in wellcontrolled micro-architectures [2-8]. Scaled natural flexible armors (figure 2-1) are excellent examples of this concept: They combine hard materials (mineralized collagen, dry keratin) with soft materials which are orders of magnitude more compliant [9, 10]. Natural scaled armors combine two properties which are typically mutually exclusive: high surface hardness for protection against puncture or laceration, combined with high flexural compliance for fast locomotion. In fish skins the hard scales are attached to a soft substrate (figure 2-1a and 1b). Under flexural deformation the scales can glide on one another, providing high compliance to the system [11-13]. Moreover, interactions between neighboring scales can improve the penetration resistance [14], and distribute the localized puncture force over a larger area to prevent excessive strains in the underlying tissues, thereby delaying blunt injuries [10, 15, 16]. Experiments on synthetic scaled systems made of hexagonal glass plates on elastomeric substrates showed that discrete glass plates not only provide flexural compliance to the system, but also increase puncture resistance by up to 70% compared to a continuous glass layer [9]. Decreasing the size of the plates reduces their flexural span which delays fracture up to a point where the scales are small enough to tilt from the action of the sharp indenter [9, 10, 17]. The tilting of individual plates is indeed an important

failure mode in scaled skin which is prominent in animals with very hard scales such as in alligator gar [10]. A mechanical criterion was recently proposed for the tilting and instability of hard plates on a soft substrate [10]. Experiments on 3D printed scales have later suggested that the indented scale can be stabilized by neighboring scales, and that scale geometry and arrangement have a deep impact on this mechanism [4]. Despite these recent advances, the mechanics of scaled skins is still not fully understood. For example, how scales interact during flexural deformation and puncture, how they distribute concentrated forces over wide areas, and how the geometry and arrangement of the scales govern mechanical performance are important effects that are not fully understood.

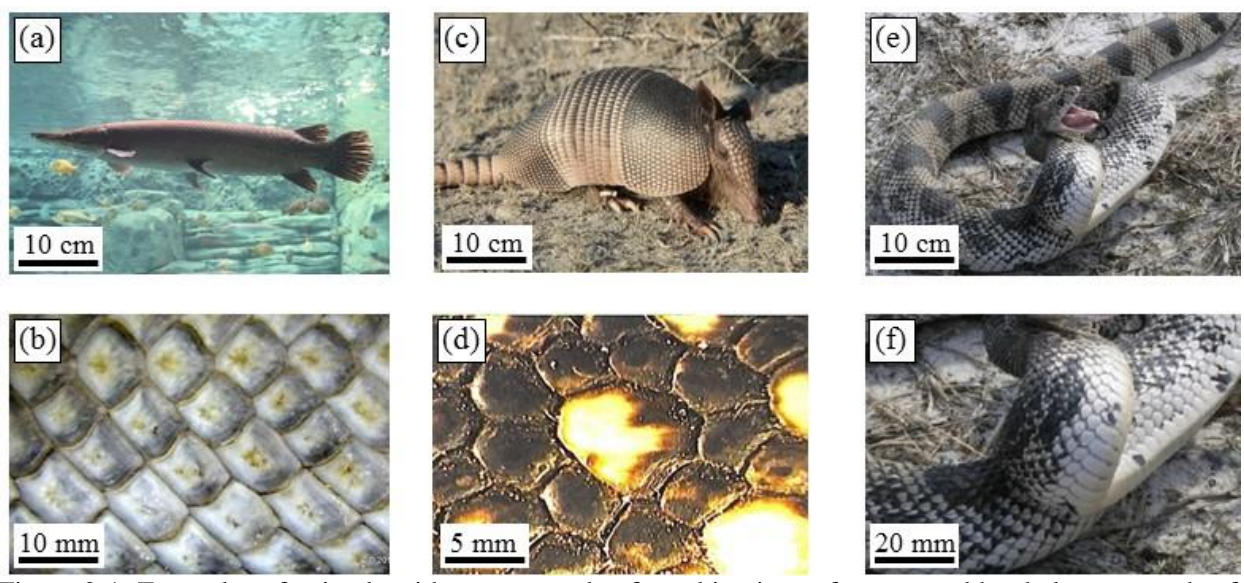


Figure 2-1: Examples of animals with armors made of combinations of segmented hard elements and soft materials together: (a)-(b) alligator gar (*Atractosteus spatula*, adapted from [18]); (c)-(d) Armadillo (*Dasypus novemcinctus*, adapted from [19, 20]); (e)-(f) Northern pine snake (*Pituophis melanoleucus*, adapted from [21])

Some insights can be provided from experiments on synthetic scales [4, 22, 23], also from finite element modeling such as a 2D simulation of a scale-covered substrate under blunt indentation loading [16], and a 3D flexural modeling of a system of hard scales on a soft membrane [24]. But in the both finite element models, a limited number of scales were used. The large number of

contact regions occurring concurrently are difficult to properly capture with standard numerical methods such as finite elements where convergence is difficult (if at all possible). In this article, we propose the discrete element method (DEM) as an approach to model the deformation of scaled skins, including multiple scale-scale interactions. The discrete element method (DEM) offers a computationally efficient alternative to the conventional finite element method (FEM) by reducing the degrees of freedom in the problem [25]. DEM is also well suited for the systems containing a large number of rigid elements with complex interaction laws [25-33]. For instance, we recently used DEM on nacre which had a structure similar to fish skin: both are made of hard plates connected by much softer material [28, 29]. After validation of this numerical tool, we used DEM to explore the design space of a large number (720) of scale-covered systems with interesting combinations of puncture resistance and flexibility.

2.3 Discrete element method (DEM) for scales: formulation and validation

For this study we developed a 2D DEM model of hard scales perfectly bonded onto a soft substrate (figure 2-2a). The scales were identical and modeled as parallelograms defined by a thickness t, length 2L, and slant angle α . The bases of the scales were assumed to be perfectly bonded to a soft substrate and uniformly spaced, with a gap distance d. To model puncture, a concentrated force was applied on the upper face of the middle scale along the direction normal to the surface of the substrate (figure 2-2a), while the substrate was modeled as a half-space. The position of each scale was represented by a node coinciding with the midpoint of the lower side of the scale. Each of the nodes has three degrees of freedom: translations in the x- and y-directions, and rotation about the z-axis. The substrate was modeled as a linear elastic half-space (modulus E_s , Poisson's ratio v) with small strains. The scales were assumed to be several orders of magnitude stiffer than the

substrate [34], and therefore we modeled the scales as rigid for the purpose of efficiently capturing scale-substrate interactions (scale-scale interactions were captured using a simplified contact model that takes in account the deformability of the scale, as detailed below). For simplicity the substrate was modeled with spring elements (figure 2-2a) that captured not only the reaction of the substrate onto individual scales, but also the elastic coupling between neighboring scales. More specifically, the two reaction forces and the reaction moment from the substrate to the individual scales were captured with three "direct" stiffness coefficients α_x , α_y and α_ϕ , and the effect of the neighboring scales on a given scale were captured with another three "coupling" coefficients β_x , β_y and β_ϕ . The forces (F_x, F_y) and the moment M_z (about the z axis) on the ith node were expressed as:

$$\begin{cases} F_{x}^{(i)} = \frac{E_{s}Lt}{(1-v^{2})} (\alpha_{x} \frac{u_{x}^{(i)}}{t} - \beta_{x} (\frac{u_{x}^{(i-1)}}{t} + \frac{u_{x}^{(i+1)}}{t})) \\ F_{y}^{(i)} = \frac{E_{s}Lt}{(1-v^{2})} (\alpha_{y} \frac{u_{y}^{(i)}}{t} - \beta_{y} (\frac{u_{y}^{(i-1)}}{t} + \frac{u_{y}^{(i+1)}}{t})) \\ M_{z}^{(i)} = \frac{E_{s}L^{3}}{(1-v^{2})} (\alpha_{\phi} \phi^{(i)} - \beta_{\phi} (\phi^{(i-1)} + \phi^{(i+1)})) \end{cases}$$

$$(2.1)$$

Where E_s is the Young's modulus of the substrate, and v is the Poisson's ratio of the substrate. u_x , and u_y are the nodal displacements in the x- and y-directions, respectively, and ϕ is the nodal inplane rotation. To appreciate the effect of coupling between the scales, consider a simple example where all the scales are clamped, except scale i+1 which is displaced by $u_x^{(i+1)} > 0$. Displacing that scale deforms the surrounding substrate, so that a force $F_x^{(i)} < 0$ must be applied onto scale i to keep it immobile (equation (2.1)). To calibrate the coefficients α_x , α_y , α_ϕ , β_x , β_y and β_ϕ we used Boussinesq's and Cerruti's close-form solution for the substrate as an elastic half-space where we assumed that the substrate is adequately thick [35, 36]. For the case of thin substrate assumption,

other theories are available to be used which is beyond the scope of this work [37-39]. We considered three scales on the elastic half-space, first subjecting the middle scale to a tangential displacement u_x (figure 2-2b) while the other two scales were clamped.

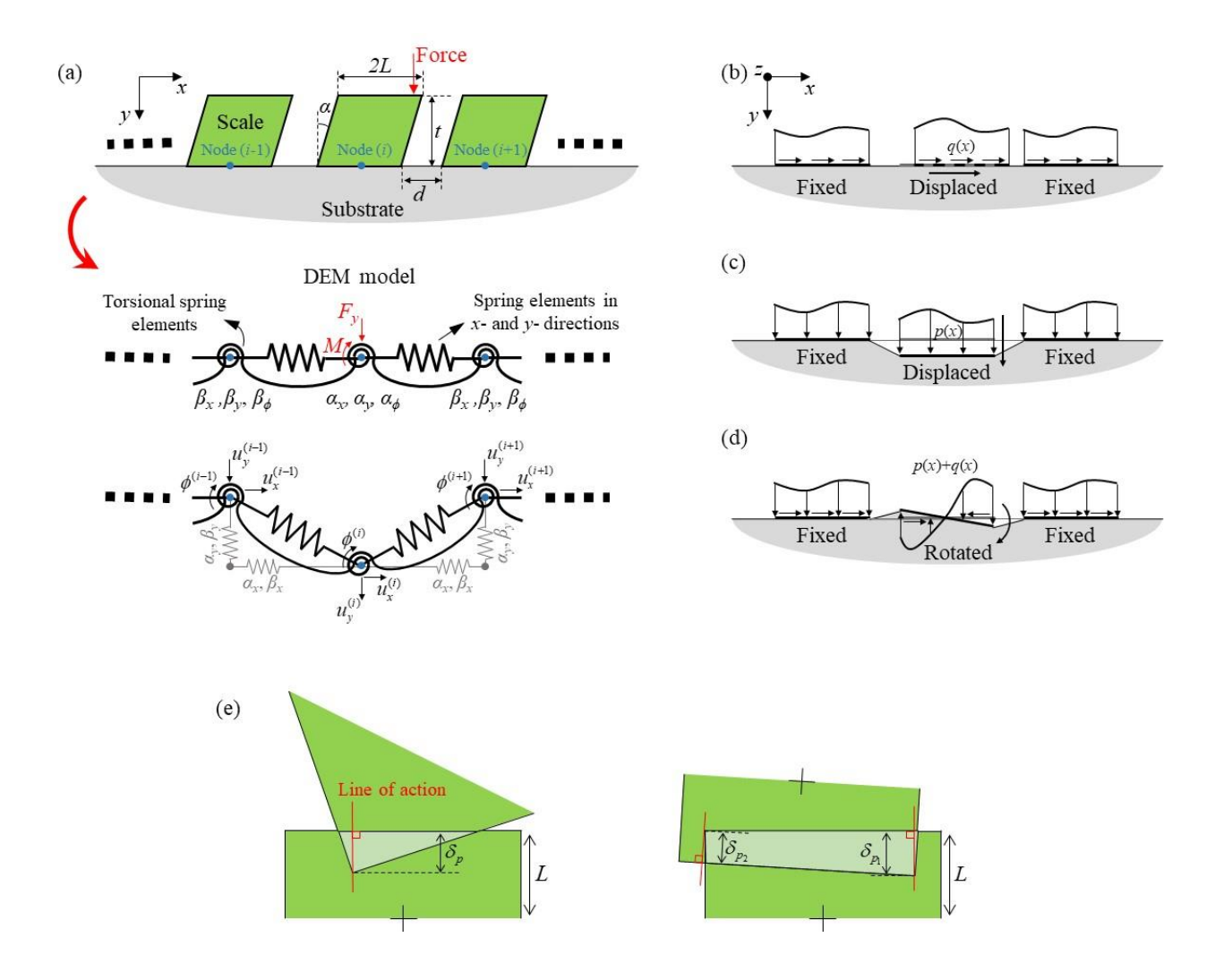


Figure 2-2: (a) The system of hard scales attached to a soft substrate, The DEM model in which the substrate is replaced by spring elements in the x- and y-directions, and torsional spring elements; The distribution of the shear load q(x) and the normal load p(x) for the models with (b) a horizontal displacement boundary condition (the surfaces at the sides are fixed, and the middle one is displaced); (c) a vertical displacement boundary condition (the surfaces at the sides are fixed, and the middle one is displaced); (d) applying a rotation boundary condition (the surfaces at the sides are fixed, and the middle one is rotated) which makes both the shear and normal loads on the surfaces (q(x) + p(x)); (e) Intersection of two scales with a triangle shape which makes a force along the line of action (the red line), or with a four sided shape which makes two separate forces along their line of actions (the red lines).

The relation between the tangential displacement u_x and the horizontal (x-direction) distributed shear load $q(\zeta, \gamma)$ on the surface of the substrate underneath the scales (figure 2-2b) is given as:

$$u_{x} = \frac{1+\nu}{\pi E_{s}} \iint q(\zeta, \gamma) \left[\frac{1-\nu}{\sqrt{(x-\zeta)^{2} + (z-\gamma)^{2}}} + \frac{\nu(x-\zeta)^{2}}{\sqrt{((x-\zeta)^{2} + (z-\gamma)^{2})^{3}}} \right] d\zeta d\gamma$$
 (2.2)

Where z is the out-of-plane direction. We obtained the distributed shear load q(x,z) from equation (2.2), which we then integrated over the area of the scales to obtain the shear force for each scale. Dividing the shear forces on the middle scale, and on the neighbouring scales by the imposed displacement of the middle scale (u_{x_0}) provided the stiffness coefficients α_x and β_x , respectively. The process was repeated for a normal displacement u_y (figure 2-2c) where we imposed a displacement u_{y_0} to the middle scale. To compute α_y and β_y we used the equation:

$$u_{y} = \frac{1 - v^{2}}{\pi E_{s}} \iint p(\zeta, \gamma) \frac{1}{\sqrt{(x - \zeta)^{2} + (z - \gamma)^{2}}} d\zeta d\gamma$$
 (2.3)

Where $p(\zeta,\gamma)$ is the distributed normal load in the vertical (y) direction on the surface of the substrate below the scales (figure 2-2c). Finally, we imposed a rotation ϕ_0 on the middle scale by still keeping the other two scales clamped (figure 2-2d). Using equations (2.2) and (2.3), we obtained the distributed shear and normal loads and the resultant moment on each scale. The coefficients α_{ϕ} and β_{ϕ} were computed by dividing the moment on the middle and neighbouring scales (respectively) by the imposed rotation on the middle scale ϕ_0 . The coefficients α_x , α_y , α_{ϕ} , β_x , β_y and β_{ϕ} are expressed as

$$\begin{cases} \alpha_{x} = \frac{\iint_{A_{m}} q(x,z)dxdz}{u_{x_{0}}} &, \quad \beta_{x} = \frac{\iint_{A_{n}} q(x,z)dxdz}{u_{x_{0}}} \\ \alpha_{y} = \frac{\iint_{A_{m}} p(x,z)dxdz}{u_{y_{0}}} &, \quad \beta_{y} = \frac{\iint_{A_{n}} p(x,z)dxdz}{u_{y_{0}}} \\ \alpha_{\phi} = \frac{\iint_{A_{m}} \left[q(x,z)(x-x_{m})\sin\phi_{0} + p(x,z)(x-x_{m})\cos\phi_{0} \right]dxdz}{\phi_{0}} \\ \beta_{\phi} = \frac{\iint_{A_{n}} \left[q(x,z)(x-x_{n})\sin\phi_{0} + p(x,z)(x-x_{n})\cos\phi_{0} \right]dxdz}{\phi_{0}} \end{cases}$$

$$(2.4)$$

In which A_m and A_n are the areas of the middle scale and either of the neighbouring scales, respectively. x_m and x_n are the x-coordinates of the midpoint of the lower side of the middle scale and either of the neighbouring scales, respectively. An important implication of this result is that individual scales can interact with their neighbors not necessarily only by direct contact but also through deformations in the substrate. Direct contact between the scales is another feature of the model which is critical to capture puncture and flexural deformations. In our model the contacting scales were assumed to be rigid and frictionless, and we used a simple yet accurate and computationally efficient contact algorithm inspired by the Winkler elastic foundation model [40]. We first used shape intersection algorithms to detect collision between pairs of scales, and we used kinematics to compute the penetration distance δ_p (figure 2-2e) between the contacting scales. The contact force was then computed from δ_p using:

$$\frac{F_{ct}}{LbE_{ct}} = C_1 \left(\frac{\delta_p}{L}\right)^{C_2} \tag{2.5}$$

Where E_{ct} is the contact modulus, and b is the out-of-plane dimension (width) of the scales. The calibration constants C_1 and C_2 were obtained using a 2D finite element model (ANSYS V16 2016, PA, US) in which the corner of one scale penetrated into the edge of another scale under controlled

displacement (figure 2-2e). From the finite element calculations we computed the resultant contact force (the interfaces were assumed to be frictionless) and determined C_I =1.1 and C_2 =0.23. We also defined the line of action of F_{ct} so that it is intersecting the penetrating corner of one the scales, and is perpendicular to the edge of the other scale (figure 2-2e). For the case of four-sided overlap area (figure 2-2e), we applied the procedure to two instances of corner contact and applied equation (2.5) twice. In addition to forces, direct contact between scales may induce moments about the out-of-plane axis z. We computed the effective nodal moment due the contact forces as:

$$M_{ij} = r_{ct} \times F_{ct,ij} \tag{2.6}$$

Where M_{ij} is the effective nodal moment induced by scale i onto neighboring scale j, r_{ct} is the position vector of the contact force relative to node i and $F_{ct,ij}$ is the contact force which scale i exerts on scale j. Since the contact model introduces geometrical nonlinearities we used the iterative Newton-Raphson method to obtain numerical solutions [28].

To validate our model we performed puncture tests on a system composed of a pair of Acrylonitrile butadiene styrene (ABS) blocks glued onto a softer elastomeric substrate. The blocks were 3D printed with a high resolution Direct Light Projector (DLP) 3D printer (Micro HiRes Machine, EnvisionTech, 2019), which produced fully dense and pore-free blocks. We tested 3D printed ABS along different directions and verified that the blocks were isotropic, with a modulus E_{ABS} GPa. The blocks were then glued onto the surface of a thick polyurethane substrate using cyanoacrylate. The polyurethane we used is four orders of magnitude softer than ABS, with a measured modulus of E_s =310 kPa (we used a Poisson's ratio v=0.5 [4]). The assumption of rigid blocks compared to the substrate, required for our DEM simulation, was therefore verified. For the puncture test, a

needle was pressed on the upper surface of one of the blocks, which caused the substrate to deform and the blocks to displace and tilt (figure 2-3a).

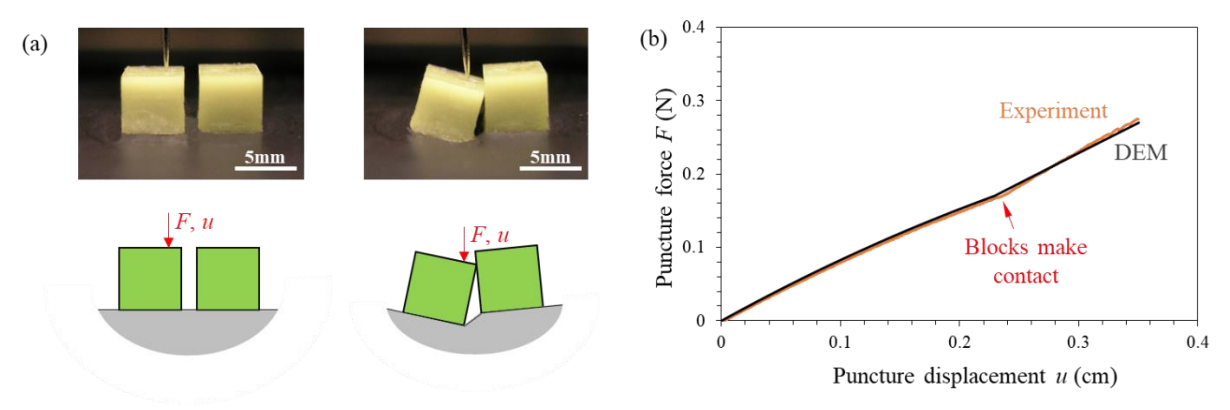


Figure 2-3: (a) Experimental and DEM puncture tests on a pair of ABS blocks on a polyurethane substrate; (b) Force-displacement curve showing a good agreement between the experimental and DEM results.

For validation we compared the force-displacement curves obtained experimentally and through DEM, which showed excellent agreement (figure 2-3b). The model properly captured the initial stiffness of the system and the onset of contact between the blocks. Following contact, the stiffness of the system suddenly increased (which shows as a 'kink' on the puncture force-displacement curve in figure 2-3b), a phenomenon that the DEM model also accurately captured.

2.4 Parametric study and exploration of geometry-puncture resistance relationships We used the DEM model to systematically explore the effects of scale geometry and arrangement on puncture resistance. In this first study, we focused on parallelogram-shaped scales placed at regular intervals over the softer substrate. Since there is no length scale associated with the elastic deformation, we use non-dimensional geometrical parameters: the aspect ratio of the scales (L/t), the slant angle of the scales (α), and the normalized gap distance between the scales (d/t). Figure

2-4 illustrates models with different combinations of these three geometrical parameters, showing that this approach covered a wide range of possible scale designs.

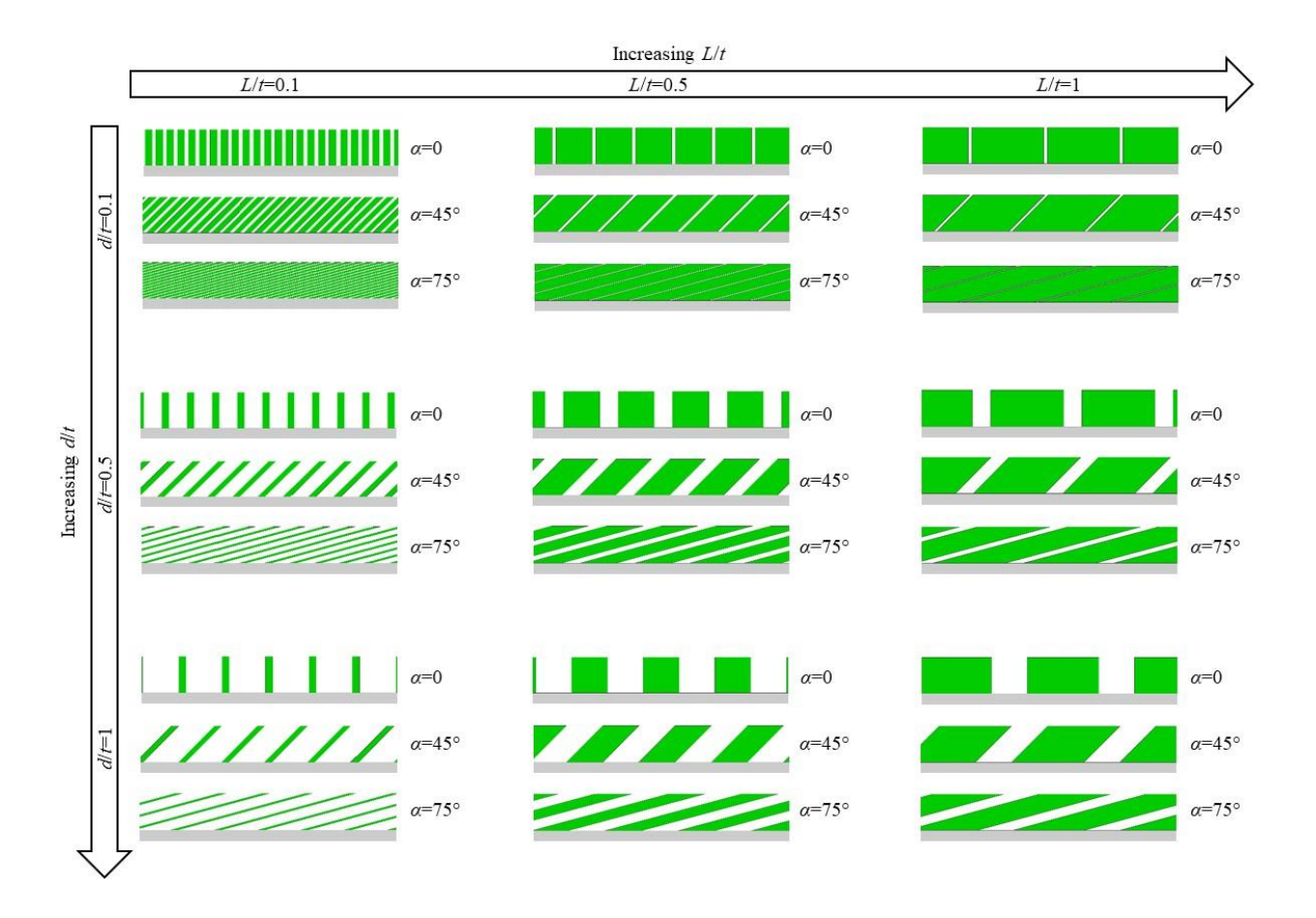


Figure 2-4: Models with different combinations of scale gaps (d/t), aspect ratios (L/t) and slant angles (α) .

A first inspection reveals that some designs do not provide adequate coverage, leaving the substrate directly exposed to outside mechanical threats. This issue occurs for all designs with no slant angle (α =0), and more generally when the spacing of the scale is too large and/or the slant angle is too low. On the other hand, designs providing good coverage involve neighboring scales that overlap. To characterize the extent of coverage for each design we defined a non-dimensional coverage parameter λ = t_s/t where t is the thickness of the scales, and t_s is obtained by first drawing a vertical line from the upper right corner of a scale. t_s then was computed as the sum of the intersect lengths

between that line and the neighboring scales (figure 2-5). By this measure, λ ranges from $\lambda = 0$ (no coverage) to $\lambda = 1$ (full coverage).

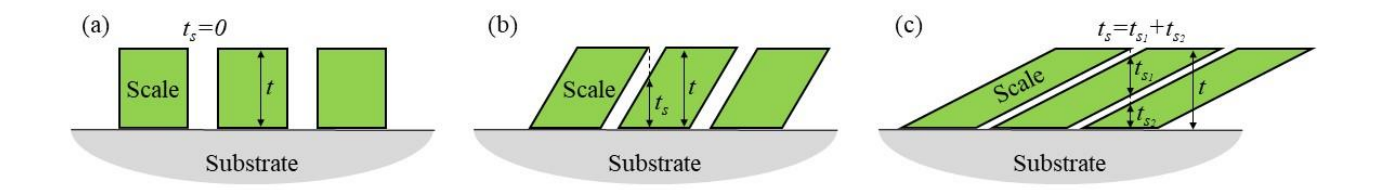


Figure 2-5: Diagrams showing three examples on how to compute ts and $\lambda = ts/t$: (a) Example with no scale overall and no coverage ($\lambda = 0$); (b) Example with two scales overlapping, leading to intermediate λ ; (c) Example with three scales overlapping, leading to high λ .

For all models, we imposed a vertical force on the upper right corner of the middle scale so that the force applied the largest possible tilting moment on the scale, which represented the "worstcase scenario" for loading. We first present the effect of each parameter on the puncture forcedisplacement curves (figure 2-6). For all results, we normalized the applied force on the middle scale as $F^*=F(1-v^2)/E_sLt$ (consistent with equation (2.1)) and the displacement of the punctured point as $u^*=u/t$. Figure 2-6a shows the effect of the slant angle α on the deformation of the system for a fixed aspect ratio of L/t=1 and gap of d/t=0.1. Initially, the imposed force simultaneously pushes the scales into the substrate and increases the tilt angle. At the initial stage the puncture stiffness is relatively low, especially at larger slant angles (figure 2-6b) because of the larger moment arm of the applied force. At some point during the simulation the scales start contacting each other (on the snapshots of figure 2-6a, the contact areas are marked in red and on the puncture force-displacement curves in figure 2-6b a (x) symbol marks every new contact event). For the cases of $\alpha = 0^{\circ}$ and $\alpha = 45^{\circ}$ the punctured scale contacts with the neighboring scales at about u/t=0.08, which translates into a kink on the force-displacement curve and a stiffer response. For the case of α =0, the corner of the punctured scale slides on the side of the neighboring scale with

little resistance and the contact force between the scales is mostly horizontal. Introducing a slant angle generates a vertical component to the contact force and a much stiffer response (this result is consistent with our previous experimental study on 3D printed scales [4]). For the model with the largest slant angle (α =75°) the initial contact occurs earlier due to the larger tilting moment. The first four contacts do not have a significant effect on the stiffness because of the high tilting moments in the scales. By engaging more scales by contact during loading, the resistance from the contact eventually overcomes the high tilting moment and the stiffness starts increasing. The postcontact stiffness also increases significantly with the scale slant angle. Interestingly, the puncture force can become high enough that additional scales enter contact (figure 2-6a), which distributes the puncture force over an even greater area. Figure 2-6c shows the effect of varying the aspect ratio on the response of the system, with a fixed gap of d/t=0.1 and fixed slant angle of $\alpha=45^{\circ}$. Larger aspect ratios cause less penetration, but larger tilting moments induced by the loading in the punctured scale, which implies that individual scales offer less resistance to tilting resulting in low initial stiffness (figure 2-6d). In contrast, smaller scales (smaller L/t) penetrate more into the substrate but showed less tilting. This stability effects the post-contact stiffness of the system as well, where the contacting scales with smaller aspect ratios show more resistance against tilting resulting in higher system stiffness (figure 2-6d). Finally, figure 2-6e and 6f show the effect of the gap size for a fixed aspect ratio of L/t=0.5 and slant angle of $\alpha=45^{\circ}$. The gap size has no significant effect on the initial stiffness of the systems and little effect on post contact stiffness. The main effect of increasing d/t was to delay scale-scale contact (figure 2-6f).

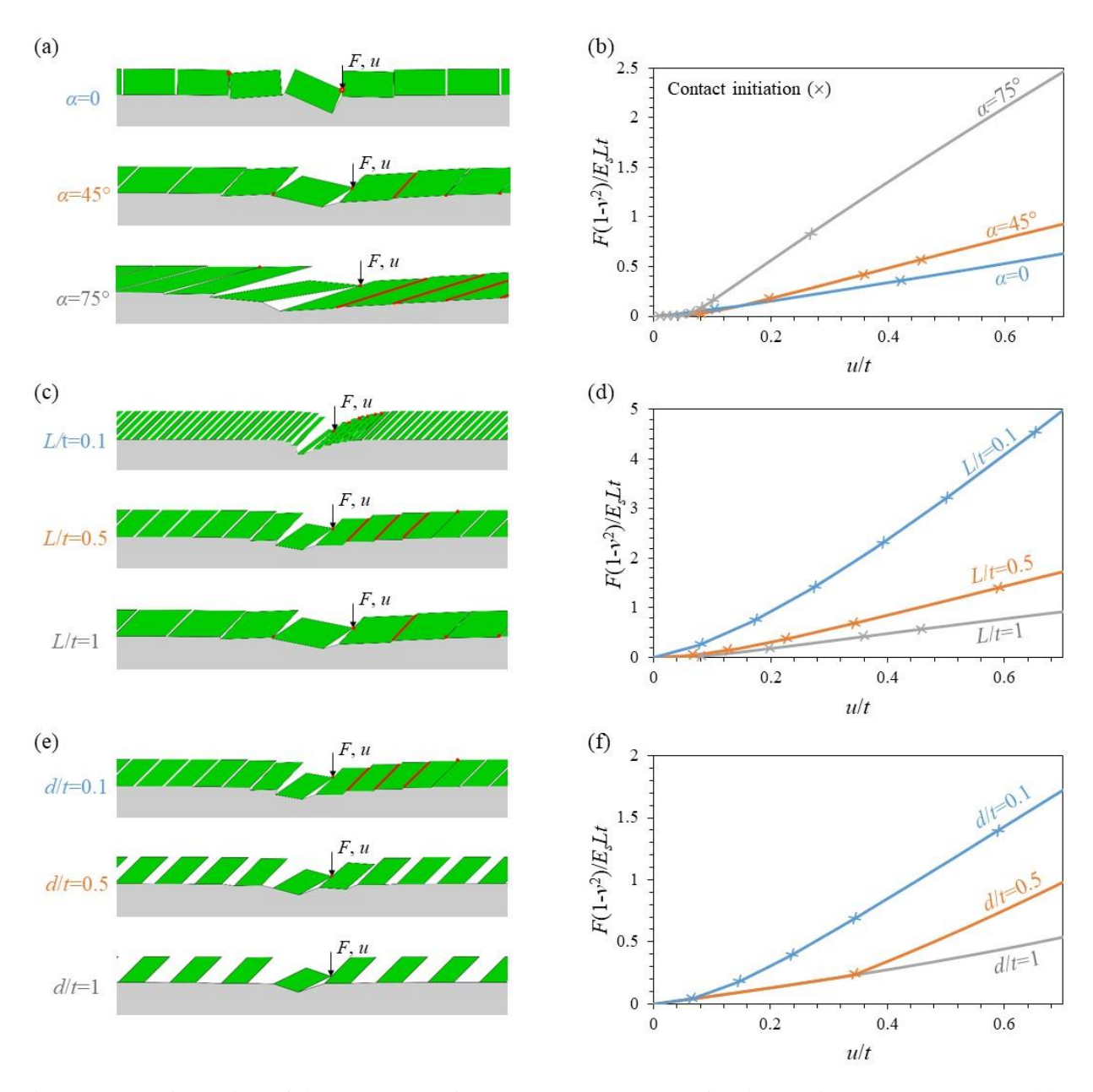


Figure 2-6: Deformation of three systems of scales at u/t=0.7 on a soft substrate in a puncture test, and the related force-displacement curves: for (a) and (b) a fixed aspect ratio of L/t=1 and a gap size of d/t=0.1, (c) and (d) a fixed gap size of d/t=0.1 and a slant angle of $\alpha=45^{\circ}$, (e) and (f) a fixed aspect ratio of L/t=0.5 and a slant angle of $\alpha=45^{\circ}$.

In addition to puncture stiffness, we considered the puncture resistance of the scaled surface. There are several possible failure modes for this system, including fracture in the scales, failure of the interface or tearing of the substrate. However, in this study the combination of the materials,

geometries and load range was such that we did not observe any of these failure modes. Instead, we focused on a failure mode that occurred by tilting of the indented scale. In this failure mode the indented scale tilts from the action of the needle, and when the tilt reaches a critical angle ϕ_c =tan⁻¹(μ) (where μ is the friction coefficient between the scale and the needle), the needle suddenly slides on the surface of the tilted scale and finds its way into the substrate (figure 2-7a).

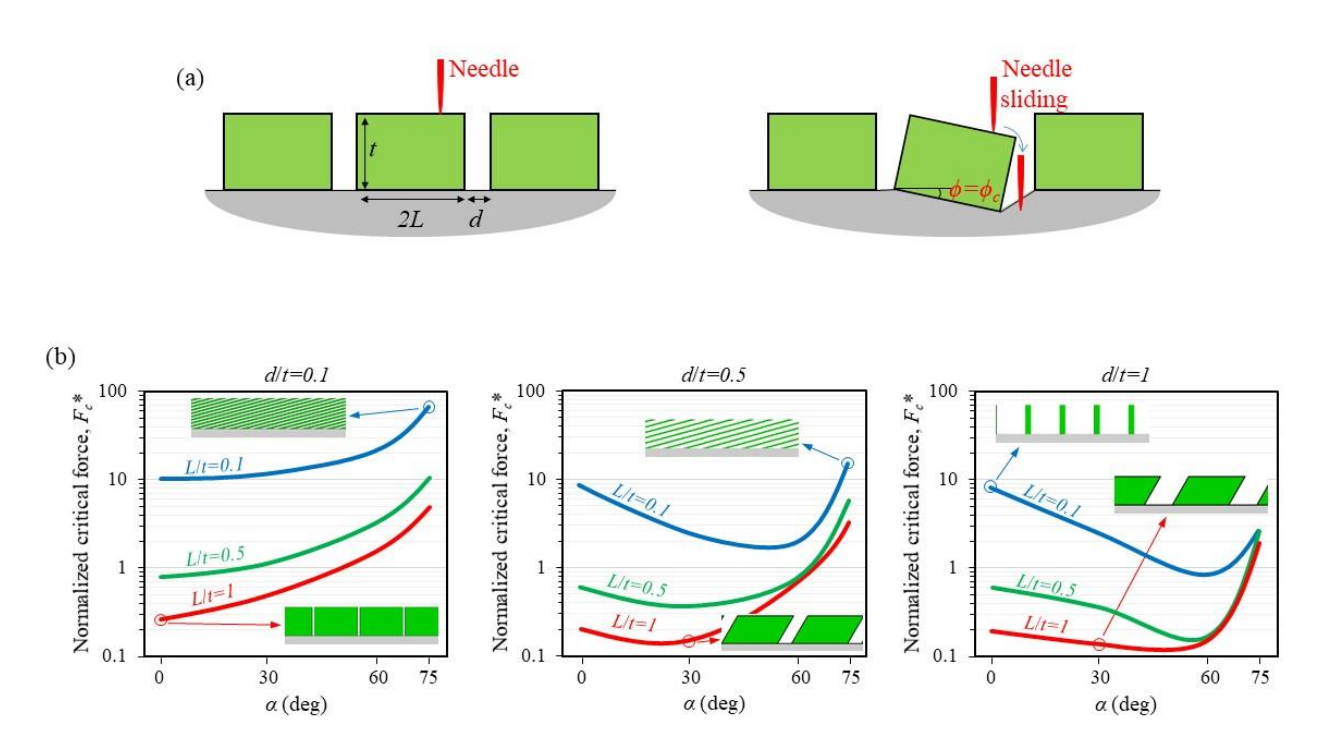


Figure 2-7: (a) Reaching the critical angle causes the needle to slide off the scale surface; (b) the effect of the slant angle (α), the aspect ratio (L/t) and the gap (d/t) on the critical force of the system. The critical force is denoted as F_c and is normalized by $F_c*=F_c (1-v^2)/E_sLt$.

This failure mode was identified on scales from gar fish and duplicated in puncture experiments on 3D printed scales [4, 17]. For each of the models discussed above, we computed a critical force, corresponding to the point where the tilting of the scale reached a critical angle which we took as $\phi_c = 10^\circ$ to be consistent with previous experiments [17]. Figure 2-7b shows that the gap size, aspect ratio and slant angle, all had a significant effect on the critical force. In general, decreasing the gap between the scales (d/t) increased the critical force, because early contact between the

scales increased stability and delayed tilting. Smaller scales (small L/t) were also more stable, because of the reduced lever arm of the applied force. Higher slant angles also increased the critical force as long as the scales contacted early in the puncture process. If the contact was delayed because of a large initial gap between scales, larger slant angles led to larger lever arm for the force and less stability. Compounding all these effects, the smallest aspect ratio (L/t=0.1), the smallest gap (d/t=0.1) and the largest slant angle (α =75°) produced the system with the highest critical force ($F_c(1-v^2)/ELt$ =64). Figure 2-8 maps the puncture stiffness and the critical force for all models of scale designs, showing a strong correlation between these two properties. The highest puncture stiffness was achieved for the case with an aspect ratio of L/t=0.1, a slant angle of α =75°, and a gap of d/t=0.1. This system also has the highest critical force. Among all the design parameters considered here, we found that the slant angle had the most significant effect on the puncture stiffness and critical force.

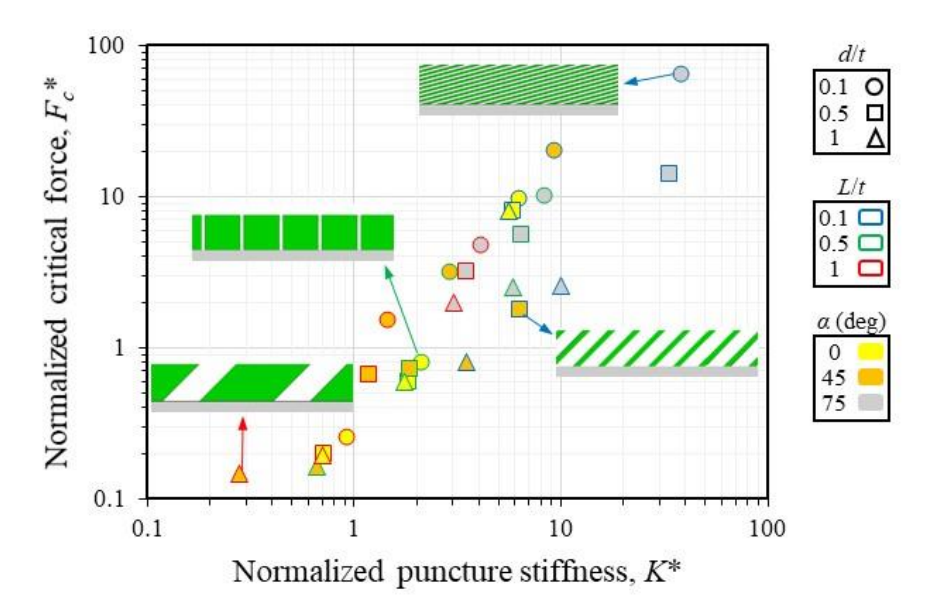


Figure 2-8: The relation between the normalized stiffness and the critical force for different combinations of slant angle (α), aspect ratio (L/t) and gap (d/t). The stiffness and critical force are denoted as K and F_c , and are normalized by $K^* = K/E_s t$, and $F_c^* = F_c (1-v^2)/E_s L t$, respectively.

Contact interaction between scales not only improves critical force, it also improves how the puncture force is distributed onto the substrate (see, for example, figure 2-6a). To better illustrate this effect, figure 2-9 shows the spatial distribution of vertical reaction forces from the substrate onto the scales, for models with different slant angles (under the same puncture force). In the model with no slant angle (α =0), only one scale is engaged by the point force, and the force is transmitted to the substrate over a small area. This concentrated distribution could lead to flexural failure of the scale, or damage in the underlying tissues ("blunt damage"). As the slant angle is increased, more scales enter in contact and distribute the force over a larger region of the substrate. This effect is very pronounced for the case α =75°, where scales tilt and contact in "domino effect" that involve about eight scales, distributing the puncture force over a large surface. Slanted scales can therefore improve the critical force of the system by distributing the force over a wider area.

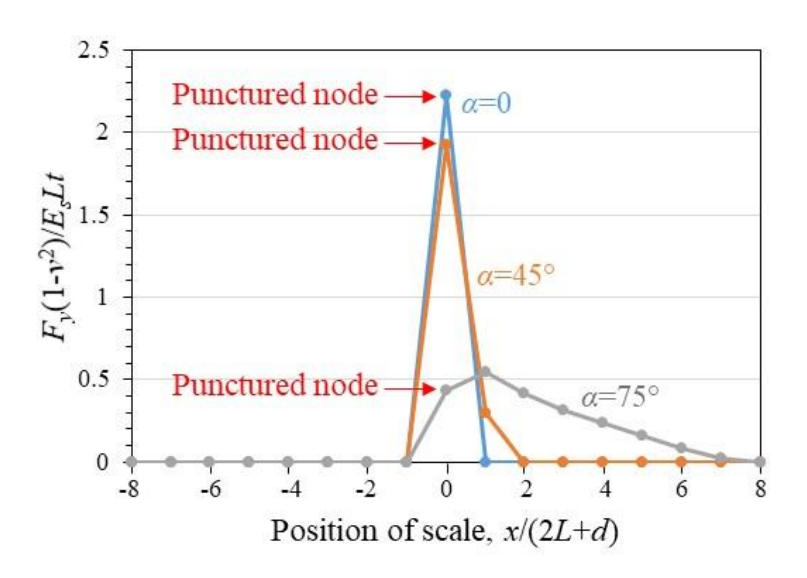


Figure 2-9: Force distribution over the models with different slant angles in a puncture test

2.5 Hard scales on a soft membrane: flexural compliance

In addition to resistance to puncture, flexural compliance is a desired property in scaled skin. In this section we used the DEM model to explore how the architecture of the scales affects flexural stiffness. In the model, a set of scales is perfectly bonded to a thin membrane of thickness h, depth b, and modulus E_m (figure 2-10a). The membrane was modeled with nonlinear co-rotational Euler-Bernoulli beam elements which assumed linear elasticity and small strains within the membrane, but allowed for arbitrarily large elemental rotations. The section of the membrane located below the rigid scales was also assumed to be rigid (figure 2-10a). In order to induce flexural deformations to the model, two self-equilibrated moments M were imposed at the ends of the membrane, inducing a state of pure bending. Figure 2-10b shows the bending moment-curvature response for a membrane covered with cubic scales. Initially the flexural deformation of the thin membrane is the only contributor to the bending moment, so that the flexural stiffness is very low. As curvature increases the scales contact each other, which is characterized by an abrupt stiffening. In that second stage, the contact forces between the scales are balanced by tension in the membrane. These two forces create a couple which becomes the largest contributor to flexural stiffness. To better appreciate this mechanism we partitioned the total strain energy in the DEM model into the contributions from bending and axial strain energy in the membrane (figure 2-10c). In the initial stage the energy from axial stretch of the membrane is negligible compared to the energy from flexural deformation. After contact of the scales however, the energy from axial deformation increases dramatically.

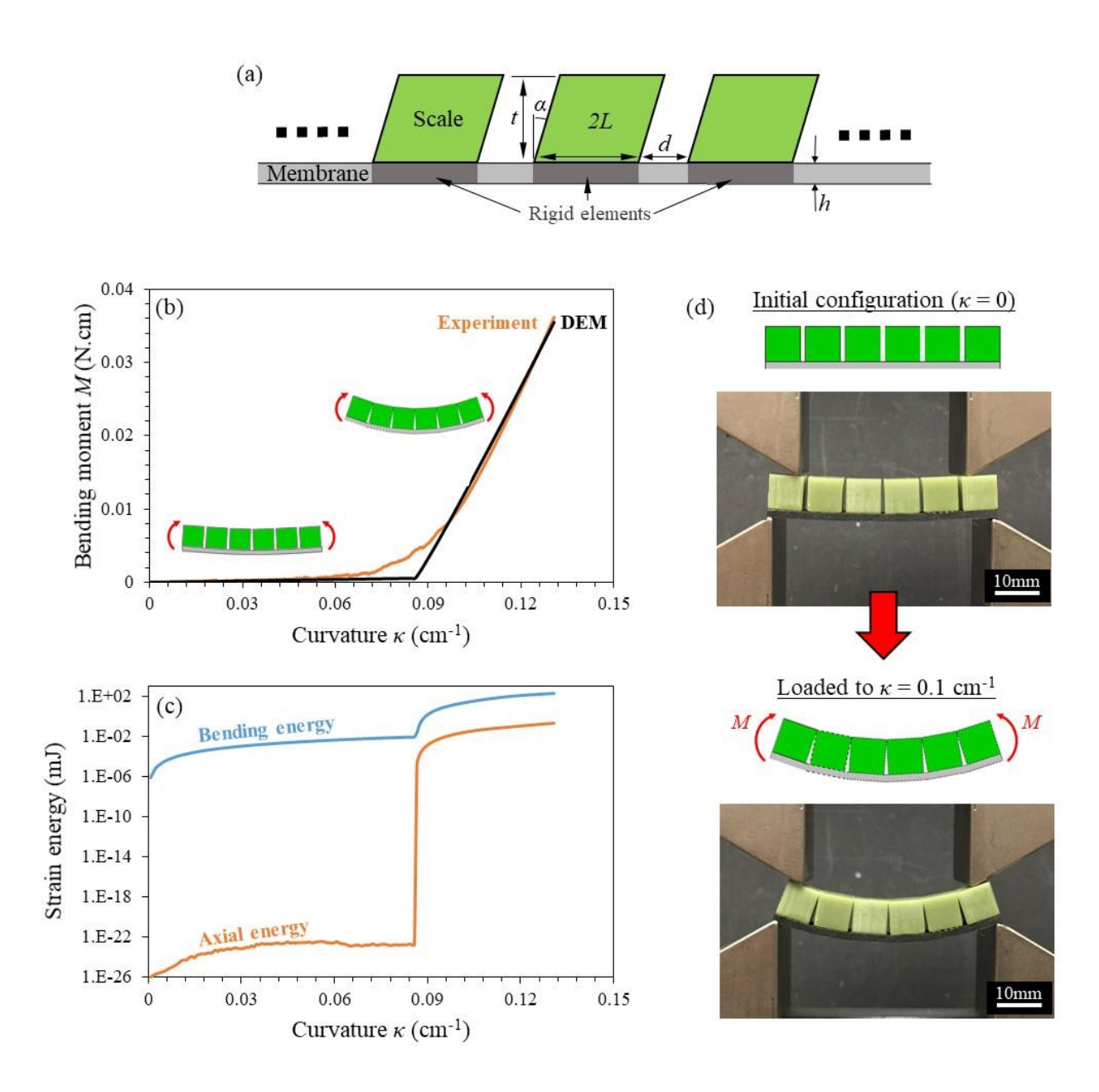


Figure 2-10: (a) Schematic for the DEM flexural model; (b) Bending moment-curvature curves showing good agreement between the experiment and DEM results; (c) Evolution of strain energy from axial stresses and strain energy form bending stresses during loading, computed from the DEM simulations. (d) Comparison between a DEM simulation and an experiment on 3D printed blocks on elastomer strip.

To validate the flexural models we also fabricated and tested a membrane covered by ABS cubic scales (8mm×8mm×8mm). The scales were 3D-printed and glued onto a 1mm thick strip of polyurethane (Young's modulus =4.5 MPa, measured in three-point bending). In the experiment,

pure bending was induced in the membrane using a four-point bending configuration (figure 2-10d). Figure 2-10b shows an excellent agreement between the experiment and the DEM model, except near the contact point. In the DEM model, contact is initiated simultaneously between all the scales which gives rise to a sharp transition in stiffness. In the experiments contact was initiated at slightly different deformation stage due to imperfections, which gave rise to a more progressive transition in the slope. We used the DEM approach to explore the effect of the scale geometry and arrangement on the flexural compliance of the scaled-membrane system. The moment was normalized according to classical beam theory as $M^*=Mt/E_mI_m$, and the curvature normalized as $\kappa^*=\kappa t$. Figure 2-11 shows the effect of slant angle, scale length and scale gap. The normalized moment-curvature response followed the behavior described above: initially negligible stiffness, followed by rapid stiffening immediately after the scales enter contact. Interestingly, the post contact behavior shows softening, because the sliding of the contact points increase the moment arm on individual scales, effectively making the entire structure more compliant (softening is absent for cases with no slant, α =0 because the contact points remain at the corner of the scales during the entire simulation). The deformation at which the scales contact, the amount of stiffening and softening depend largely on the geometric parameters. In addition, we observed that for designs with high slant angles, large scale size or small gap, the conformation induced a 'zigzagged' deformation in the membrane.

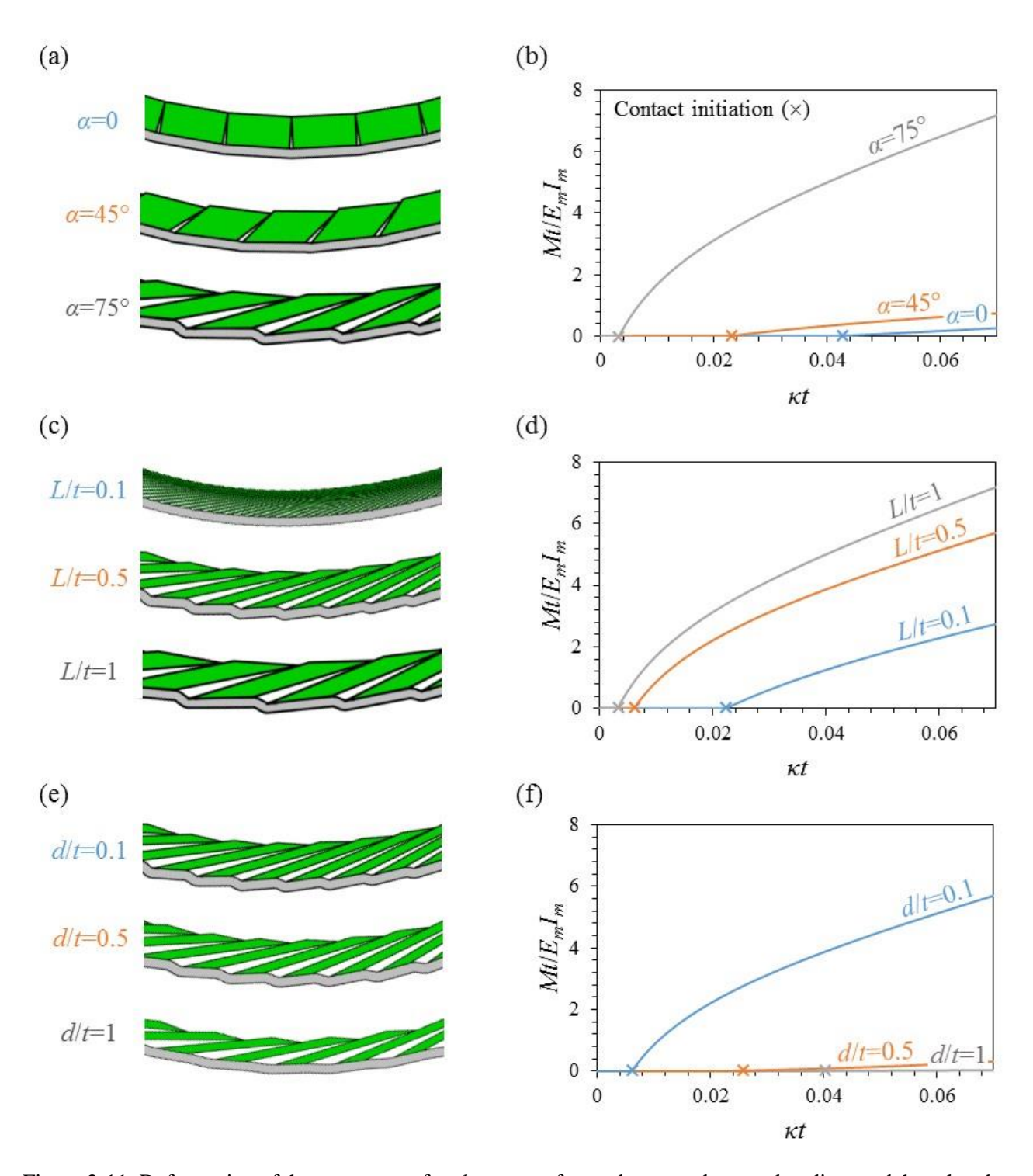


Figure 2-11: Deformation of three systems of scales on a soft membrane under pure bending, and the related moment - curvature curves: for (a) and (b) a fixed aspect ratio of L/t=1 and a gap size of d/t=0.1, (c) and (d) a fixed gap size of d/t=0.1 and a slant angle of $\alpha=75^{\circ}$, and (e) and (f) a fixed aspect ratio of L/t=0.5 and a slant angle of $\alpha=75^{\circ}$.

Figure 2-12 summarizes the flexural compliance for different combinations of gap sizes (d/t), aspect ratios (L/t) and slant angles (α) . For all models, we considered a constant total membrane length of $L_{\text{whole}}/t = 100$. also, we put a limitation on loading where the system is loaded up to a maximum end rotation of 180°. In some designs, contact was never initiated in the simulation due to geometry (large gap sizes) and, therefore, were unaffected by the scale angle; these cases were plotted as unfilled dots in figure 2-12. Considering all other cases in which contact occurs during the loading (filled dots in figure 2-12), contact significantly decreases the flexural compliance of the system by up to three orders of magnitude. For small slant angles of α =0° and α =30°, the highest flexural compliance is for the models with the smallest gap (d/t=0.1) and the smallest aspect ratio (L/t=0.1). For slant angles of α =60° and α =75°, the highest flexural compliance is for the model with d/t=0.5, L/t=0.1, and the model with d/t=1, L/t=0.1, respectively. For the models with large slant angles, larger gaps therefore increased the flexibility to the system. Also, by increasing the aspect ratio of the scales the system gets stiffer, so smaller aspect ratios are desirable.

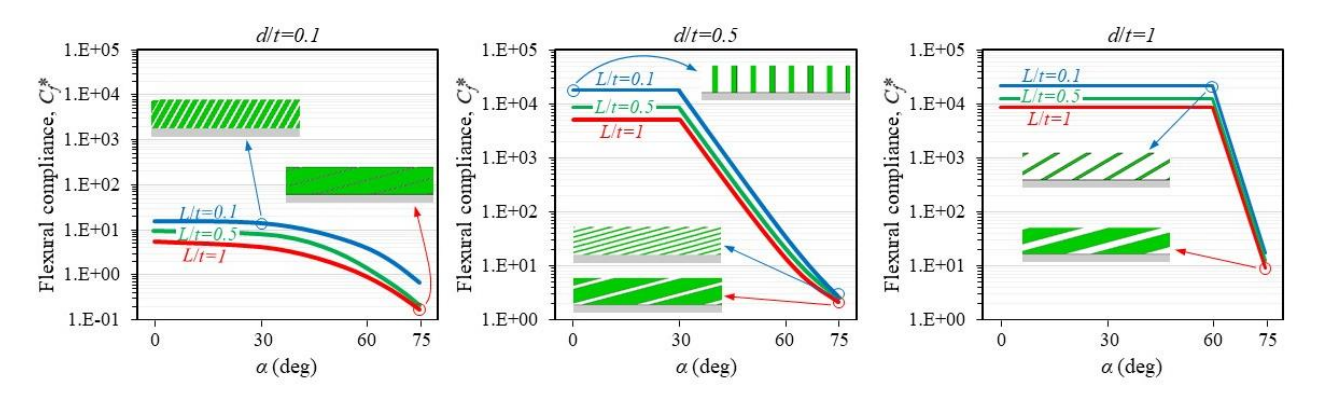


Figure 2-12: The effect of the gap size, aspect ratio and slant angle on the flexural compliance of a series of scales on a soft membrane. The flexural compliance is denoted as C_f and normalized by $C_f *= C_f E_m I_m$.

2.6 Optimum mechanical performance

From the previous sections, it is clear that several of the design parameters have conflicting effects on puncture resistance and flexural compliance. For example, increasing slant angle increases

puncture resistance, but also decreases flexural compliance. In this section we seek designs which offer optimum combinations of four mechanical properties: (i) the coverage parameter λ (determined using geometry, figure 2-5) (ii) the critical force (force at which the indented scale become mechanically instable), (iii) the penetration resistance (defined as the inverse of the maximum penetration of the scales into the substrate when the punctured scale reaches the critical tilting angle), (iv) the flexural compliance (defined as the inverse of the maximum slope in the moment-curvature curve). In order to find the best design, we parameterized the scale gap size d/t $= \{0.1, 0.2, ..., 1\}$, aspect ratio $L/t = \{0.025, 0.05, 0.1, 0.2, ..., 1\}$, and slant angle $\alpha = \{0^{\circ}, 15^{\circ}, 15$..., 75°}. We eliminated the designs where the coverage λ is zero, because these designs leave the substrate partially exposed to mechanical threats. We compared a set of models with various combinations of the three design parameters (the gap size, the aspect ratio and the slant angle) using a quaternary plot to find the best design for a given design performance criteria. As the four criteria have values with different orders of magnitude, we rescaled each criterion to a range from 0 to 1 in which the minimum and the maximum of each criterion are 0 and 1, respectively. We defined a fitness score as:

$$f = (Coverage)^{m}(Critical force)^{n}(Penetration resistance)^{k}(Flexural compliance)^{l}$$
(2.7)

The individual values of m, n, k and l can be tuned to control the influence of each criterion on the fitness score, but we required m+n+k+l=1. The best designs for any combinations of m, n, k and l can therefore be displayed on a quaternary plot, shown on figure 2-13. The corners of the tetrahedron shows the four designs that optimize one of the four criteria while the other three are ignored. High coverage (m=1) is obtained with small gap size, large aspect ratio and intermediate slant angle (45°). Maximum critical force (n=1) is obtained for small gap size, small aspect ratio and large slant angle. The best penetration resistance is obtained for a large gap size. Finally, the

most flexible designs among the models (l=1) are achieved with scales with the smallest aspect ratio (L/t = 0.025) and a large slant angle (α = 60°). These four designs are very distinct, especially in terms of aspect ratio and gap distance. In order to identify the design with the best "balanced" set of properties, we sought the design that maximized f with m=n=k=l=0.25, to give equal weight to each performance metrics.

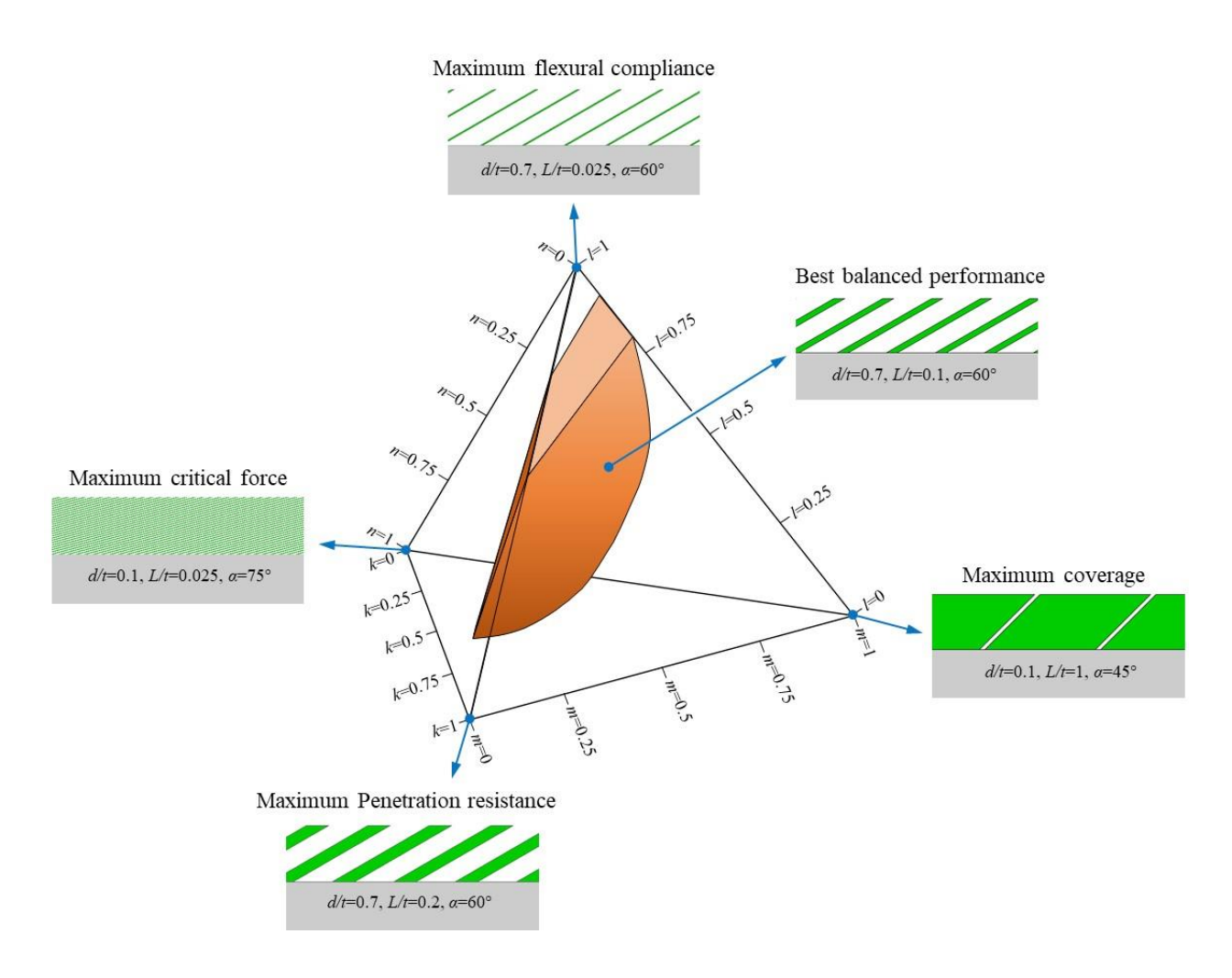


Figure 2-13: The quaternary plot showing the best designs for the fitness indices of m=1, n=1, k=1 and l=1 (the four corners of the plot). Also the best balanced design is shown for the case with (m=0.25, n=0.25, k=0.25, l=0.25).

The design with the best balanced performance was d/t=0.7, L/t=0.1 and $\alpha=60^{\circ}$. Our approach also showed that this particular design dominates not only for m=n=k=l=0.25, but also for a wide variety of fitness parameters depicted by the orange volume on figure 2-13.

2.7 Summary

In this study we proposed the discrete element method to investigate the mechanical behaviour of systems of segmented scales attached to a soft substrate and a soft membrane. DEM is appropriate for this kind of system where the scales can be assumed to be rigid compared to the surrounding materials, and we validated the simulations with puncture and flexural experiments. The focus was to learn about the effect of the architecture (the aspect ratio and slant angle of the scales) and the arrangement (the gap size between the scales) of the scales on the mechanical performance of the scaled systems. The study gives us useful insights into the mechanics of this type of system, optimization of its mechanical performance, and eventually, a better design of synthetic fish-skin-like protective systems. The computational efficiency of DEM allows us to run a large number of nonlinear models (720 Models) with different combinations of the design parameters. To identify the best designs, we considered four criteria: critical force, coverage, penetration resistance and flexural compliance. The results show that the contact between the scales play a critical role in the behaviour of the system. The contact helps to distribute the load over a wider area therefore the system becomes more resistant to tilting and penetration. The main conclusions are as follow:

- The models with a high stiffness have a high critical force as well.
- The model with the highest critical force requires the smallest gap size and aspect ratio, and the largest slant angles.
- The smallest gap size, the largest aspect ratio and a moderate slant angle of 45° give the best coverage.

- Contact makes the force distribution occur over a wider area which results in a higher critical force and penetration resistance. On the other hand, too many contact points has negative effects on the penetration resistance.
- To have the highest flexural compliance the aspect ratio needs to be the smallest.
- There is limitation on the positive effect of the slant angle on the flexural compliance: too large slant angle decreases the flexibility of the system.

We used a quaternary plot to examine the influence of the design parameters (gap size, aspect ratio and slant angle) on the four mechanical properties: coverage, critical force, penetration resistance and flexural compliance. The quaternary plot shows that changing each design parameter can improve one mechanical property while having a negative effect on the other ones. Also, based on which mechanical properties are more important to be considered, we give a weight to each criterion (m, n, k and l), which results in different combinations of design parameters. The best response of the system considering the four criteria with the equal weights (m=0.25, n=0.25, k=0.25 and l=0.25) belongs to the model with a small aspect ratio (L/t=0.1), intermediate gap size (d/t=0.7) and large slant angle ($\alpha=60^{\circ}$). This article provides a strong basis for future design of synthetic fish-skin-like protective systems. Further simulations would be needed to optimize the design parameters for specific applications and boundary conditions, and could include material nonlinearity in the substrate for better accuracy at large deformations. Adding nonlinearities and unusual behavior to the substrate could indeed enrich the problem and possibly lead to new and interesting interactions between the scales and the substrate. The focus on this DEM-based method is on systems where the scales are orders of magnitude stiffer than the substrate, which is relevant for many types of flexural armor (biological and engineered). For the cases where the deformation of individual scales cannot be neglected, other numerical approaches such as finite elements must

be used. Finite element is however much more expensive computationally because of contact penalty methods and much greater number of degrees of freedom.

2.8 Acknowledgments

This work was supported by a Discovery Grant from the Natural Sciences and Engineering Research Council of Canada. A.S. was partially supported by a McGill Engineering Doctoral Award.

2.9 References

- 1. Ritchie, R.O., *The conflicts between strength and toughness*. Nature Materials, 2011. **10**(11): p. 817-822.
- 2. Wegst, U.G.K., et al., *Bioinspired structural materials*. Nature Materials, 2014. **14**: p. 23.
- 3. Barthelat, F., *Architectured materials in engineering and biology: fabrication, structure, mechanics and performance.* International Materials Reviews, 2015. **60**(8): p. 413-430.
- 4. Martini, R., Y. Balit, and F. Barthelat, *A comparative study of bio-inspired protective scales using 3D printing and mechanical testing*. Acta Biomaterialia, 2017. **55**: p. 360-372.
- 5. Rajabi, H., et al., Effect of microstructure on the mechanical and damping behaviour of dragonfly wing veins. Royal Society Open Science, 2016. **3**(2): p. 160006.
- 6. Porter, M.M., et al., *Highly deformable bones: Unusual deformation mechanisms of seahorse armor.* Acta Biomaterialia, 2013. **9**(6): p. 6763-6770.
- 7. Yang, W., et al., *Natural Flexible Dermal Armor*. Advanced Materials, 2013. **25**(1): p. 31-48.
- 8. Rajabi, H., et al., *Resilin microjoints: a smart design strategy to avoid failure in dragonfly wings.* Scientific Reports, 2016. **6**: p. 39039.
- 9. Chintapalli, R.K., et al., *Fabrication, testing and modeling of a new flexible armor inspired from natural fish scales and osteoderms.* Bioinspiration & Biomimetics, 2014. **9**(3): p. 036005.
- 10. Martini, R. and F. Barthelat, *Stretch-and-release fabrication, testing and optimization of a flexible ceramic armor inspired from fish scales.* Bioinspiration & Biomimetics, 2016. **11**(6): p. 066001.
- 11. Funk, N., et al., *Bioinspired Fabrication and Characterization of a Synthetic Fish Skin for the Protection of Soft Materials*. ACS Applied Materials & Interfaces, 2015. **7**(10): p. 5972-5983.
- 12. Rudykh, S., C. Ortiz, and M.C. Boyce, *Flexibility and protection by design: imbricated hybrid microstructures of bio-inspired armor.* Soft Matter, 2015. **11**(13): p. 2547-2554.

- 13. Vernerey, F.J. and F. Barthelat, *Skin and scales of teleost fish: Simple structure but high performance and multiple functions.* Journal of the Mechanics and Physics of Solids, 2014. **68**: p. 66-76.
- 14. Vernerey, F.J. and F. Barthelat, *On the mechanics of fishscale structures*. International Journal of Solids and Structures, 2010. **47**(17): p. 2268-2275.
- 15. Zhu, D.J., et al., *Puncture resistance of the scaled skin from striped bass: Collective mechanisms and inspiration for new flexible armor designs.* Journal of the Mechanical Behavior of Biomedical Materials, 2013. **24**: p. 30-40.
- 16. Browning, A., C. Ortiz, and M.C. Boyce, *Mechanics of composite elasmoid fish scale assemblies and their bioinspired analogues*. Journal of the Mechanical Behavior of Biomedical Materials, 2013. **19**: p. 75-86.
- 17. Martini, R. and F. Barthelat, *Stability of hard plates on soft substrates and application to the design of bioinspired segmented armor*. Journal of the Mechanics and Physics of Solids, 2016. **92**: p. 195-209.
- 18. Nelson, O. *Illinois Gar Summit I*. 2014; Available from: http://moxostoma.com/illinois-gar-summit-i-feb-2014/.
- 19. Chen, I.H., et al., *Armadillo armor: Mechanical testing and micro-structural evaluation.* Journal of the Mechanical Behavior of Biomedical Materials, 2011. **4**(5): p. 713-722.
- 20. Garst, W. and G.S. Garst, *Warren and Genevieve Garst Photographic Colletion*. 1985, Colorado State University.
- 21. Burger, J. and R.T. Zappalorti, *The Northern Pine Snake (Pituophis melanoleucus) its Life History, Behavior and Conservation.* Reptiles-Classification, Evolution and Systems. 2011, New York: Nova Science Publishers, Inc.
- 22. Chintapalli, R.K., et al., *Fabrication, testing and modeling of a new flexible armor inspired from natural fish scales and osteoderms.* Bioinspiration & Biomimetics, 2014. **9**(3).
- 23. Connors, M., et al., *Bioinspired design of flexible armor based on chiton scales*. Nature Communications, 2019. **10**(1): p. 5413.
- 24. Vernerey, F.J., K. Musiket, and F. Barthelat, *Mechanics of fish skin: A computational approach for bio-inspired flexible composites*. International Journal of Solids and Structures, 2014. **51**(1): p. 274-283.
- 25. Dugué, M., et al., *Indentation of interlocked assemblies: 3D discrete simulations and experiments.* Computational Materials Science, 2013. **79**: p. 591-598.
- 26. Pro, J.W., et al., *GPU-based simulations of fracture in idealized brick and mortar composites*. Journal of the Mechanics and Physics of Solids, 2015. **80**: p. 68-85.
- 27. Bolander, J.E. and S. Saito, *Fracture analyses using spring networks with random geometry*. Engineering Fracture Mechanics, 1998. **61**(5): p. 569-591.
- 28. Abid, N., M. Mirkhalaf, and F. Barthelat, *Discrete-element modeling of nacre-like materials: Effects of random microstructures on strain localization and mechanical performance*. Journal of the Mechanics and Physics of Solids, 2018. **112**: p. 385-402.
- 29. Abid, N., J.W. Pro, and F. Barthelat, *Fracture mechanics of nacre-like materials using discrete-element models: Effects of microstructure, interfaces and randomness.* Journal of the Mechanics and Physics of Solids, 2019. **124**: p. 350-365.
- 30. Lim, R.K., et al., *High-performance simulation of fracture in idealized 'brick and mortar' composites using adaptive Monte Carlo minimization on the GPU*. The International Journal of High Performance Computing Applications, 2015. **30**(2): p. 186-199.

- 31. Pro, J.W., et al., *The impact of stochastic microstructures on the macroscopic fracture properties of brick and mortar composites.* Extreme Mechanics Letters, 2015. **5**: p. 1-9.
- 32. Pro, J.W. and F. Barthelat, *Discrete element models of tooth enamel, a complex three-dimensional biological composite.* Acta Biomaterialia, 2019. **94**: p. 536-552.
- 33. Pro, J.W. and F. Barthelat, *Discrete element models of fracture in tooth enamel: Failure mode competition and statistical effects.* Journal of the Mechanics and Physics of Solids, 2020. **137**: p. 103868.
- 34. Zhu, D.J., et al., *Structure and Mechanical Performance of a "Modern" Fish Scale*. Advanced Engineering Materials, 2012. **14**(4): p. B185-B194.
- 35. Barber, J.R., *Elasticity*. 2002: Springer.
- 36. Okumura, I.A., *ON THE GENERALIZATION OF CERRUTI'S PROBLEM IN AN ELASTIC HALF-SPACE*. Doboku Gakkai Ronbunshu, 1995. **1995**(519): p. 1-10.
- Wu, J. and C.Q. Ru, *Spherical indentation of an elastic layer on a rigid substrate revisited.* Thin Solid Films, 2019. **669**: p. 500-508.
- 38. Lin, Y.-Y., C.-F. Chang, and W.-T. Lee, *Effects of thickness on the largely-deformed JKR* (*Johnson–Kendall–Roberts*) test of soft elastic layers. International Journal of Solids and Structures, 2008. **45**(7): p. 2220-2232.
- 39. Li, M. and M. Dai, A simple method for spherical indentation of an elastic thin layer with surface tension bonded to a rigid substrate. Applied Mathematical Modelling, 2020. **81**: p. 653-662.
- 40. Johnson, K.L., *Contact mechanics*. 1987: Cambridge university press.

Link between the chapter 2 and chapter 3

In the previous chapter (chapter 2), we proposed discrete element method (DEM) as an approach to model a scale-covered system with two different configurations: hard scales on a soft substrate, and hard scales on a asoft membrane. After validating the models with experiments, we investigated the puncture resistance and flexural compliance of the system, and the effect of the scales on the mechanics and the performance. We showed that by optimizing the geometries and the arrangement of the scales we can improve the flexural compliance, within limitations (by increasing the flexural compliance, the puncture resistance decreases). In the next chapter (chapter 3), inspired from nature, we approached a different solution to provide flexibility for the system, which was imposing wrinkles in the system. We explored the post-buckling stability of a scaled membrane in the mode I and mode II configurations, and how to control a buckling mode using scales.

Chapter 3

Bioinspired buckling of scaled skins

Chapter 3: Bioinspired buckling of scaled skins

Ali Shafiei¹, J. William Pro¹ and Francois Barthelat^{1,2}*

¹ Department of Mechanical Engineering, McGill University, 817 Sherbrooke Street West, Montreal, QC H3A 2K6, Canada

² Department of Mechanical Engineering, University of Colorado, 427 UCB, 1111 Engineering Dr, Boulder, CO 80309, United States

* Correspondence to: francois.barthelat@colorado.edu

3.1 Abstract

Natural flexural armors combine hard, discrete scales attached to soft tissues, providing unique combinations of surface hardness (for protection) and flexibility (for unimpeded motion). Scaled skins are now inspiring synthetic protective materials which offer attractive properties, but which still suffer from limited trade-offs between flexibility and protection. In particular, bending a scaled skin with the scales on the intrados side jams the scales and stiffen the system significantly, which is not desirable in systems like gloves where scales must cover the palm side. Nature appears to have solved this problem by creating scaled skins that can form wrinkles and folds, a very effective mechanism to accommodate large bending deformations and to maintain flexural compliance. This study is inspired from these observations: we explored how rigid scales on a soft membrane can buckle and fold in a controlled way. We examined the energetics of buckling and stability of different buckling modes using a combination of discrete element modeling (DEM) and experiments. In particular, we demonstrate how scales can induce a stable mode II buckling, which is required for the formation of wrinkles and which could increase the overall flexural compliance and agility of bioinspired protective elements.

Keywords: Bioinspiration, discrete element method, segmented hard material, buckling, stability

3.2 Introduction

The need for protection against predation and other threats in nature has led to high performance protective systems that evolved over millions of years. Among natural flexible armor, scaled skins are common in animals including fish, snakes, lizards, and armadillos. The main idea in scaled skins is to cover flexible tissues with hard plates of finite sizes [1-5]. The hard plates provide surface hardness and resistance to puncture and laceration [6-9], while also maintaining high flexural compliance due to the ability of discrete scales to move relative to one another. These systems have been inspiring synthetic scaled protective systems [2], [1-5], where a central design challenge is to combine high puncture resistance with flexural compliance [2, 10-19]. In these systems the architecture and arrangement of the scales can be tuned to maximize combinations of compliance and protection [1-3, 10, 11, 15, 17, 20, 21]. However, a major challenge remains: It is difficult to achieve high compliance when hard scales are placed on the "intrados" side of the skin (i.e. inside the curvature) because at large flexural deformations the scales come closer together, enter contact and can jam, causing significant stiffening in flexion [10, 11, 16, 22, 23]. This scenario is not observed in flexible skins made purely of soft tissues, for example in the skin on the palm of human hands. When the hand closes the skin undergoes flexural deformations combined with compression in the plan of the skin, because the skin is offset by ~10mm from the rotation axes of the joints. The skin can buckle and form wrinkles to accommodate deformations (Fig. 1a, [24]), which maintains large compliance even when the hand is completely closed. In contrast, we recently covered the palm of Kevlar gloves with alumina scales following a stretch and release protocol [11]. This glove is impervious to lacerations and sharp punctures, but the wearer of the glove feels a sharp stiffening as they close their hands and as the ceramic scales jam together (Fig. 1b). In this glove the scales completely suppress the wrinkling and folding

mechanisms which are so important for the overall compliance of skin (and also for the compliance of a scale-less protective glove). Is it possible to create scaled skins that can buckle and form wrinkles? This design, which would be very attractive for regions of high deformation like the palm of a glove, does not exist in synthetic systems. Interestingly however, buckling and wrinkling of scaled skins do exist in nature. Figure 3.1d and 3.1e show examples of a snake and a lizard with sections of their bodies undergoing high flexural deformations. The intrados side of the scaled skin clearly forms wrinkles to accommodate for large deformations without resistance, preventing the scales from jamming together in these regions of high compression. Can we duplicate these buckling and folding mechanisms in synthetic scaled skins? The objective of this work is to investigate how hard scales on a flexible membrane affect the buckling energy landscape, and how in certain cases the stability of buckling modes can be manipulated.

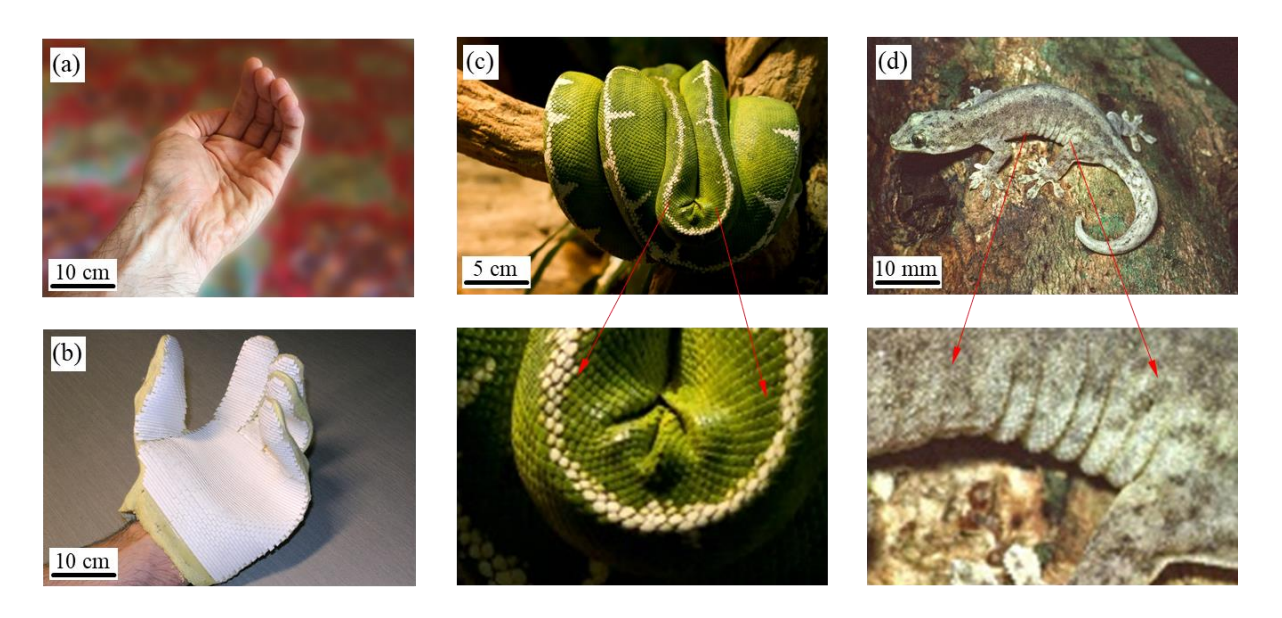


Figure 3-1: (a) Buckling / folding / flexure of skin at the palm of a hand allows for high compliance; (b) However hard ceramic scales at the palm of a Kevlar glove suppress these mechanisms: The scales jam and significant stiffening is felt when the hand is closed. Nature demonstrates that the buckling / folding of scaled skins is possible: (c) Emerald tree boa snake (*Corallus caninus*, the photo taken by William Warby [25]); (d) Christmas Island chained gecko (*Lepidodactylus listeri*, adapted from [26]).

To investigate these mechanisms we used the discrete element method (DEM), a computational efficient approach which was initially developed by Cundall and Strack for granular materials [27] and which was more recently used to model deformation and fracture in staggered composites such as enamel, nacre, Bouligand-type structures, and fish-skin-like material [16, 28-32]. For this study we applied DEM to the buckling of scaled membranes, and after validation against experiments, we examined the effect of the architecture and the arrangement of the scales on buckling response and stability of different buckling modes.

3.3 DEM model setup and validation

The objective of this work is to capture the mechanics of deformation of bioinspired scaled membranes using 2D models and experiments, focusing on the interplay between membrane deformation and scale-scale interactions. These mechanisms involve contact mechanics and large deformations, making them computationally expensive to capture with traditional modeling approach such as finite elements. As an alternative we used the discrete element method (DEM), which is much more computationally efficient for this type of problem [27]. The main assumption of this modeling approach is that the scales are rigid in comparison to the membrane on which they are attached. Each scale was therefore modeled as a discrete element with its own given geometry and three degrees of freedom (two translations and one rotation). The scales were perfectly bonded on the surface of a 2D flexible membrane which was modeled with a series of nonlinear beam elements [16]. While the scales were assumed to be rigid compared to the membrane, their elastic deformation was taken into account in the case of direct contact with other scales (more details are provided below). The membrane was modeled as a linear elastic material (modulus *E*) with second moment of area *I* (which included the effect of membrane thickness) using nonlinear co-rotational

Euler-Bernoulli beam elements which were allowed to have large rotations. To induce buckling numerically we introduced an infinitesimally small imperfection in the membrane, in the form of an initial curvature $\kappa^* = 10^{-4}$ ($\kappa^* = \kappa L_m$ where κ is the curvature of the membrane and L_m is the length of the membrane). Buckling of the membrane was produced by clamping one end while imposing a clamped-longitudinal compressive displacement $\delta_L^* = \delta_L/L_m$ onto the other end (Figure 3-2a). More details on the DEM formulation we used can be found in [16]. This nonlinear system was solved using the iterative Newton-Raphson method [16, 29]. We first present results from the DEM modeling of a plain membrane (free of scales), which we used for validation. The DEM buckling model was compared with buckling experiments on a strip of polyurethane (Young's modulus = 4.5 MPa, measured in three-point bending) with a length $L_m = 50$ mm, thickness $t_m = 1.4$ mm thick and a width $w_m = 10$ mm. These buckling experiments were conducted in displacement controlled mode on a dual column universal testing machine (ADMET, model eXpert 5000, MA US) which continuously recorded the axial force F_L as δ_L was increased at a quasi-static rate. Figure 3-2 shows two representative snapshots of these experiments and a representative F_L - δ_L curve. As expected, the initial response is linear up to a critical force F_{cr} which marks the onset of buckling. Beyond the point the increasing stresses in the membranes are offset by the geometric softening of buckling, so that the force is decreasing with displacement. The DEM model of the bare membrane is in very good agreement with the experiments in terms of initial stiffness and critical force at buckling. The forces in the buckling region are lower than in the DEM model which we attributed to imperfections in the membrane [33]. We also compared these results with Euler's theoretical critical load of a beam with identical end conditions given by [34]:

$$F_{cr} = \frac{4\pi^2 EI}{L_m^2} \tag{3.1}$$

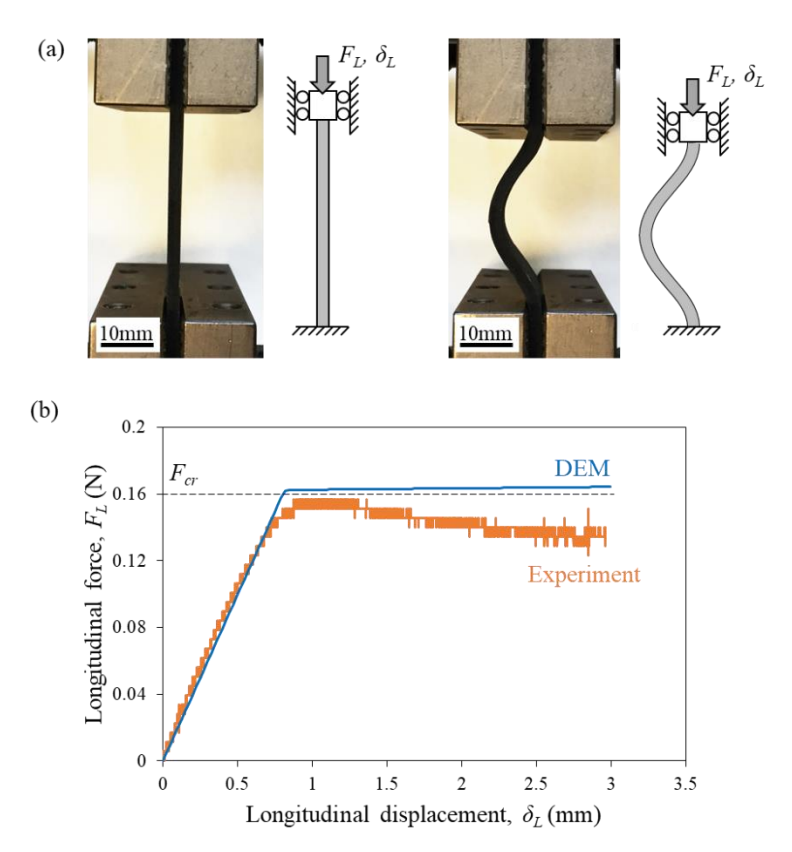


Figure 3-2: (a) Snapshots and schematics of a buckling experiment on a bare polyurethane membrane with fixed-ends conditions (no rotation); (b) Corresponding longitudinal force – longitudinal displacement curves.

Using the experimental parameters we computed a theoretical critical force $F_{cr} = 0.162$ (N) which is also in agreement with the DEM model and buckling experiments (Figure 3-2b). The next step was to develop DEM models with hard scales perfectly bonded onto the membrane (figure 3-3a). We placed N_s identical scales with normalized length L/L_m and normalized thickness t/L_m on the elastic membrane. The scales were uniformly spaced with a normalized gap distance d/L_m . These geometrical parameters are therefore related by the equation $L/L_m = (1 + (N_s+1) d/L_m)/N_s$. The thickness of the membrane was on the same order as the thickness of the scales or thinner, and therefore we assumed that the segments of the membrane which were bonded to the scales were perfectly rigid. Only the sections of the membrane which were "free-standing" between the scales were allowed to deform. In the model, the scales could also interact by direct contact. Scale-to-

scale collisions were detected using a shape intersection algorithm (Sutherland-Hodgman polygon clipping [35]) which detected whether a vertex entered the contour of the scale. When a scale-to-scale collision was detected we first established whether interaction occurred by "sharp contact" where a corner of a scale penetrates a flat edge of another scale, or by "flat contact" where the neighboring edges from contacting scales interpenetrate and make a four-sided-shape overlap (in this case, the shape intersection algorithm detects two penetrating corners). For the case of a sharp contact the penetration distance δ_p was determined as defined on Figure 3-3b. δ_p was then used to compute the contact force—using a model inspired by a Winkler elastic foundation [16, 36]. Assuming that the scales are frictionless the contact force F_{ct} for a "sharp" contact is written:

$$\frac{F_{ct}}{LwE_{ct}} = C_1 \left(\frac{\delta_p}{L}\right)^{C_2} \tag{3.2}$$

Where E_{ct} is the contact modulus, and w is the out-of-plane width of the scales. The interpenetration of the scales was a streamlined was a streamlined approach to capturing the localized deformation of the scales due to contact forces. To calibrate C_1 and C_2 we used a 2D finite element model of a sharp contact between two identical square scales (ANSYS, V16 2016, PA, US) where one of the scales was rotated by $\phi_0 = 45^\circ$ (incidence angle) from the other one. In this model one scale penetrates the other under controlled displacement [16], and the normalized resultant contact force F_{ct}/LwE_{ct} was computed as a function of the normalized penetration δ_p/L (figure 3-3d). These results were then fitted with equation (3.2) to determine the constants in model (2): $C_1 = 1.1$ and $C_2 = 0.23$. We repeated the test with different angles of incidence for the penetrating scale (figure 3-3d) and obtained almost identical values for C_1 and C_2 . An important ingredient in the scale-scale contact model is the line of action of the contact force F_{ct} , because it governs the moment generated by F_{ct} on individual scales, which in turn govern their rotation. Our

definition of the line of action for a "sharp" contact is shown on Figure 3-3b: The line of action was defined as a line perpendicular to the edge of the flat contact and intersecting the tip of the sharp contacting scale. The other contact configuration of interest is the "flat" contact, where the domain of intersection between the scales is four-sided (figure 3-3c). For this case we simply applied equation (3.2) twice to compute two contact forces (and two distinct lines of actions) generated by the normal penetration δ_{p_1} and δ_{p_2} .

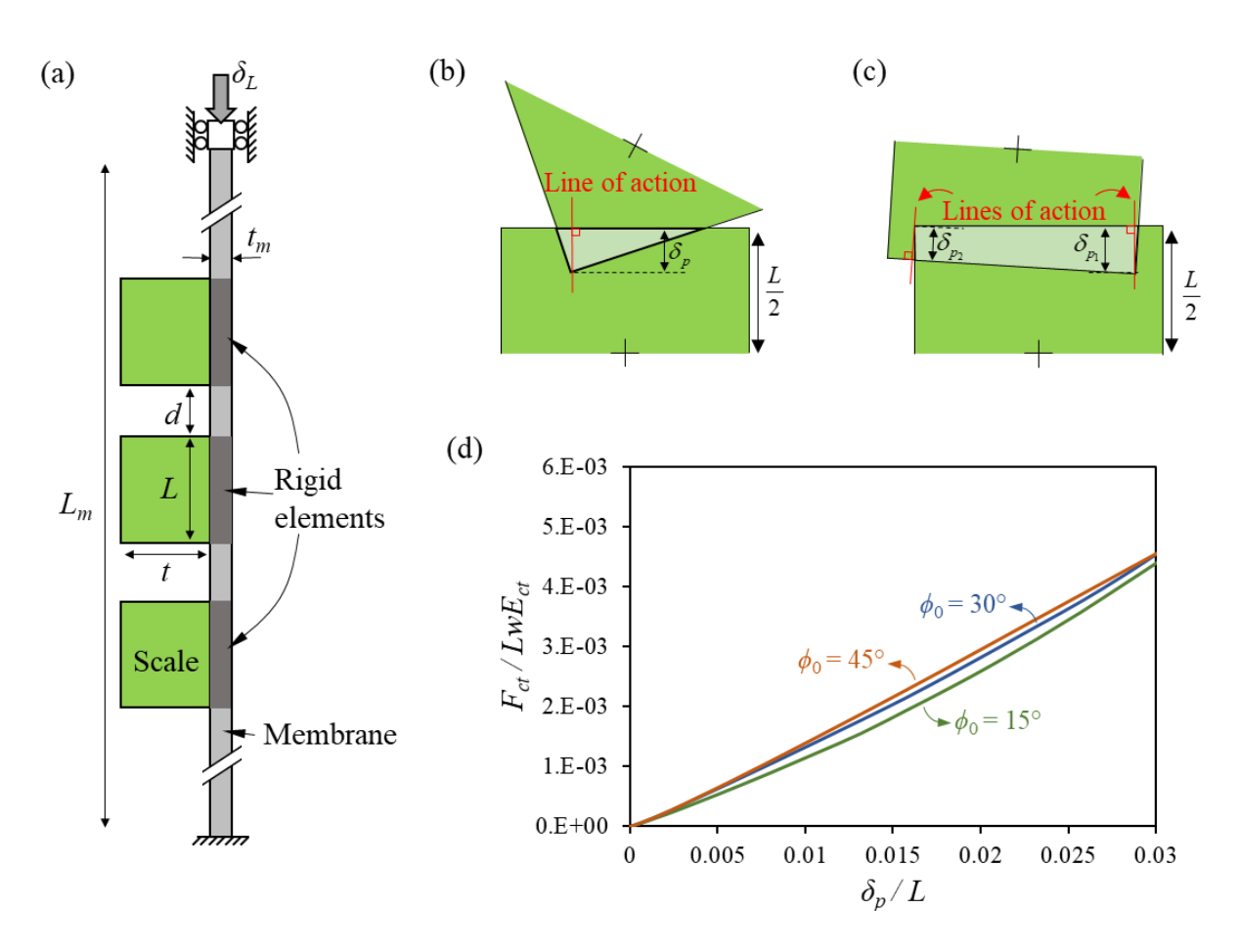


Figure 3-3: (a) DEM model of a system of hard scales bonded onto a soft membrane with fixed-ends conditions; Schematic showing the penetration of two scales for the case of (b) a "sharp" contact and (c) a "flat" contact. For both cases the lines of action of the contact forces are shown in red; (d) The normalized resultant contact as a function of the normalized penetration for the models with different incidence angles, which was used to obtain the constants C_1 and C_2 .

For validation, we compared a full DEM model of the scaled membrane (including contacts) with experiments. Buckling experiments were performed on a strip of polyurethane covered with scales. The scale dimensions were t = 2.5 mm, L = 7.75 mm, w = 10 mm and were 3D printed with a high resolution Direct Light Projector (DLP) 3D printer (EnvisionTech Micro HiRes) which produced fully dense, isotropic and pore-free scales with a Young's modulus of 3 GPa (measured experimentally [16]). The scales were then glued onto the surface of the membrane using cyanoacrylate and with a gap distance of d=0.5mm. The scaled membrane was placed into a loading machine and buckled following the same protocol as for the bare membrane. Since the scales were only attached to one side of the membrane, the system was not symmetric and there were two asymmetric mode I buckling. Following a terminology we previously used to characterize the flexural response of scaled membrane [11], we defined the "mode I-extrados" buckling as the buckling configuration where the scales, placed on the "extrados" side of the bent membrane, move apart as bending deformations increase (figure 3-4a). We defined the "mode Iintrados" buckling as the buckling configuration where the scales, placed on the "intrados" side of the bent membrane, move closer together and may enter contact as bending increases (figure 3-4b). To steer the experiments into either of the mode I-extrados or -intrados, we imposed a small pre-curvature ($\kappa \approx 0.0005$) to the system. Figure 3-4c shows the experimental F_L - δ_L curves for mode I-intrados and mode I-extrados buckling modes, together with the results from the bare membrane for comparison. As expected the scales made the membrane significantly stiffer, which also increased the critical buckling force by a factor of ~3. The effect of the scales on the initial stiffness and critical force was identical for the two buckling modes, and the two buckling responses were identical until the scales entered contact. For the mode I-extrados, the scales moved away from one another and the deformation mechanism was unchanged until the end of the

experiment. On the other hand, for the mode I-intrados buckling mode and starting at δ_L =1.2mm the scales started to enter contact in the mode I-intrados buckling, which added significant stiffening to the buckling response. We observed a transition regime where the scales progressively entered contact (1.2 < δ_L < 4.2 mm), followed by an extremely stiff regime where all scales where in contact ($\delta_L > 4.2$ mm). In this particular regime, a large contact force is generated between the scales, balanced by a large tension in the membrane that predominantly acted as a tensile ligament. This "jamming" effect is what generates unwanted stiffening on bio-inspired scaled skin, for example at the palm of gloves (figure 3-1b, [11]). Another effect of contacting scales in the intrados mode is the redistribution and "equalization" of flexural deformations. Figure 3-4a and 4b show snapshots of the buckled scaled membrane well into the stiffening regime (δ_L =6 mm). Mode Iextrados shows flexural deformations which are localized at the ends and at the middle of the membrane. In contrast, the membrane in mode I-intrados shows more distributed flexural deformations, so most of the membrane forms an almost perfect arc of circle. This effect is better seen by plotting the local curvature of the membrane as function of position (Figure 3-4d), showing a near-uniform curvature along most of the membrane. The scales can therefore be used not only to stiffen the membrane and to increase the buckling critical force, but also to control the buckled geometry (in the next section we also explore how the scales can be used to manipulate the stability of the system). Finally, figure 3-4 also shows that DEM predictions are in excellent agreement with the experiments, except in the mode I-intrados stiffening where the DEM model overestimates the force (but the onsets of the transitions are captured accurately). We attributed this discrepancy with imperfections in the geometry of the 3D printed scales (imperfect, rounded corners) and their spacing. Nevertheless, the level of accuracy of the DEM model was deemed sufficient to use it as exploratory tool for the design of the scaled membranes, focusing on the postbuckling regimes.

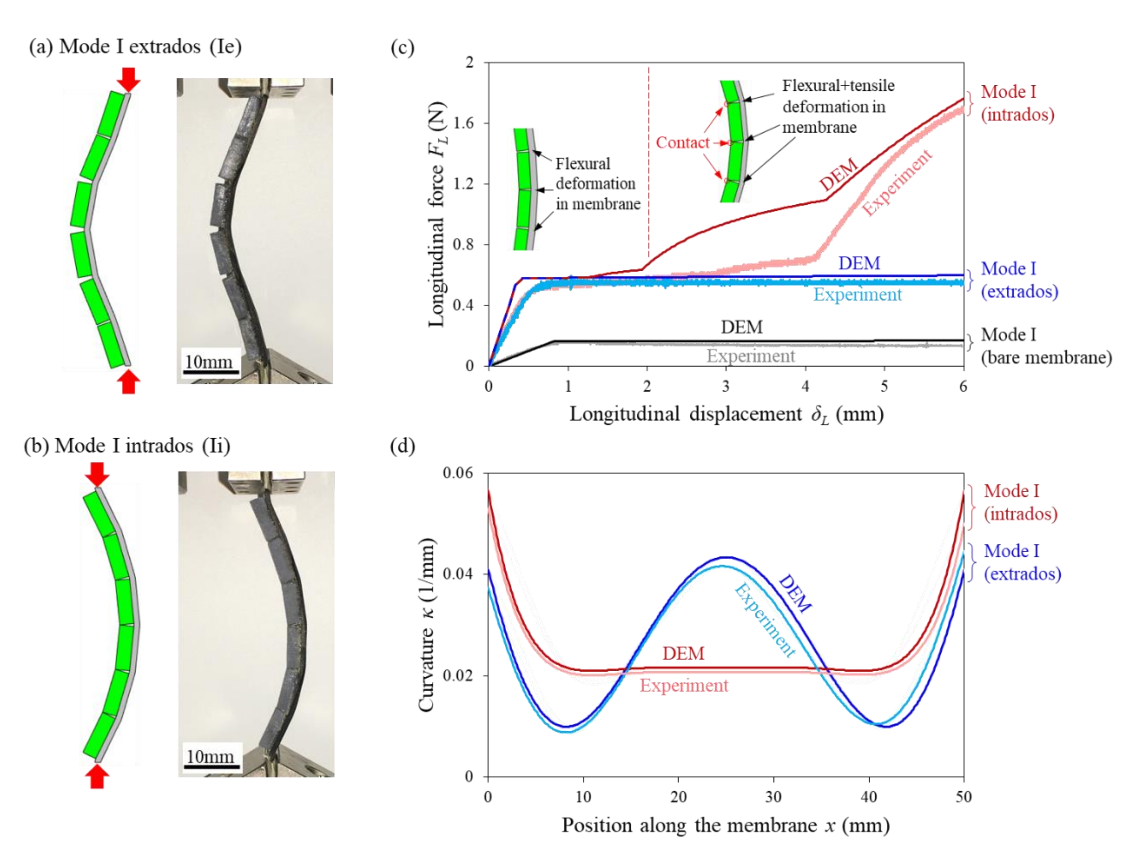


Figure 3-4: Experimental and DEM buckling test on a scaled polyurethene strip where the system buckles into (a) mode I-extrados and (b) mode I-intrados; (c) longitudinal force-longitudinal displacement curves showing a good agreement between the experimental and DEM results; (d) Curvature of the membrane as a function of the position along the membrane in the mode I-extrados and mode I-intrados configurations at loading point δ_L =6mm.

3.4 Post-buckling response

Mode I buckling is the only stable mode for a simple and uniform column or membrane in compression. Higher buckling modes exist in theory, but they are not seen in practice because they are unstable. In this study we hypothesised that the scales can be used to manipulate the stability of higher order modes. In particular, we were interested in promoting mode II buckling, which can

create wrinkles in natural scaled skin as seen in snake and lizard skins (Fig. 1). We first started by investigating the stability of a bare membrane in buckling. A buckled system tends to stay in a configuration with the lowest strain energy, therefore, the mode shapes which have a local minimum energy are stable [34]. A possible approach to assess stability is to disturb the buckled configuration with a transverse load and to examine the change in energy and force, and whether these changes induce the system to return to the stable configuration when the disturbance is removed. Here we used the DEM models to apply a transverse displacement to the buckled membrane, while monitoring total strain energy. Figure 3-5a shows a membrane subjected to a normalized longitudinal displacement of $\delta_L^* = \delta_L/L_m = 0.1$ and buckled in mode I (We kept the longitudinal displacement δ_L^* =0.1 constant for this numerical experiment). Initially the transverse defection of the midpoint is δ_T^* =-0.19 and the force F_T^* is equal to zero (figure 3-5b), and the system is in a stable equilibrium which occupies a state of minimum energy. We then imposed a transverse displacement to the mid-point of the membrane to steer the system away from that first stable equilibrium position. Figure 3-5b and 5c show the corresponding transverse force F_T^* applied at the mid-point (normalized by $F_T^* = F_T L_m^2 / EI$), and the strain energy of the membrane U^* (normalized by $U^* = U/U_0$ where U_0 is equal to the strain energy of the bare membrane in the mode I) during the transverse displacement, respectively. As the midpoint of the membrane is displaced to the right, F_T^* increases, and the system then undergoes a bifurcation at point δ_T^* =-0.18 to transition from a "C" shape to a "S" shape deformation profile. Following this transition F_T^* decreases as δ_T^* is increased further, to reach $F_T^*=0$ at $\delta_T^*=0$. This state of the membrane corresponds to mode I buckling, another equilibrium solution, which is unstable. Increasing δ_T from that point takes the system to the symmetric mode I buckling configuration, following an antisymmetric F_T^* - δ_T^* response and a symmetric U^* - δ_T^* response.

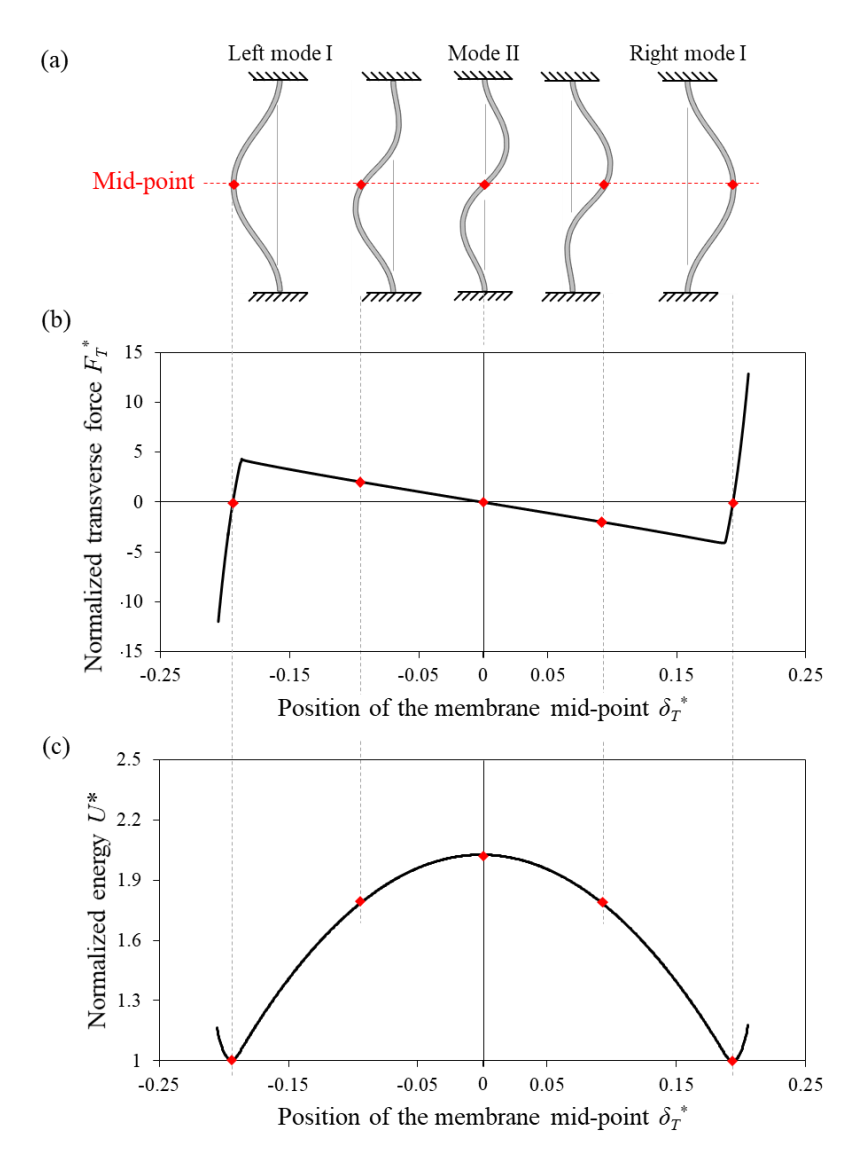


Figure 3-5: Buckling results from DEM on a bare membrane: (a) Buckling profiles, (b) force landscape and (c) strain energy landscape. To generate this plot a transverse displacement is applied to the mid-point of the membrane.

This simple approach therefore captures the main buckling characteristics of a bare membrane: by two symmetric and stable mode I buckling modes, and one unstable mode II buckling mode. In the next step, we investigated the effect of the scales in the post-buckling behaviour of the system. Figure 3-6 shows how scales bonded on the membrane (in this example the size of the scales was t/L_m =0.05 and L/L_m =0.15) can drastically change the energy landscape of buckling (if the scales are close enough). If the scales are far apart (blue line in figure 3-6) no contact is made during

buckling, and the only effect of the scales is stiffening (i.e higher strain energy in the system). If the scales are close enough (green and red lines in figure 3-6), the scales enter contact during buckling in mode I-intrados, which greatly increases the strain energy and changes the shapes in the energy curve, with a significant rise in energy on the intrados side (right side on the graph). As a result, the mode II positions are shifted to the right (but they remain unstable). We also note that the mode Ii becomes a higher energy mode compared to Ie, and that Ie is more stable (i.e. the energy barriers around Ii are steeper than around Ie). Reducing the gap between the scales (which adds more scales on the membrane) accentuates these effects.

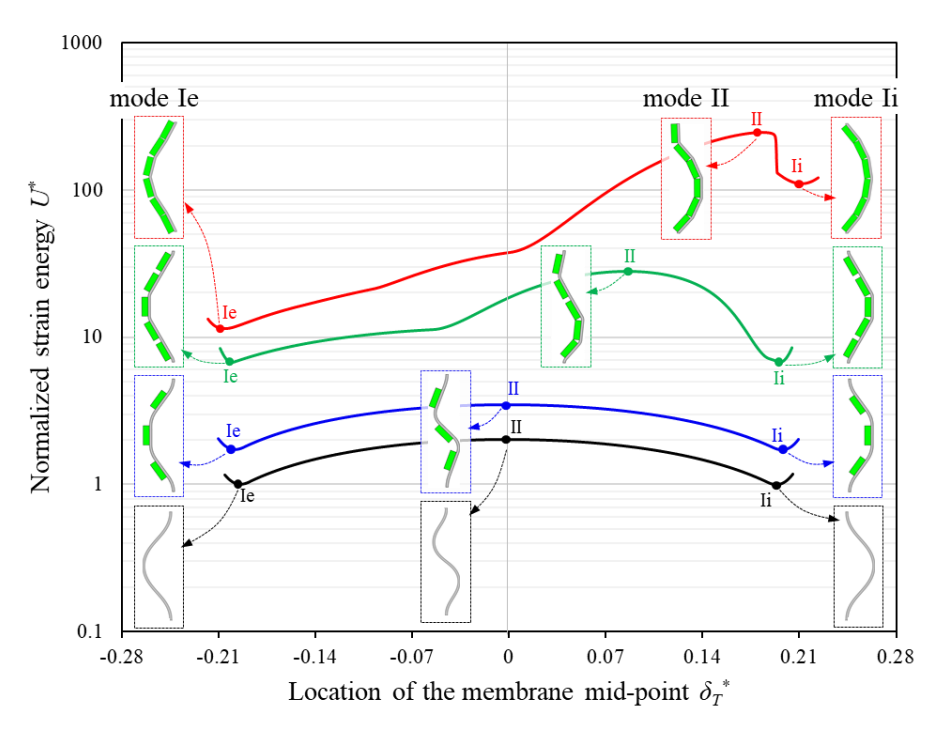
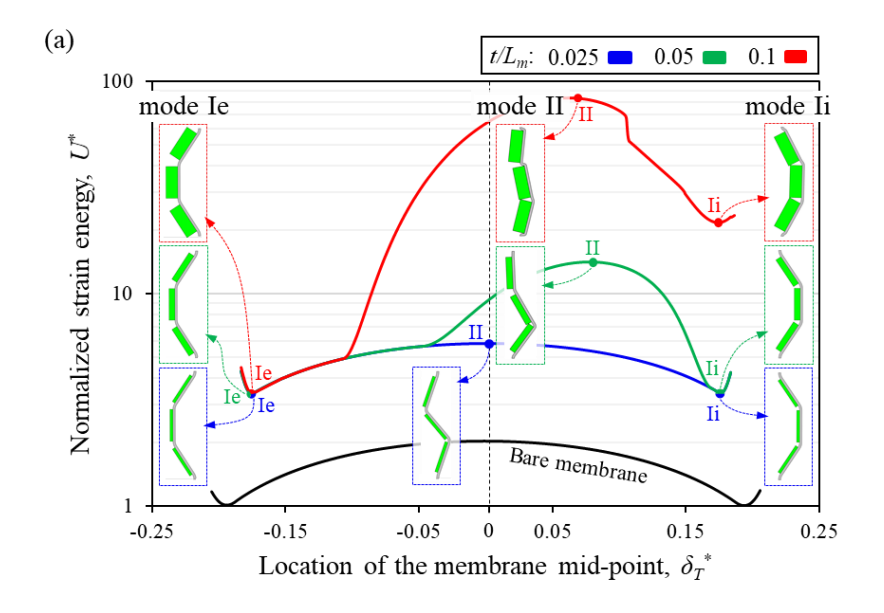


Figure 3-6: Buckling energy landscape for a bare membrane and a membrane uniformly covered by three, five and six scales with fixed sizes of $t/L_m = 0.05$ and $L/L_m = 0.15$.

These effects and asymmetries can also be amplified further with thicker scales and larger numbers of (shorter) scales, as shown on Figure 3-7. Figure 3-7b also shows an extreme configuration where the system is completely jammed around the mode Ie buckling configuration. In this design the scales generate so much locking with such high energy barriers that is it not possible to evolve the

system towards mode II and mode Ie buckling. We also captured this phenomenon in experiments where two different models were loaded transversely about a jammed configuration using a wire where one end was glued to the middle of the membrane and the other end was pulled horizontally to the right (figure 3-8).



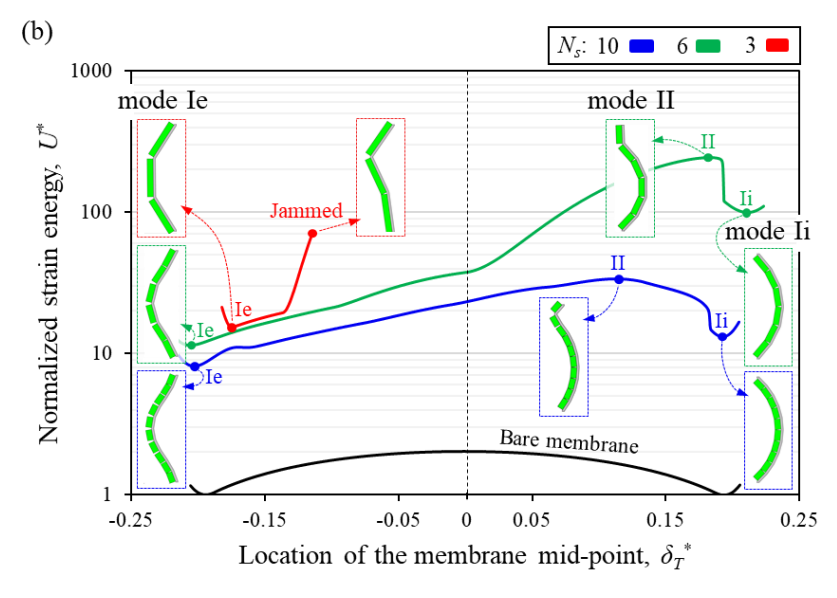


Figure 3-7: Buckling energy landscape for three different scaled membranes: (a) Varying scale thickness with a fixed gap distance of d/L_m =0.05 and scale number of N_s =3; (b) Varying number (and length) of the scales for a fixed gap distance of d/L_m =0.01 and scale thickness of t/L_m =0.05. The energy of the bare membrane is also shown for comparison.

In these experiments, the only buckling mode that could be achieved was mode Ie. Increasing the transverse force instead resulted in the delamination of the scales from the membrane or failure in the membrane itself. This type of design can be used to only trigger and promote mode Ie, while forbidding the other buckling modes entirely.

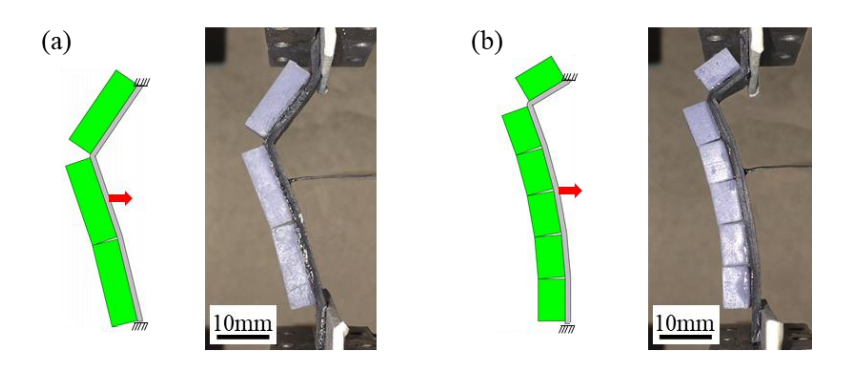


Figure 3-8: DEM and experimental results on scaled membranes in jammed configurations: with (a) t/L_m =0.1, N_s =3, d/L_m =0.01 and (b) t/L_m =0.1, N_s =6, d/L_m =0.01.

3.5 Buckling of symmetrically scaled membranes

The results above are representative of a large parametric study on scale size and spacing, and while these parameters can change the buckling energy landscape significantly, we did not identify any design that could increase the stability of mode II buckling. Additional design explorations however revealed that bonding scales on both sides of the membrane could be a powerful approach to stabilizing mode II. Figure 3-10a shows the energy landscape for membranes with scales $(t/L_m=0.04 \text{ and } d/L_m=0.05)$ bonded to either the left or the right surface of the membrane. As expected, the energy results are asymmetric and both produce higher energy on the intrados side and an unstable mode II buckling mode. Figure 3-10b shows the results of "superimposing" these two designs by bonding the same scales to both left and the right surfaces of the membrane. This

symmetric design takes advantage of the stiffening mechanism associated with contacting scales in both buckling directions, and creates a symmetric energy landscape. The most interesting feature of this design is the emergence of a mode II buckling which is stable, while also preserving the stability of the two modes I. We could validate this result experimentally, creating a scaled membrane with a stable mode II buckling mode (Figure 3-10b).

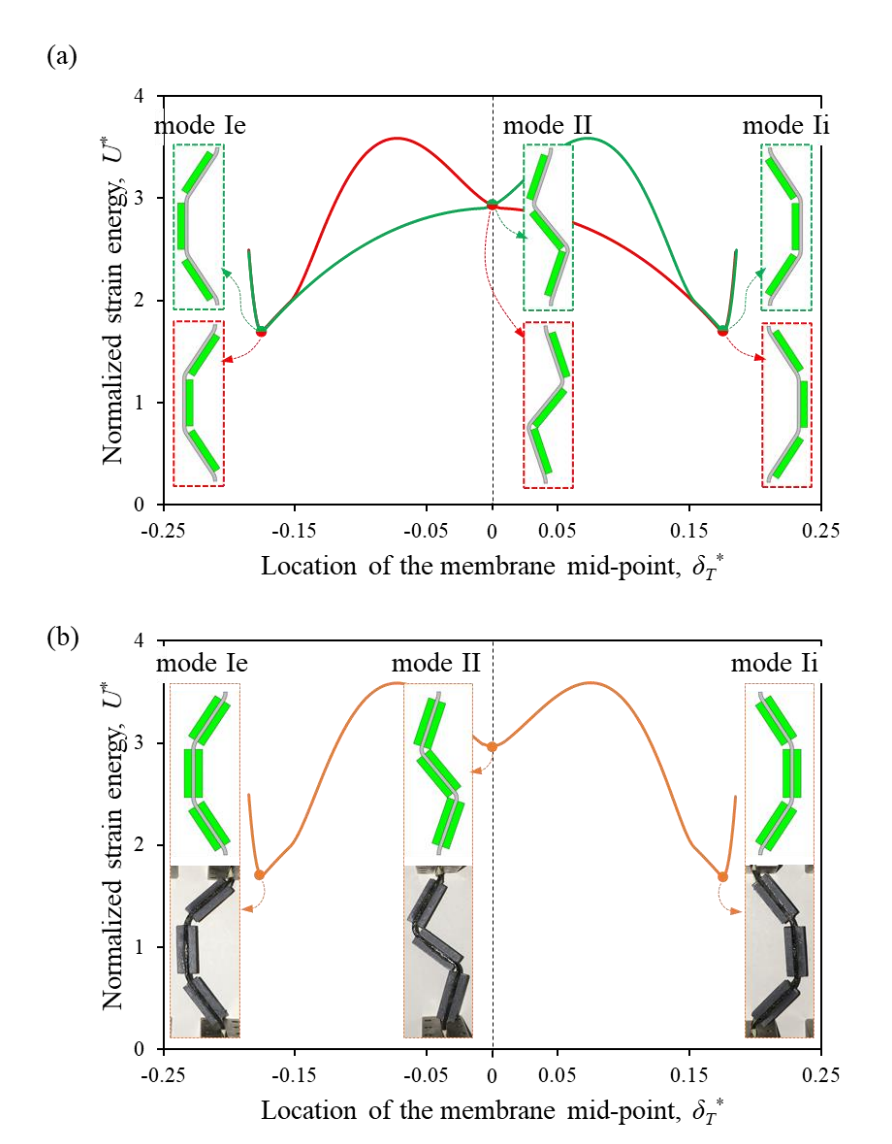


Figure 3-10: (a) Buckling energy landscape for two models symmetric from one another; (b) the two designs are combined to create a stable mode II.

In these symmetric designs, the geometrical parameters (t/L_m , d/L_m , N_s) can be adjusted to increase or decrease the stability of mode II. For example, increasing the thickness of the scale increases the stability of mode II buckling but only up to t/L_m =0.06. Increasing the thickness to t/L_m =0.09 made the maximum strain energy shift to δ_T^* =0 and, as a result, makes the mode II an unstable configuration. Figure 3-11b and 11c show how the spacing of the scales and the number of scales can be tuned to create a stable model II buckling.

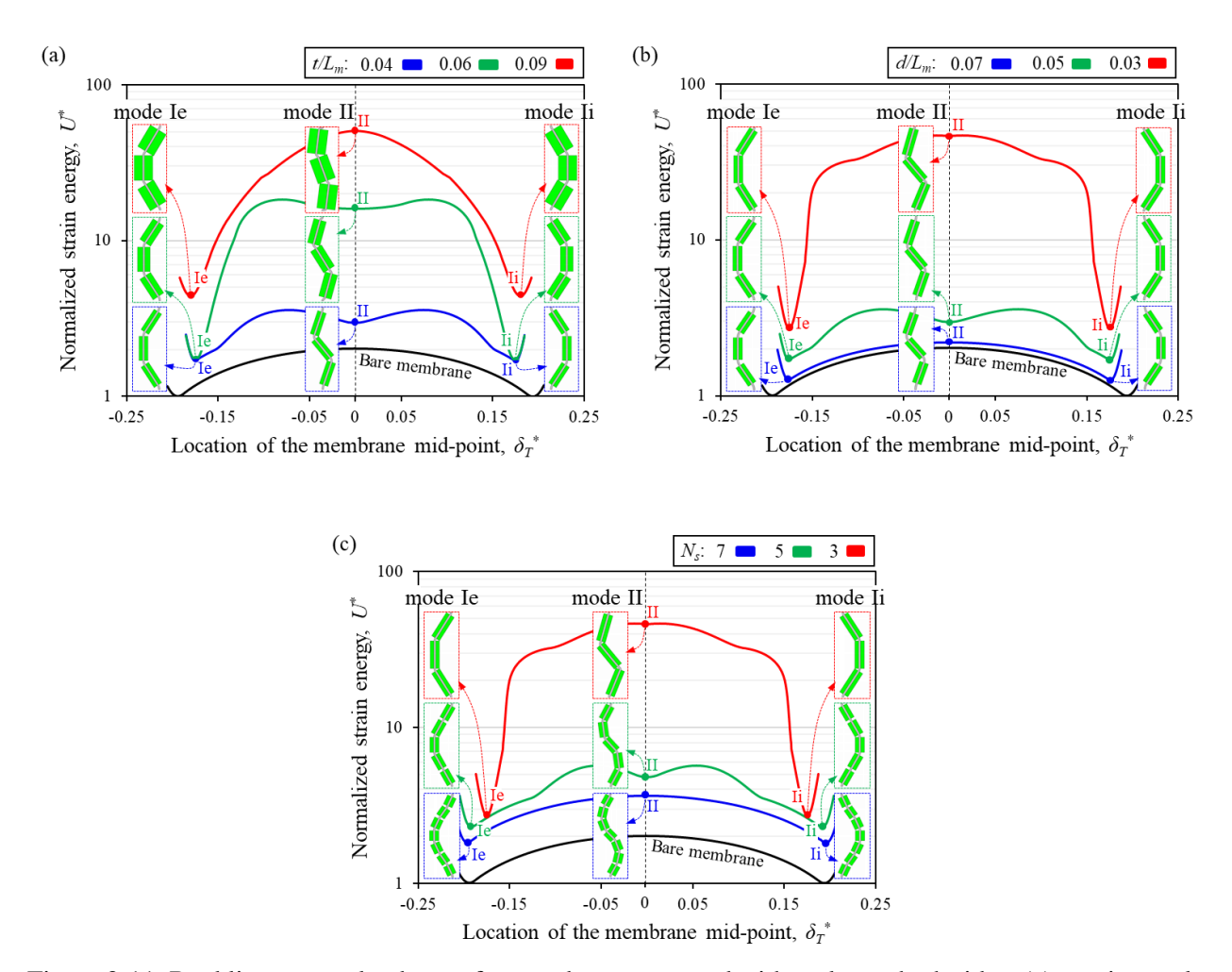


Figure 3-11: Buckling energy landscape for membranes covered with scales on both sides: (a) varying scale thickness for fixed gap distance of d/L_m =0.05 and scale number of N_s =3; (b) varying scale spacing for fixed scale thickness of t/L_m =0.04 and scale number of N_s =3; (c) varying number (and therefore length) of scales for fixed gap distance of d/L_m =0.03 and scale thickness of t/L_m =0.04.

3.6 Summary

A variety of bio-inspired scaled protective systems with useful combinations of flexibility and protection have recently been developed. However synthetic scaled skins stiffen in mode I intrados bending, which reduces the flexibility and dexterity or protective elements like gloves. Nature on the other hand displays examples of scaled skins that can buckle and form wrinkles to accommodate large deformations, a phenomenon which requires higher buckling modes. Inspired from these observations, we explored how rigid scales on a soft membrane impact the energetics of buckling and stability. The main conclusions are as follows:

- Scales increase the strain energy stored in the system by stiffening the membrane and by making direct contact.
- If the scales (bonded on one side of the membrane) are close enough to go in contact in the mode I-intrados, this mode creates a higher energy, and mode I-extrados becomes a more stable configuration.
- "Jamming" was observed in some designs. This phenomenon can be used to achieve particular buckling modes while excluding others.
- By adding scales onto both faces of a membrane and creating symmetric design, we could create and manipulate a stable buckling mode II.

Greater control of buckling in bio-inspired scaled membrane should lead to better designs of synthetic scale-covered systems. This study provides a strong basis for future designs that guide scaled membrane into specific buckling mode configurations by judicious design and arrangement of rigid protective scales. In particular, the creation of stable mode II buckling configurations can induce wrinkles and folds which can increase the overall flexural compliance and agility of bioinspired protective elements. A prime application of these mechanisms is therefore flexible

protection, but there could be other applications in foldable structures or metamaterials where high control and programmability over buckling is desirable. The models we presented here (DEM and 3D printed) are highly idealized and relatively far from natural scaled skin. There are however many obstacles to overcome before a comparison between our model and natural scaled skin can be successful: Non-linearities and anisotropies in biological tissues, effect of hydration, rate effects, and last for not least 3D effects. The current model presented here is simplified, but it can nevertheless guide the design of synthetic scales. In addition the design space for scaled skin is vast, and in this study we only focused on 2D rectangular scales. Scales with slanted sides and which overlap, or 3D scales with more complex geometries are known to have a profound impacts on scale-scale interactions and on overall mechanical properties [2-4, 37]. It is also highly probable that buckling is also affect by these additional geometrical features. Further work is needed to examine how enriching the geometry of the scales can be used to access additional buckling modes. These designs may also include non-uniform scales to generate localized deformation mechanisms or to adapt to specific combinations of deformation and constraints [38]. In addition, in this study we only considered perfectly bonded scales and smooth and continuous membranes in this study. In the future, designing and dispersing imperfections in the membrane or incorporating partially debonded scales could be combined to the design of scales for additional tunability of material response [39].

3.7 Acknowledgments

This work was supported by a Discovery Grant from the Natural Sciences and Engineering Research Council of Canada. A.S. was partially supported by a McGill Engineering Doctoral Award.

3.8 References

- 1. Barthelat, F., *Architectured materials in engineering and biology: fabrication, structure, mechanics and performance.* International Materials Reviews, 2015. **60**(8): p. 413-430.
- 2. Martini, R., Y. Balit, and F. Barthelat, *A comparative study of bio-inspired protective scales using 3D printing and mechanical testing.* Acta Biomaterialia, 2017. **55**: p. 360-372.
- 3. Yang, W., et al., *Natural Flexible Dermal Armor*. Advanced Materials, 2013. **25**(1): p. 31-48.
- 4. Vernerey, F.J. and F. Barthelat, *On the mechanics of fishscale structures*. International Journal of Solids and Structures, 2010. **47**(17): p. 2268-2275.
- 5. Mirkhalaf, M., T. Zhou, and F. Barthelat, *Simultaneous improvements of strength and toughness in topologically interlocked ceramics*. Proceedings of the National Academy of Sciences, 2018. **115**(37): p. 9128-9133.
- 6. Ghods, S., et al., *Designed for resistance to puncture: The dynamic response of fish scales.*Journal of the Mechanical Behavior of Biomedical Materials, 2019. **90**: p. 451-459.
- 7. Zhu, D., et al., *Structure and Mechanical Performance of a "Modern" Fish Scale*. Advanced Engineering Materials, 2012. **14**(4): p. B185-B194.
- 8. Garrano, A.M.C., et al., *On the mechanical behavior of scales from Cyprinus carpio.* Journal of the Mechanical Behavior of Biomedical Materials, 2012. **7**: p. 17-29.
- 9. Meyers, M.A., et al., *Battle in the Amazon: Arapaima versus Piranha*. Advanced Engineering Materials, 2012. **14**(5): p. B279-B288.
- 10. Funk, N., et al., *Bioinspired Fabrication and Characterization of a Synthetic Fish Skin for the Protection of Soft Materials*. ACS Applied Materials & Interfaces, 2015. **7**(10): p. 5972-5983.
- 11. Martini, R. and F. Barthelat, *Stretch-and-release fabrication, testing and optimization of a flexible ceramic armor inspired from fish scales.* Bioinspiration & Biomimetics, 2016. **11**(6): p. 066001.
- 12. Porter, M.M., et al., 3D-printing and mechanics of bio-inspired articulated and multi-material structures. Journal of the Mechanical Behavior of Biomedical Materials, 2017. 73: p. 114-126.
- 13. Martini, R. and F. Barthelat, *Stability of hard plates on soft substrates and application to the design of bioinspired segmented armor*. Journal of the Mechanics and Physics of Solids, 2016. **92**: p. 195-209.
- 14. Chintapalli, R.K., et al., Fabrication, testing and modeling of a new flexible armor inspired from natural fish scales and osteoderms. Bioinspiration & Biomimetics, 2014. **9**(3): p. 036005.
- 15. Vernerey, F.J. and F. Barthelat, *Skin and scales of teleost fish: Simple structure but high performance and multiple functions.* Journal of the Mechanics and Physics of Solids, 2014. **68**: p. 66-76.
- 16. Shafiei, A., et al., *The very hard and the very soft: Modeling bio-inspired scaled skins using the discrete element method.* Journal of the Mechanics and Physics of Solids, 2020: p. 104176.
- 17. Rudykh, S., C. Ortiz, and M.C. Boyce, *Flexibility and protection by design: imbricated hybrid microstructures of bio-inspired armor*. Soft Matter, 2015. **11**(13): p. 2547-2554.

- 18. Rudykh, S. and M.C. Boyce, Analysis of elasmoid fish imbricated layered scale-tissue systems and their bio-inspired analogues at finite strains and bending. Ima Journal of Applied Mathematics, 2014. **79**(5): p. 830-847.
- 19. Tatari, M., et al., *Bending behavior of biomimetic scale covered beam with tunable stiffness scales.* Scientific Reports, 2020. **10**(1): p. 8.
- 20. Yang, W., et al., Flexible Dermal Armor in Nature. JOM, 2012. **64**(4): p. 475-485.
- 21. Ali, H., H. Ebrahimi, and R. Ghosh, *Bending of biomimetic scale covered beams under discrete non-periodic engagement*. International Journal of Solids and Structures, 2019. **166**: p. 22-31.
- 22. Ghosh, R., H. Ebrahimi, and A. Vaziri, *Contact kinematics of biomimetic scales*. Applied Physics Letters, 2014. **105**(23).
- 23. Ghosh, R., H. Ebrahimi, and A. Vaziri, *Non-ideal effects in bending response of soft substrates covered with biomimetic scales.* Journal of the Mechanical Behavior of Biomedical Materials, 2017. **72**: p. 1-5.
- 24. Wang, Q.M. and X.H. Zhao, Beyond wrinkles: Multimodal surface instabilities for multifunctional patterning. Mrs Bulletin, 2016. **41**(2): p. 115-122.
- 25. Warby, W. *Emerald Tree Boa Snake*. [Digital photo] 2008 [cited 2020 May 11]; Available from: https://www.flickr.com/photos/wwarby/.
- 26. Cogger, H., N.M. Mitchell, and J. Woinarski, *Lepidodactylus listeri*. 2017, The IUCN Red List of Threatened Species.
- 27. Cundall, P.A. and O.D.L. Strack, *Discrete numerical-model for granular assemblies*. Geotechnique, 1979. **29**(1): p. 47-65.
- 28. Abid, N., J.W. Pro, and F. Barthelat, *Fracture mechanics of nacre-like materials using discrete-element models: Effects of microstructure, interfaces and randomness.* Journal of the Mechanics and Physics of Solids, 2019. **124**: p. 350-365.
- 29. Abid, N., M. Mirkhalaf, and F. Barthelat, *Discrete-element modeling of nacre-like materials: Effects of random microstructures on strain localization and mechanical performance*. Journal of the Mechanics and Physics of Solids, 2018. **112**: p. 385-402.
- 30. Pro, J.W. and F. Barthelat, *Discrete element models of tooth enamel, a complex three-dimensional biological composite.* Acta Biomaterialia, 2019. **94**: p. 536-552.
- 31. Pro, J.W. and F. Barthelat, *Discrete element models of fracture in tooth enamel: Failure mode competition and statistical effects.* Journal of the Mechanics and Physics of Solids, 2020. **137**: p. 103868.
- 32. Pro, J.W. and F. Barthelat, *Is the Bouligand architecture tougher than regular cross-ply laminates? A discrete element method study.* Extreme Mechanics Letters, 2020. **41**: p. 101042.
- 33. Case, J., L. Chilver, and C.T.F. Ross, 18 Buckling of columns and beams, in Strength of Materials and Structures (Fourth Edition), J. Case, L. Chilver, and C.T.F. Ross, Editors. 1999, Butterworth-Heinemann: London. p. 424-457.
- 34. Timoshenko, S. and J.M. Gere, *Theory of elastic stability*. 2009, Dover Publications: Mineola, N.Y.
- 35. Sutherland, I.E. and G.W. Hodgman, *Reentrant polygon clipping*. Commun. ACM, 1974. **17**(1): p. 32–42.
- 36. Johnson, K.L., *Contact mechanics*. 1987: Cambridge university press.

- 37. Varshney, S., et al., *Morphometric structural diversity of a natural armor assembly investigated by 2D continuum strain analysis*. Journal of Structural Biology, 2015. **192**(3): p. 487-499.
- 38. Connors, M., et al., *Bioinspired design of flexible armor based on chiton scales*. Nature Communications, 2019. **10**(1): p. 5413.
- 39. Budiansky, B. and J.W. Hutchinson. *Dynamic buckling of imperfection-sensitive structures*. 1966. Berlin, Heidelberg: Springer Berlin Heidelberg.

Link between chapter 3 and chapter 4

In previous chapters (chapter 2 and chapter 3), we developed a 2D DEM model and explored the puncture and flexural mechanics of fish-skin-like systems. We studied the effect of the aspect ratio of the scales, the scale slant angle and the gap distance between the scales on the mechanical performance of the system (puncture resistance and flexural compliance). These chapters provided some helpful insights into the mechanics of scale-covered scales, however, some aspects cannot be examined using a 2D model such as the effect of the scales base shape. In the upcoming chapter, we made a 3D DEM model using ABAQUS/CAE to study the 3D mechanics of fish-skin-like systems. We investigated the effect of the geometries (base shape and slant angle) and the arrangement of the scales on the puncture resistance and the flexural compliance.

Chapter 4

3D mechanics of scaled membranes

Chapter 4: 3D mechanics of scaled membranes

Ali Shafiei¹ and François Barthelat^{1,2}*

4.1 Abstract

Scale-covered skins are excellent examples of natural flexible protective systems. With segmented hard scales bonded or embedded onto a deformable skin, these natural structures provide useful combinations of puncture resistance and flexural compliance. The interaction of the scales with the substrate and the scales themselves is the key to such high-performance systems. In this work we investigate the 3D mechanics of puncture and flexion for a range of designs for scale-covered systems, using validated discrete element models (DEM) of the scales. The scales are orders of magnitude harder and stiffer than the substrate, so that they can be considered rigid for the purpose of mechanical modeling. Our main findings are that scales with no slant angles positioned in arrays increase puncture resistance compared to isolated scales, but only by way of interactions through the substrate and with much less extent by direct contact between scale. Direct scale-scale interaction can however be much improved by slanting the scales which we also examined in this work. We also examined the in-plane kinematics of scales, and identified interlocking mechanisms between rows of scales that further increase toughness. Dart- and hexagon-shape scales combined all these mechanisms in the most effective way among the designs we explored here. This study provides new insights into the effect of the base shape and the slant angle of the scales on the mechanical behavior of scale-covered systems, which in turn can help in the design and optimization of improved protective systems.

¹ Department of Mechanical Engineering, McGill University, 817 Sherbrooke Street West, Montreal, QC H3A 2K6, Canada

² Department of Mechanical Engineering, University of Colorado, 427 UCB, 1111 Engineering Dr, Boulder, CO 80309, United States

^{*} Correspondence to: francois.barthelat@colorado.edu

Key words: Bioinspiration, 3D discrete element method, segmented hard material, puncture resistance, flexural compliance

4.2 Introduction

Natural materials often combine very hard and very soft components, in specific architectures that generate outstanding mechanical performance [1-5]. For example the skin of fish, armadillos or crocodiles consist of discrete hard scales which are orders of magnitude stiffer than the surrounding tissues and bare skin [4, 6, 7]. This specific construction enables high surface hardness and protection, while minimizing hindrance and enabling agile locomotion [4, 8-10]. Individual scales can also interact with each other by direct contact, which increases puncture resistance [8, 11, 12]. In fish skin, the scales are slanted and have overlaps which promote scale-scale interactions [13-15]. These contacts promote the distribution of highly localized puncture forces over wider areas, which can prevent blunt trauma to underlying tissue [16-19]. The construction and mechanics of fish scales and other dermal armors have been the focus of numerous studies on the effect of the geometry and arrangement of the scales on the mechanical performance, with a strong focus on puncture resistance and on flexural compliance, two mechanical properties which have been shown to be mutually exclusive [6, 9, 10, 12, 16, 18, 20-23]. Failure of a scaled skin may occur in one of two ways: by fracturing or puncturing individual scales, or by unstable tilting of the scales [8, 16, 24, 25]. Fracturing individual scales is delayed by the strength and toughness of individual scales, while unstable tilting can be delayed by direct contact between the scales [18, 21, 23] (in particular for configurations where scales overlap [8, 16, 23]). To this effect, experiments suggested that the shape and the arrangement of the scales had a significant effect on the puncture resistance and flexural compliance of the system [8, 21, 22, 25]. Experimental studies on 3D designs are however limited in terms of the geometries explored, so that the effect of the

shapes and the arrangement of the scales on the mechanical behaviour of the system is not fully understood yet. The interaction of the scales in 3D may also be captured with numerical models, but typical method such as finite elements require a large number of contact elements and a multitude of contact pairs which are computationally expensive and which can even prevent numerical convergence [23, 29, 30]. In this study we used instead the discrete element method (DEM) where we considered the scales as three dimensional rigid blocks and replaced the substrate with springs which connect the scales together and to the ground [23, 31-34]. After validating with experiments, we investigated the mechanical behaviour of scale-covered system with a variety of scale shapes and arrangements.

4.3 Modeling and validation

For this study, we investigated the puncture resistance of a 3D model of identical hard scales fully bonded onto a soft substrate which was modeled as a linear elastic half-space (Young's modulus E_s , Poisson's ratio v_s). We first modeled some of the configurations examined experimentally in our previous study [21]: Slanted square scales arranged in a square array and with overlap generated by the slandered sides of the scales (figure 4-1). Each scale was constructed from a square base with the size $2L \times 2L$, extruded in the out-of-plane direction by a thickness t and following a slant angle α_0 towards the x-direction. The scales were arranged in a square array with a uniform gap distance d (figure 4-1). To fully cover the substrate with the scales we assumed the gap distance to be very small compared to the sizes of the scales (d/L=0.005, to avoid convergence issues one must have d > 0). The objective was to model stiff scales, which are several orders of magnitude stiffer than the substrate, and therefore the scales were modeled as rigid blocks [7, 23].

The sharp puncture experiment on the scaled system was duplicated in the model by applying a vertical displacement into the center of central scale in the model (red arrow in figure 4-1).

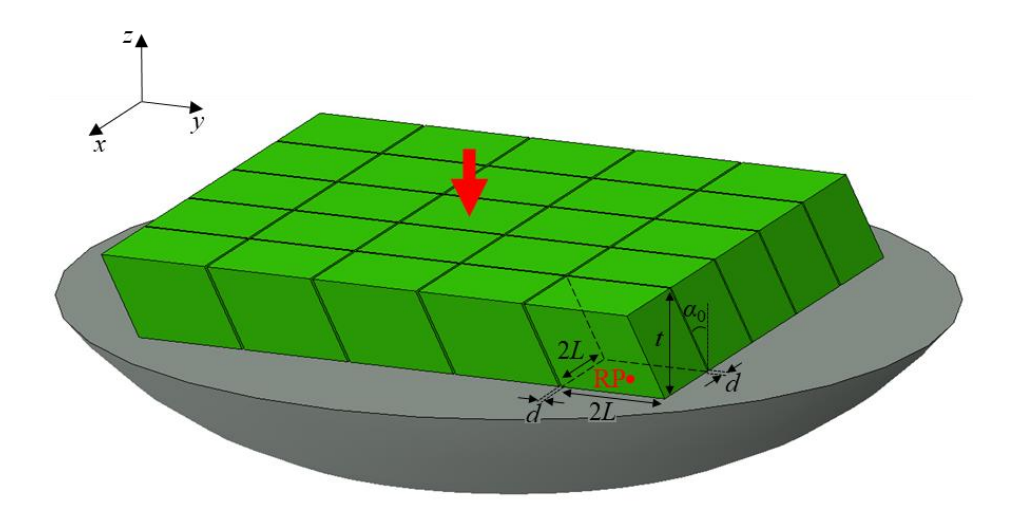


Figure 4-1: Typical system considered in this study: 5 x5 Array of hard scales bonded to a soft substrate and subjected to puncture. Key dimensions for individual scales are shown.

We used the 3D discrete element modeling capability of ABAQUS/CAE to capture the puncture mechanics of this system. Individual scales consisted of six faces where each face was made of a 4-node discrete rigid element R3D4. The displacement and rotations of the six face elements were defined in relation to a reference framework centered on a reference point associated with each scale which we placed at the centroid of the basal face of the scale (point RP on figure 4-1). The reference points were given five degrees of freedom: translation in *x*-, *y*-, *z*-directions, and rotation about the *x*- and *y*-axes. Since experiments mainly showed scale rotations about the *x*- and *y*-axes and negligible rotation about the *z*-axis (out of plane axis), that rotation was maintained to zero during the simulations to facilitate numerical convergence. To apply puncture forces to individual scales, a node was created on the top surface of the punctured scale as the loading point. A rigid connector then was defined between the loading point and the reference point of the scale, and a controlled vertical displacement was applied to the loading point (red arrow in figure 4-1). Through

the rigid connector, the applied displacement and the resulting force were transferred to the reference point of the punctured scale. The model captured the interaction of individual scales with the substrate with a system of linear springs (figure 4-2). Some of the springs captured the elastic interaction of individual scales with the substrate, and other captured the elastic interactions of each scale with its neighbors through the substrates. The scales indeed can interact through the substrate, for example pressing a scale into the substrate scale will also displace neighboring scales to some extent, depending on the separation distance between the scale and depending on the elasticity of the substrate. The system of springs was set as follows: The reference point of each scale was connected to the ground (a reference plane "far below" the surface of the substrate) by two-node connector element CONN3D2 with extensional and rotational stiffness coefficients K_{0x} , K_{0y} , K_{0z} , $K_{0\phi x}$ and $K_{0\phi y}$. Neighbouring scales were connected by their reference points by a twonode connector element CONN3D2 with "interaction" stiffness coefficients K_{1x} , K_{1y} , K_{1z} , $K_{1\phi x}$ and $K_{1\phi_{\gamma}}$. We then calibrate the stiffness coefficients using Boussinesq's and Cerruti's closed-form solutions for point forces on an elastic half-space [23, 35, 36]. For example, to obtain the coefficients K_{1x} and K_{0x} , we applied a tangential displacement u_x to the central scale while keeping all other scales immobile. The distributed shear load $q_x(\zeta, \gamma)$ on the surface of the substrate underneath the scales in x-direction was computed using [23]:

$$u_{x} = \frac{1 + v_{s}}{\pi E_{s}} \iint q_{x}(\zeta, \gamma) \left[\frac{1 - v_{s}}{\sqrt{(x - \zeta)^{2} + (z - \gamma)^{2}}} + \frac{v_{s}(x - \zeta)^{2}}{\sqrt{((x - \zeta)^{2} + (z - \gamma)^{2})^{3}}} \right] d\zeta d\gamma$$
(4.1)

We then integrated the shear load $q_x(\zeta,\gamma)$ over the area of the scales to get the shear force, which divided by the applied displacement of u_x produced the stiffness coefficients K_{0x} and K_{1x} . The same approach was used to calibrate K_{0y} and K_{1y} , except we applied a displacement u_y to the central scale to compute the shear load $q_y(\zeta,\gamma)$ in the y-direction. To obtain K_{0z} and K_{1z} , we imposed a normal

displacement u_z to the central scale and computed the normal distributed load $p(\zeta, \gamma)$ on the surface of the substrate underneath the scales using [23]:

$$u_z = \frac{1 - v_s^2}{\pi E_s} \iint p(\zeta, \gamma) \frac{1}{\sqrt{(x - \zeta)^2 + (z - \gamma)^2}} d\zeta d\gamma \tag{4.2}$$

We applied a rotation ϕ_x about the *x*-axis to the central scale, used equations (4.1) and (4.2) to obtain the distributed shear and normal loads $(q_y(\zeta,\gamma))$ and $p(\zeta,\gamma)$, and calculated the resultant moment for each scale [23]. We divided the moment on the central scale and on the neighbouring scales by the imposed rotations about either *x*-axis or *y*-axis to obtain the stiffness coefficients $K_{0\phi_x}$, $K_{1\phi_x}$, $K_{0\phi_y}$ and $K_{1\phi_y}$ respectively.

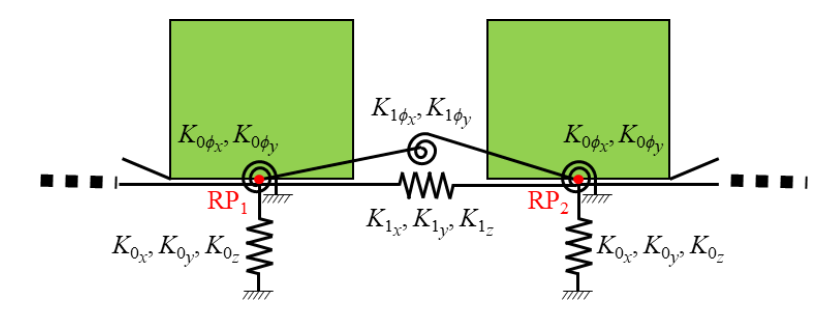


Figure 4-2: Setup of linear springs captures the interactions of individual scales with the substrate, and also the interactions between neighboring scales through the substrate.

In addition to interacting through the substrate, scales can also interact by direct contact with their neighbors. For our model we defined a frictionless contact with a linear penalty method where the contact force is proportional to the interpenetration distance between the scales. Once the model was in place and all parameters calibrated, we compared its predictions with our previous experiments [21] which consisted of a series of puncture tests on ABS scales attached onto a soft polyurethane substrate. The geometry and sizes of the scales (L = 2mm, t = 2mm and two different slant angles of $\alpha_0 = 0$ and $\alpha_0 = 63.4^{\circ}$) as well as the material properties of the substrate ($E_s = 150$ KPa) were identical to those used in the experiments [21]. In the experiments the elastic modulus

of the scales ($E_{ABS} = 3$ GPa [21]) was four orders of magnitude greater than the substrate, which indeed justified the assumption of rigid scales compared to the substrate. We considered the four different configurations shown on Figure 4-3a: An isolated scale, and three different 5×5 arrays of scales with small gap distances (d/L=0.005). Each of these models was subjected to a puncture displacement, and the corresponding reaction force was collected to generate a puncture force displacement curve (Figure 4-3b). We found good agreement between the model and the experiments in terms of puncture stiffness.

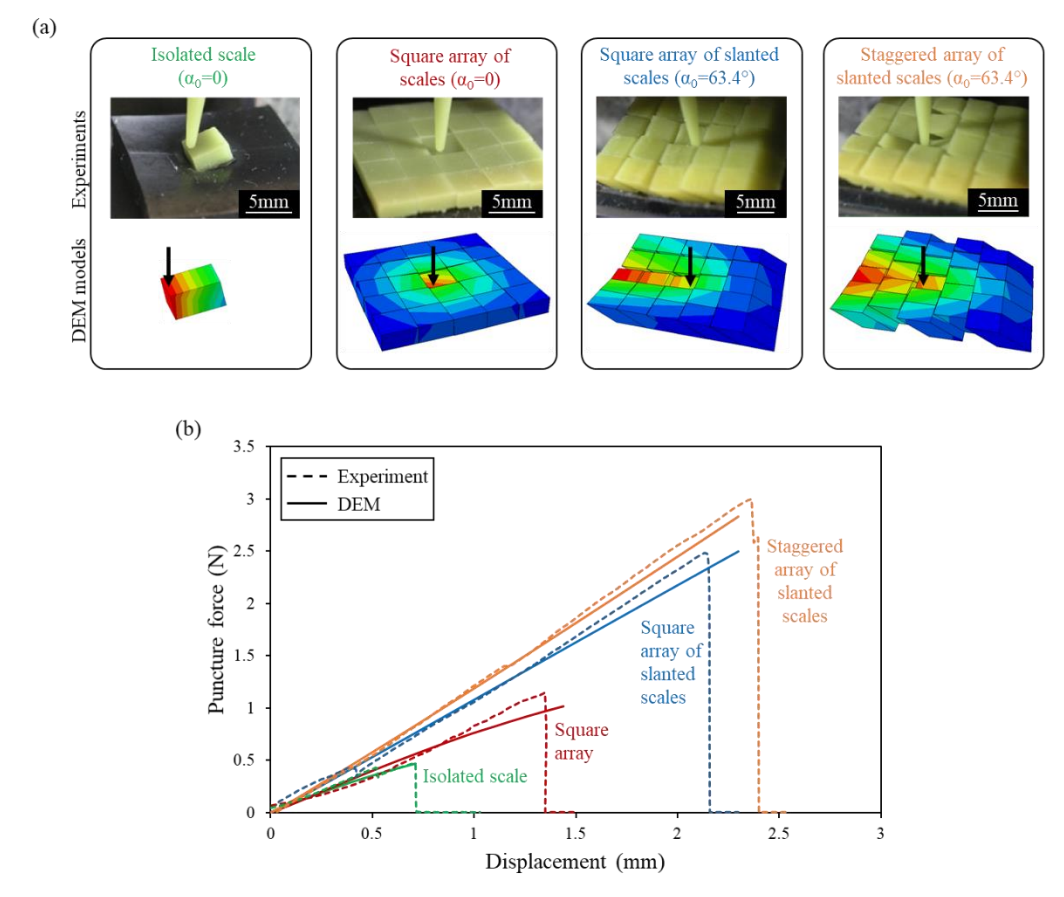


Figure 4-3: (a) Snapshots of experiments and models for a puncture test on four different designs; (b) Corresponding puncture force-displacement curves showing a good agreement between models and experiments.

The only numerical parameter we calibrated from the puncture experiments was the critical tilt angle which was defined as follows: By puncturing the top surface of the middle scale, the scale

started to tilt, and at a critical force the needle starts sliding off the scale into the substrate which is considered as a failure in the system [23]. In the experiments, this event causes a sudden drop in the puncture force on the curve (figure 4-3b). In the numerical model, failure occurs at the end point of the curve where the maximum tilting angle of the top surface of the punctured scale reaches the critical tilting angle. Our previous experiments using an ABS indenter on ABS scales [21] indicated a critical angle of $\phi_c = 13^{\circ}$ for this set of materials, a value which we therefore also used in the model.

4.4 Puncture resistance of isolated 3D scales

In the following sections of this report we used these validated models to systematically investigate the effects of the 3D scale geometry and arrangement on the response of the system. For this study we focused on scaled skins made of identical scales that were designed to cover a soft substrate entirely. Therefore we only considered scale geometries that tessellate the plane, focusing on the regular triangle, square, isosceles trapezoid, symmetric darts and regular hexagons. To isolate the effect of shape, we kept the surface area for the individual scales constant across all models. We first examined the puncture resistance of individual, isolated scales with no slant angle (figure 4-4). Our previous experiments showed that the critical force strongly depends on the location of the puncture on the surface of the scale [21]. For this study we adopted a conservative approach where for each geometry we puncture the scale at the "worst possible" location, i.e. the location leading to the least puncture resistance. This study therefore provides lower bounds for the puncture resistance of each scaled skin design. The "worst case" indentation points produce the longest moment arm δ_c of the puncture force (normalized by $\delta_c^* = \delta_c/L$) from the centroid of the scale, and they are generally located at the corners of the upper surface pf the scale (indicated by red dots on

figure 4-4). Figure 4-4 shows the puncture resistance F_c normalized by $F_c^* = F_c(1-v_s^2)/E_sL^2$ for these five geometries. Closer examination revealed that the puncture resistance is governed by two parameters: the moment arm δ_c created by the indentation force, and the rotational stiffness K_ϕ which is a function of the substrate elasticity and the scale geometry and size (normalized by $K_\phi^* = K_\phi(1-v_s^2)/E_sL^3$). The moment caused by the critical force on the punctured scale is equal to $M^* = F_c^* \times \delta_c^*$, which can also be expressed as $M^* = K_\phi^* \times \phi_c$. By combining these two equations, the puncture resistance therefore is obtained as $F_c^* = \phi_c (K_\phi^*/\delta_c^*)$ which shows that the puncture resistance is proportional to the ratio of the rotational stiffness over the moment arm. Figure 4-4 indeed shows a near-proportional relationship between K_ϕ^*/δ_c^* and puncture resistance. The dart and hexagon shapes show the highest puncture resistance.

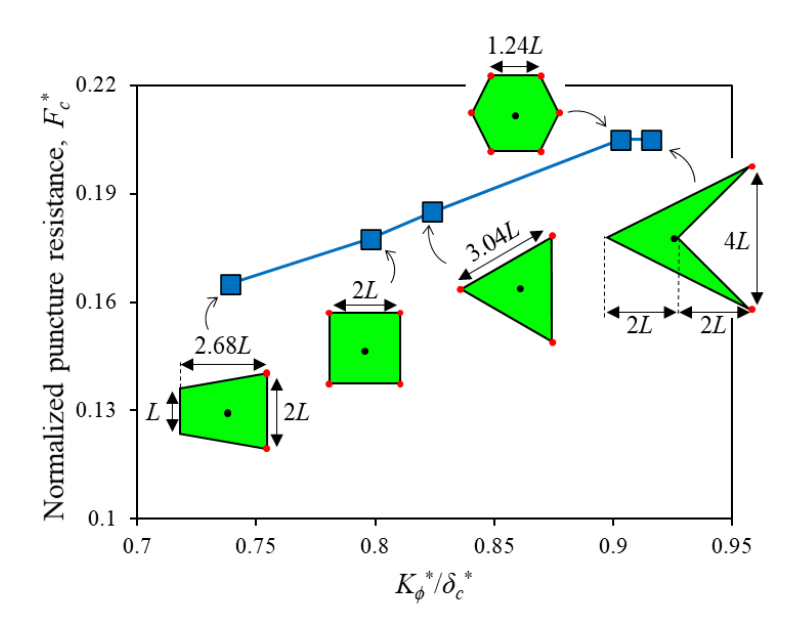


Figure 4-4: Puncture resistance of isolated scales with five different base shapes as function of rotational stiffness. All the scales have an equal base area.

4.5 Puncture resistance of arrays of scales

In the next steps, we considered the puncture resistance of arrays of scales. Figure 4-5 shows the different combinations of base shapes and arrangements which we examined. For the shapes of triangle, square and trapezoid, we considered two possible arrangements: "arrayed scales" and "staggered scales". Other shapes like the dart and the hexagon only had one possible tiling configuration. The corresponding 3D arrays of scales for these designs were created by extruding the 2D patterns along the out-of-plane direction by a distance equal to the thickness of the scales, while creating very small gaps (d/L=0.005) between the 3D scales to avoid convergence issues.

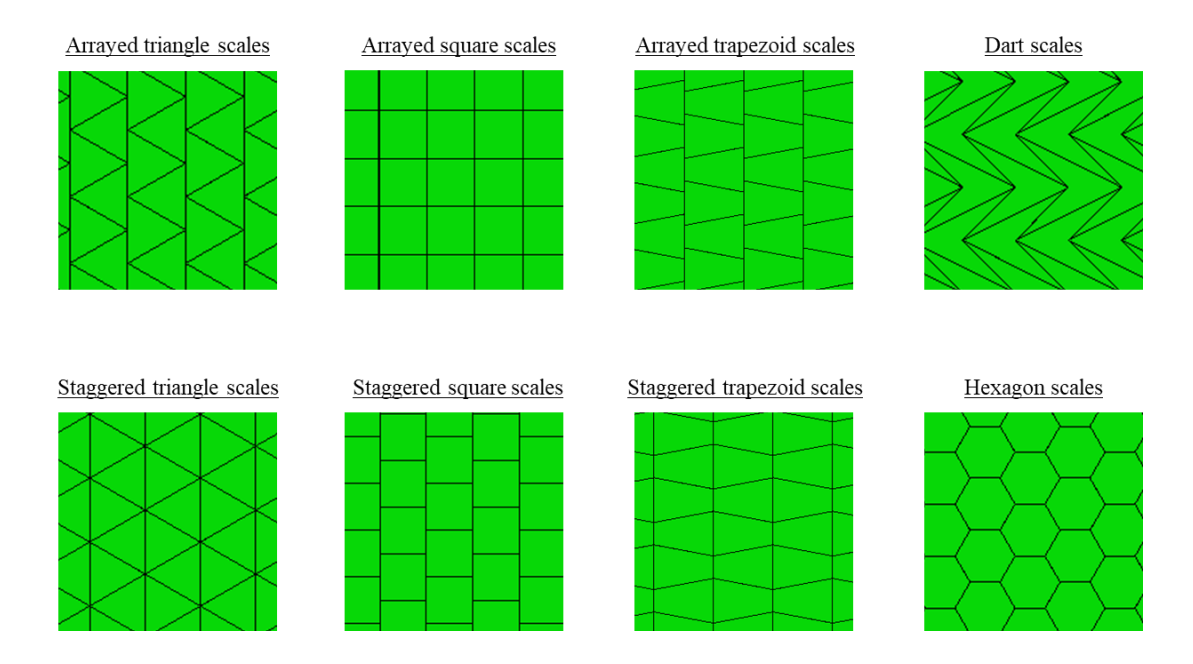


Figure 4-5: Eight designs for the base shape and arrangements we considered in this study

Figure 4-6a compares the puncture resistance of systems with different base shapes and different arrangements of scales. To emphasize the effect of scale-scale interactions, we normalized the puncture resistance of each array of scales by the puncture resistance of one isolated scale with the same geometry. As expected, the array of scales produced a significantly increased puncture

resistance compared to isolated scales, with improvements by factors of 4 to 8. The highest improvements were for the hexagonal and dart scales, which were 20-30% higher than the rest of the designs. Closer examination of the models made it evident that surrounding the indented scales with other scales stabilizes the indented scale. More specifically, the interactions of the scales by direct contact and through the substrates increase the rotational stiffness of the indented scales, with the effect of delaying tilting and increasing puncture resistance. To highlight these effects, we ran additional models where we turned off the contact algorithm, that is scale-to-scale interpenetrated without producing any contact force. The scales could still however interact elastically through the substrate. Even when direct contact was turned off, scales directly neighboring the indented scales (marked by orange dots on fig. 6a) still had a significant stabilizing effect on the indented scale, while scales further away had negligible effects. These effects were assessed by examination of the coupling stiffness for each neighboring scales, where a coupling stiffness larger than $K_{1_i}/K_{0_i} > 0.01$ was considered effective. The designs that promoted effective neighbour interactions in terms of number of interactions and configuration produced higher puncture resistances (blue columns on fig. 6a). Dart- and hexagon-shape scales were the most effective in this regard, increasing the puncture resistance by almost six times of magnitude compared to the isolated-scale models. To further establish the various contributions to puncture resistance, we ran a third set of models where this time direct scale-to-scale contact was enabled, but where the scale to scale interaction stiffness through the substrate mostly turned off (the corresponding stiffness terms were reduced to 4% of their original value, further reductions creating convergence issues). In this set of models the scales therefore mainly interacted by direct contact. Figure 4-6a (grey columns) shows that all puncture resistances in this this set of models are significantly lower than the other sets, with puncture resistance barely above the puncture

resistance of isolated scales. This indicates an important and unexpected feature of the puncture mechanism: neighboring scales stabilize the indented scale predominantly by elastic interaction

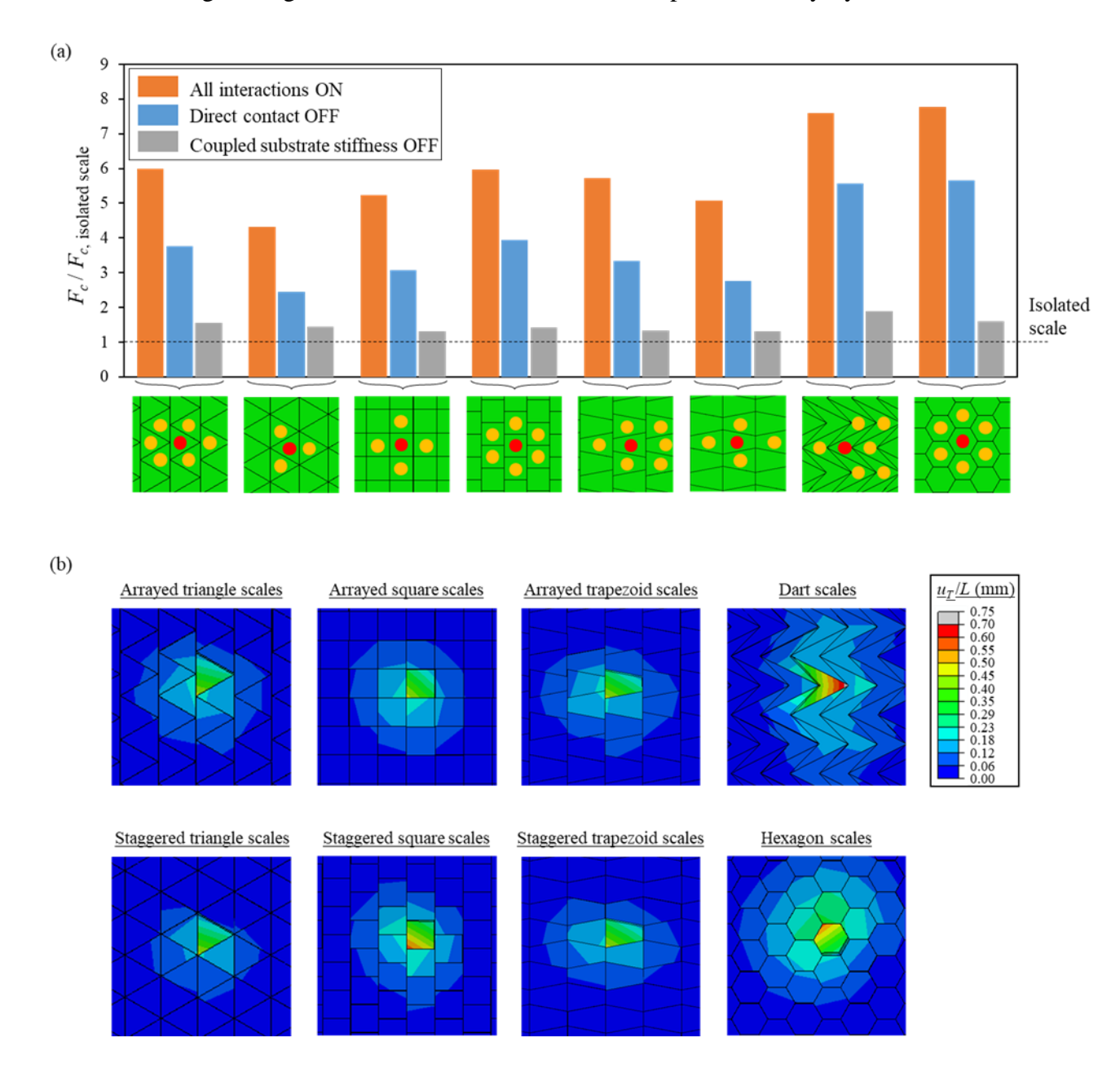


Figure 4-6: (a) Puncture resistance for eight difference scale arrays normalized by the puncture resistance of an isolated scale with the same geometry. For each design, results with full interaction and only partial interaction through substrate or through direct contact are shown. The punctured scales are marked with red dots, and the effective neighboring scales are marked by orange dots; (b) the displacement distribution in the complete model at the point where the punctured scale reached the critical tilting angle.

through the substrate, but by a much lesser extent by direct contact between the scales (at least with non-slanted sides). Finally, we note that scale-scale interactions not only delay the tilting of the indented scale, but also distributes the load over a larger area (figure 4-6b). Because mechanical interactions were more pronounced for dart- and hexagon-shape scales, the re-distribution of the puncture load over wide area was more effective for these geometries. By examining the displacements of the scales near the puncture site we identified another mechanism where the scales generate interlocking, preventing the collective motion of groups of scales in the in-plane direction. The interlocking mechanism functions differently in different in-plane directions. Figure 4-7a shows examples where in some models a row of scales in y-direction can easily slide against the neighbouring rows with no constraint from contact. On the other hand, shown in figure 4-7b, a row of scales in x-direction hinders the movement of the neighboring rows in this direction by contact (scales are interlocked). This interlocking mechanism engages a larger number of scales,

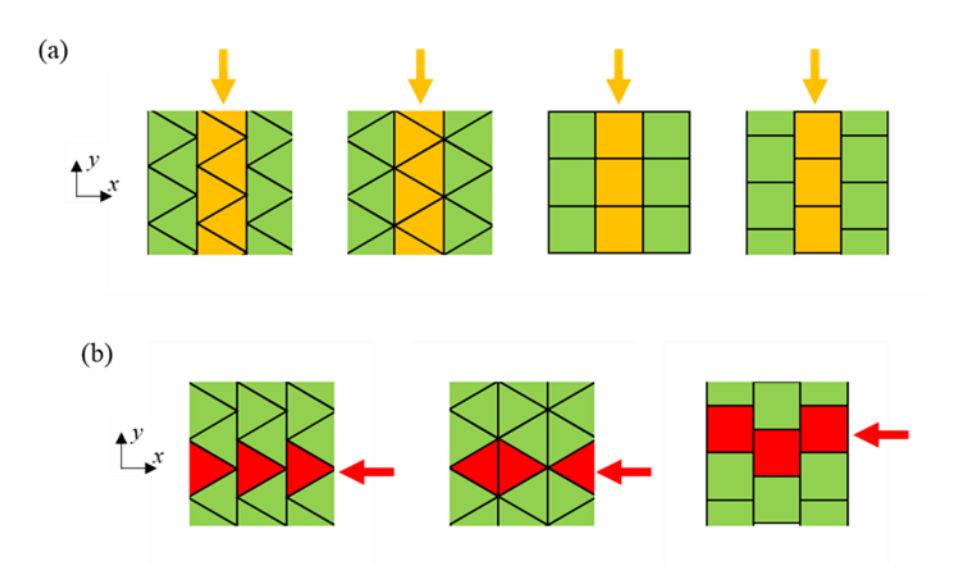


Figure 4-7: In-plane sliding of rows of scales may be (a) kinematically allowed by the shape and arrangement of the scales or (b) prevented because of interlocking.

which therefore can improve the puncture resistance of the system. In the "arrayed square scales" model, the free motion of the rows of scales is seen in both x- and y-directions, while the interlocking mechanism occurs along the diagonal (x=y) of the scale. In the "dart scales" and "hexagon scales" models, the interlocking mechanism exists in any in-plane directions, which is considered as an advantage in terms of resistance against tilting (will be discussed next).

4.6 Effects of slant angles in arrays of scales

The previous section discusses how the effects of direct contact for the case of non-slanted scales with straight sides is small, but this effect can be increased by slanting the sides of the scales. In this section we explored the mechanics of arrays of scales with a slant angle towards three possible directions (figure 4-8): a slant angle of $\alpha_0 = 60^\circ$ towards the *x*-direction, a slant angle of $\alpha_{45} = 60^\circ$ towards the diagonal (*x*=*y*) direction, and a slant angle of $\alpha_{90} = 60^\circ$ towards the *y*-direction.

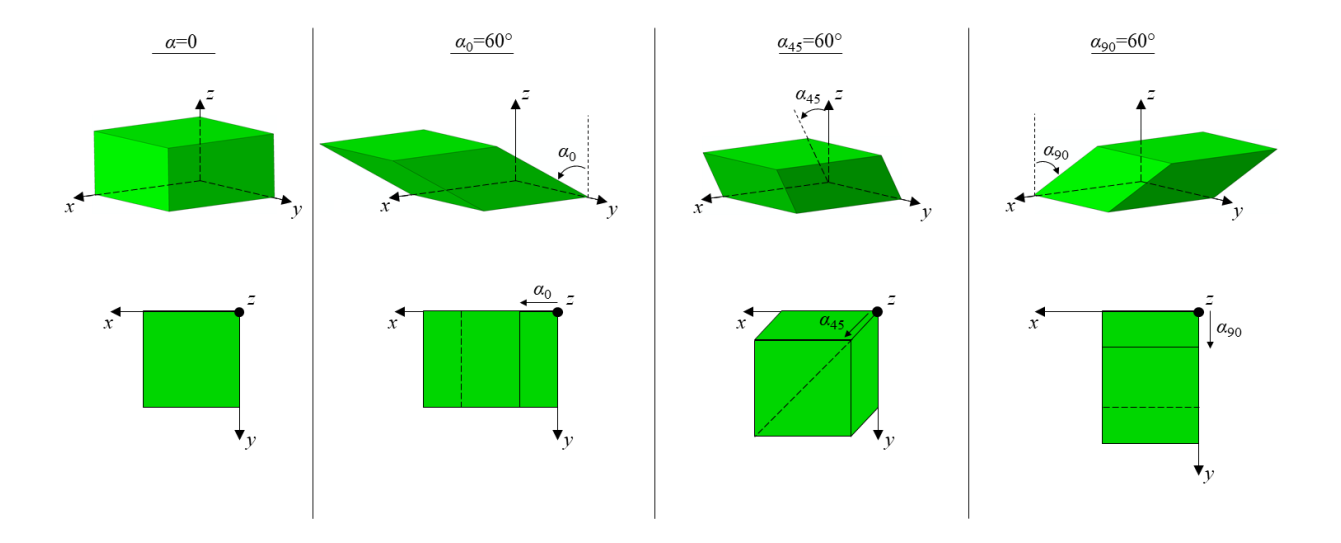


Figure 4-8: Starting from scales with straight faces, we considered 60 degree slant angles towards three different directions.

Figure 4-9a shows that slanting the scales towards any of the three directions (α_0 , α_{45} and α_{90}) roughly doubles the puncture resistance. This added stabilization effect can be explained by the slant angle changing the direction of the contact force towards the vertical direction, so this force generates a higher moment about the center of the scale. Slanted designs also result in more scales involved in the puncture mechanism through direct contact mechanism. The results show that slant angle in specific directions are more effective than others. Giving a slant angle to the scales toward the *x*-direction promotes interlocking, which results in a high puncture resistance. The "arrayed square scales" model with $\alpha_{45} = 60^{\circ}$ shows the highest resistance against tilting compared to the other slant angles (α_0 and α_{90}), since the interlocking mechanism occurs along the diagonal (*x*=*y*) of the scale. Finally, figure 4-9a and 9b show that the dart shape and hexagon shapes have a superior puncture resistance because the interlocking mechanism occurs over multiple directions and between a large number of scales.

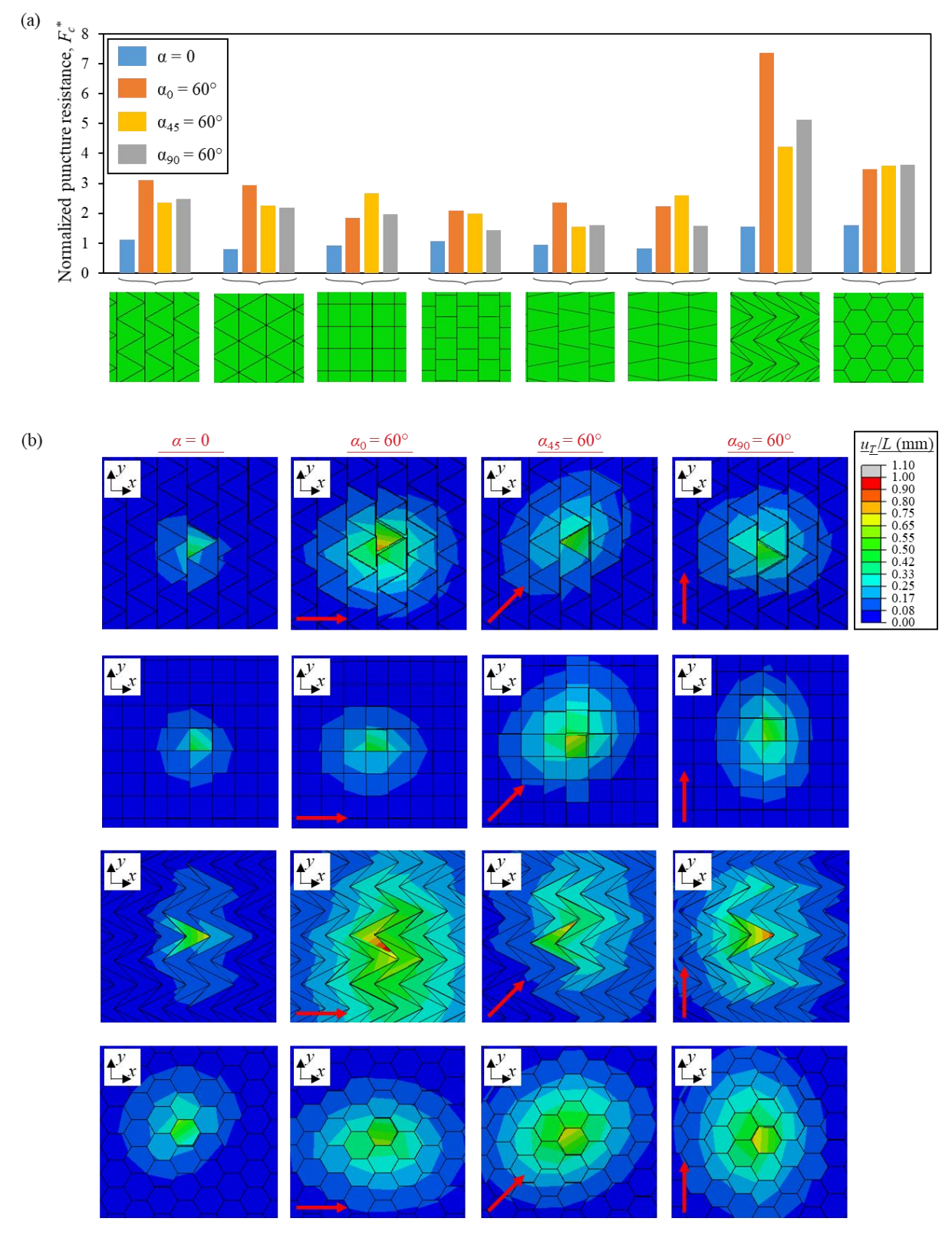


Figure 4-9: (a) Puncture resistance of arrays of scales. Within each design the effect of slant angle is also shown; (b) In-plane displacement maps for these designs. The red arrows show the direction of the slant angle.

4.7 Flexural response

In addition to puncture resistance, flexural compliance is another important criterion for flexible protective system. In this section, we created numerical models to investigate the effect of the base shape, the arrangement and the slant angle of the scales on the overall flexural compliance of the scaled skin. We used the same modeling configuration as in section 2 to create the scales, but this time the scales were bonded onto a membrane composed of linear elastic 8-nodes brick elements C3D8R with a modulus E_m and Poisson's ratio v_m and a very small gap distance of d/L=0.005 (figure 4-10a and b). We built a $10L\times10L\times1.5L$ membrane placed in a three-point bending with a support span length of 8L. Our first task were to duplicate our flexural experiments [21] and for this purpose we used $E_m = 700$ kPa, $v_m = 0.5$, L=2 mm and t=2 mm. The scaled membrane was loaded in flexion by a narrow rigid plate (figure 4-10a and b) aligned either with the x-direction (figure 4-10a) or with the y-direction (figure 4-10b).

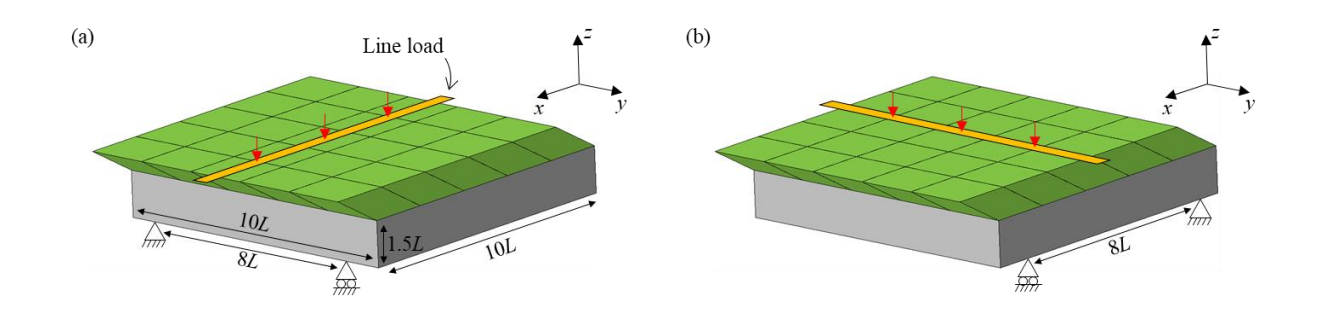


Figure 4-10: Configuration for the three-point bending (experiments and models). We considered two orientations for the loading pin (load line): (a) parallel to x-direction and (b) parallel to y-direction.

The model predictions in terms of force-deflection are compared with the experiments (from [21]) in figure 4-11. No fitting procedure or calibration of parameters was used for this comparison, and the predicted force-deflection curves show a good agreement with the experimental results (figure 4-11b and d).

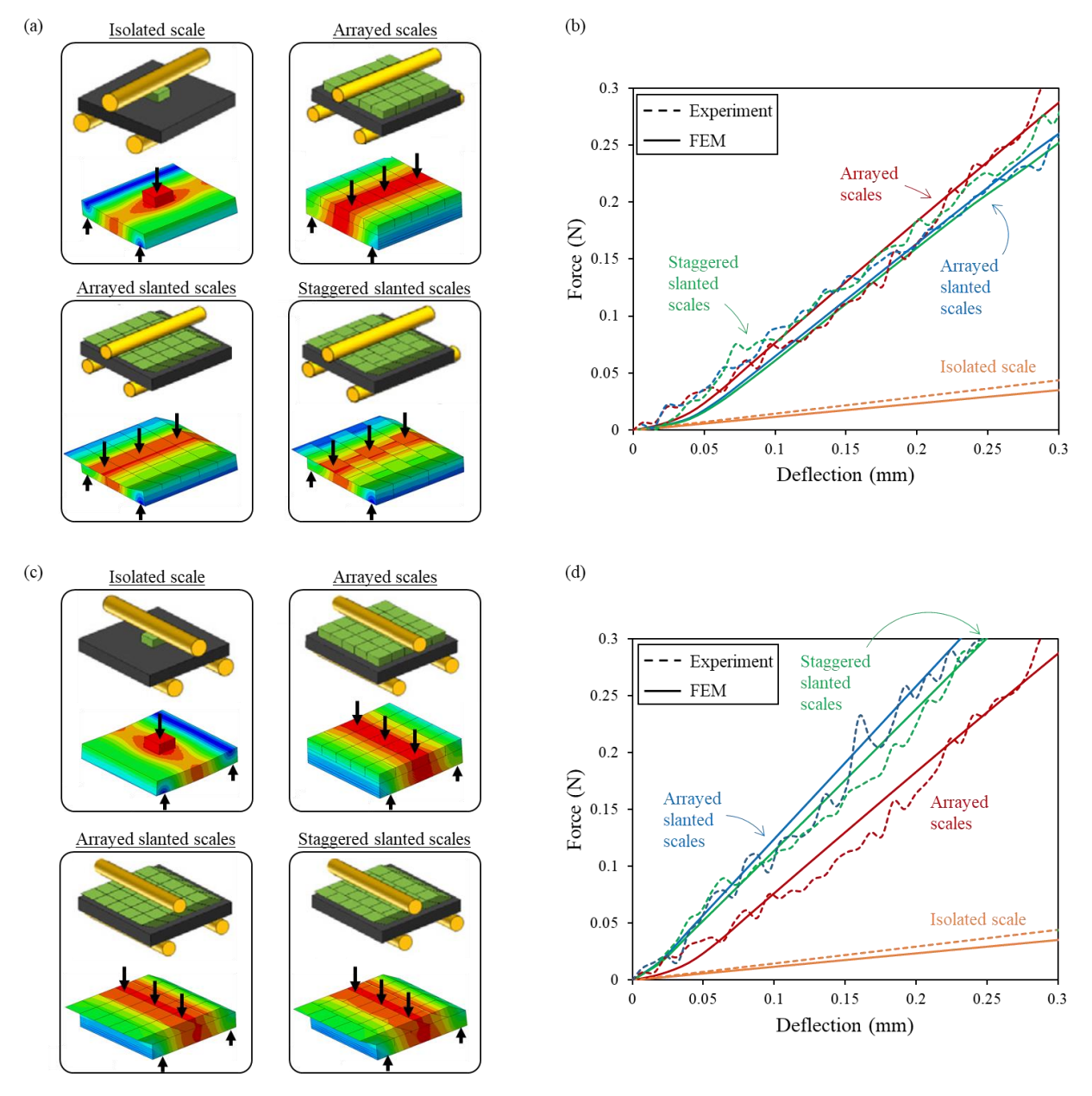
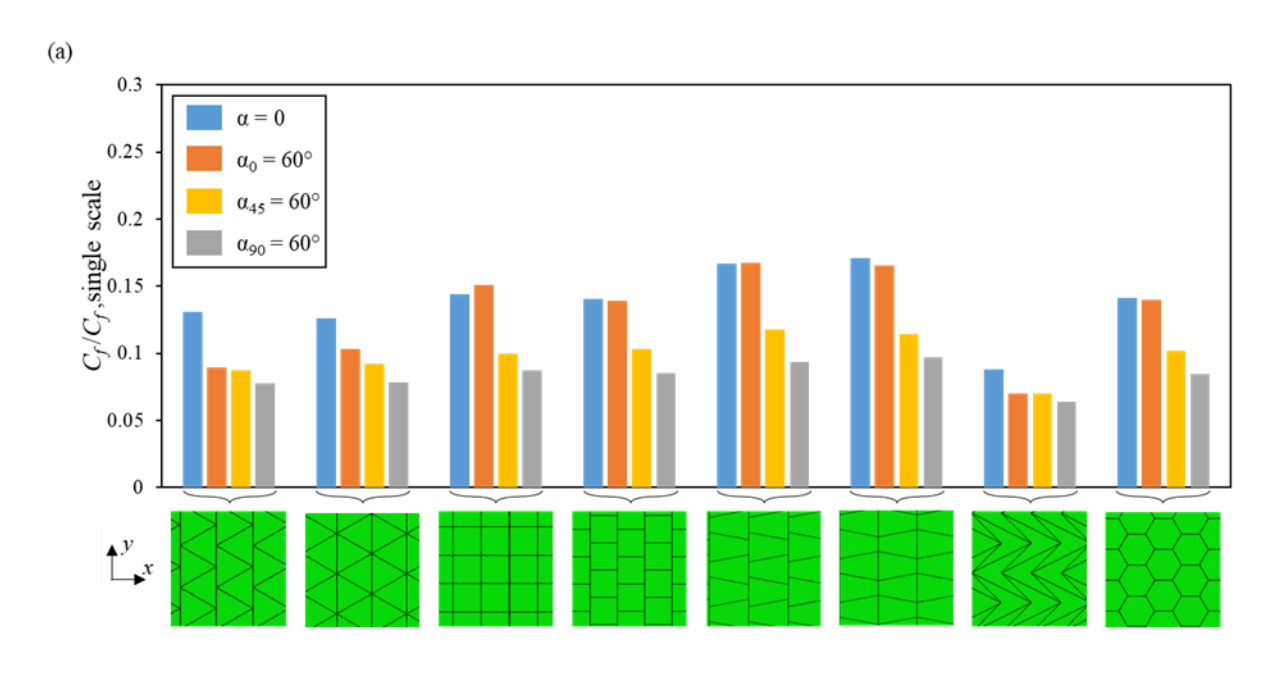


Figure 4-11: (a) Three-point flexural tests (diagrams and DEM results) on arrays of scales bonded onto a soft membrane where the line load is parallel to *x*-direction and (b) corresponding force deflection curves from experiments and DEM models, showing good agreements; (c) Same test with the line load parallel to *y*-direction with (d) corresponding force deflection curves from experiments and DEM models also showing good agreements.

The flexural model can now be extended to other base shapes. Figure 4-12 shows the normalized flexural compliance C_f^* (normalized by $C_f^* = C_f E_m I_m / L^3$ where I_m is the second moment of the area

of the membrane) for the models with different combinations of base shapes, slant angles and arrangements.



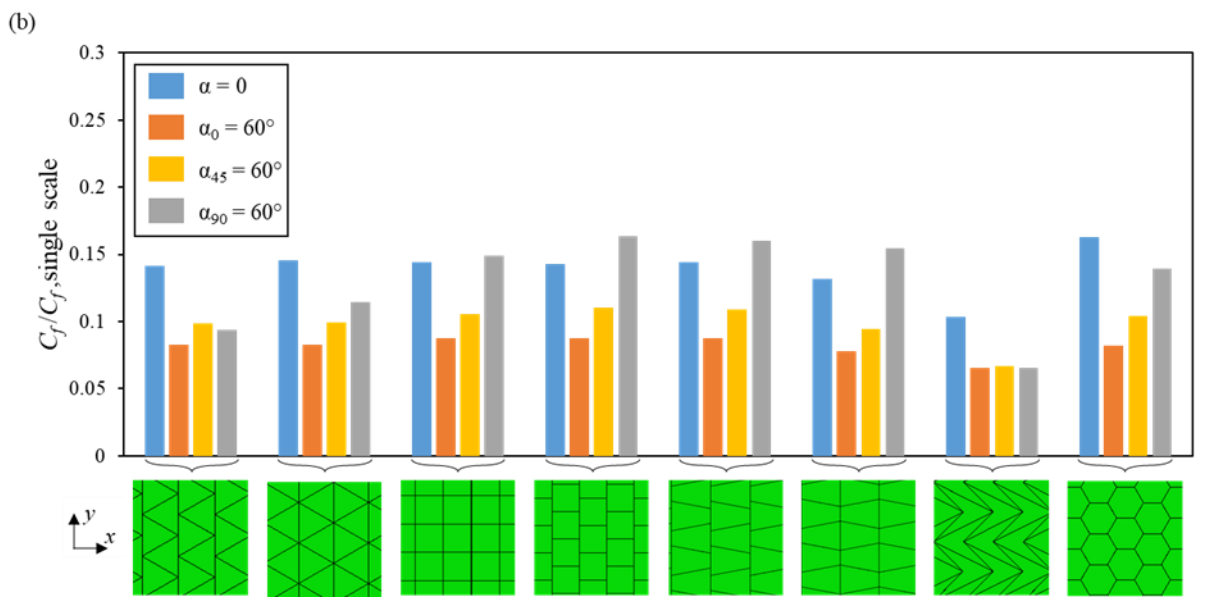


Figure 4-12: Flexural compliance of arrays of scales on soft membrane with different combinations of base shapes, slant angles and arrangements and where the line load is applied (a) parallel to the *x*-direction and (b) parallel to the *y*-direction.

Compared to an isolated scale because of the very small gap distance between the scales and also the direct contact, the scales limit the flexion of the membrane, and as a result the flexural compliance in all the scaled systems decreases by 85% - 93%. The dart is the shape with the largest geometrical size, and therefore for this shape the stiffening in flexion was more pronounced than for the other shapes. Moreover, the interlocking mechanism which is more pronounced in the "dart scales" was beneficial to puncture performance, but our results show that it is detrimental to flexural compliance. This observation, along with similar trends from other scale geometries, confirms that puncture resistance and flexural compliance are mutually exclusive [16, 21, 23]. The results (figure 4-12) also show that for design purpose, the orientation that we set the three-point bending configuration must be considered, because depending on the orientation, the models show different flexural response. If the direction of the slant angle is parallel to the orientation of the line load the system shows a higher flexural compliance, while the lowest flexural compliance happens when the slant angle direction is perpendicular to the line load orientation.

4.8 Summary

In this study we explored the mechanisms of puncture and flexural deformation in soft substrates and membranes covered with rigid scales of various shapes and arrangements. The discrete element modeling approach we used for this work was validated with puncture and flexural experiments. This modeling method brought more insights than the experiments, because a broader range of geometries and interaction parameters could be used, and the mechanisms involved in puncture and flexion could be explored with greater details. Our main findings are as follow:

- For scales with no slant angles, the puncture resistance increases mainly by elastic interactions through the substrate, and with much less extent by direct contact between the scales.
- The interlocking mechanism between rows of scales plays an important role in engaging a larger number of scales during loading, which results in a higher puncture resistance
- Slant angle towards any directions improve the puncture resistance of the system, however,
 a slant angle towards the direction with interlocking mechanism makes the effect of the
 slant angle more pronounced.
- Dart- and hexagon-shape scales show the best performance in terms of puncture resistance compared to the other models
- To have a better flexural performance, the direction of the slant angle must be considered parallel to the orientation of the three-point bending configuration

This exploration of mechanisms finally produced a comparative database of the flexure-compliance performance of various designs, which can be conveniently summarized using the Ashby chart showed on figure 4-13. Isolated scale (with any base shapes) shows the highest flexural compliance but the puncture resistance is the lowest. Covering the substrate with scales improves the puncture resistance, but, at the cost of low flexibility. Simple system of "arrayed square scales" with no slant angles (α =0) increases the puncture resistance by five times. By only giving a slant angle of α 45=60° to the scales, we can improve the puncture resistance even more by about three times of the model with no slant angle. Changing the base shape of the scales also has a significant effect on puncture resistance. When all these effects and mechanisms are combined they can produce a puncture resistance about 42 times higher than an isolated scale ("dart scales"

model with α_0 =60° slant). This puncture resistance only come at the cost of a small decrease in compliance compared to the other designs.

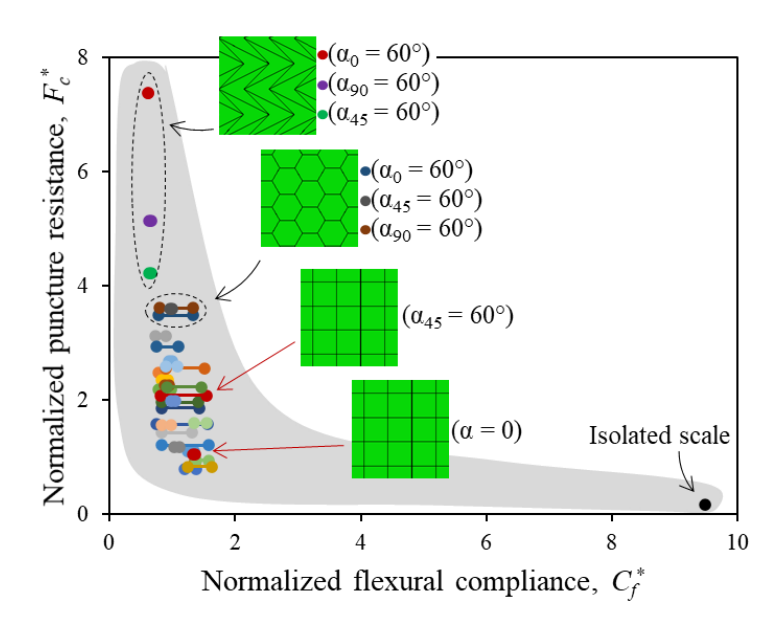


Figure 4-13: Ashby chart showing the normalized puncture resistance and the normalized flexural compliance for different combinations of base shapes, slant angles and arrangements.

This study provides new insights into the effect of the base shape and the slant angle of the scales on the mechanical behavior of a scale-covered system and the interlocking mechanism of the scales, which in turn can help in the design and optimization of improved protective systems.

4.9 Acknowledgements

This work was supported by a Discovery Grant from the Natural Sciences and Engineering Research Council of Canada. A.S. was partially supported by a McGill Engineering Doctoral Award.

4.10 References

- 1. Wegst, U.G.K., et al., *Bioinspired structural materials*. Nature Materials, 2014. **14**: p. 23.
- 2. Chen, P.Y., J. McKittrick, and M.A. Meyers, *Biological materials: Functional adaptations and bioinspired designs*. Progress in Materials Science, 2012. **57**(8): p. 1492-1704.
- 3. Rajabi, H., et al., *Effect of microstructure on the mechanical and damping behaviour of dragonfly wing veins*. Royal Society Open Science, 2016. **3**(2): p. 160006.
- 4. Chen, I.H., et al., *Armadillo armor: Mechanical testing and micro-structural evaluation.* Journal of the Mechanical Behavior of Biomedical Materials, 2011. **4**(5): p. 713-722.
- 5. Barthelat, F., *Architectured materials in engineering and biology: fabrication, structure, mechanics and performance.* International Materials Reviews, 2015. **60**(8): p. 413-430.
- 6. Chintapalli, R.K., et al., Fabrication, testing and modeling of a new flexible armor inspired from natural fish scales and osteoderms. Bioinspiration & Biomimetics, 2014. **9**(3): p. 036005.
- 7. Zhu, D.J., et al., *Structure and Mechanical Performance of a "Modern" Fish Scale*. Advanced Engineering Materials, 2012. **14**(4): p. B185-B194.
- 8. Yang, W., et al., *Natural Flexible Dermal Armor*. Advanced Materials, 2013. **25**(1): p. 31-48.
- 9. Vernerey, F.J. and F. Barthelat, *Skin and scales of teleost fish: Simple structure but high performance and multiple functions.* Journal of the Mechanics and Physics of Solids, 2014. **68**: p. 66-76.
- 10. Rudykh, S. and M.C. Boyce, Analysis of elasmoid fish imbricated layered scale-tissue systems and their bio-inspired analogues at finite strains and bending. IMA Journal of Applied Mathematics, 2014. **79**(5): p. 830-847.
- 11. Szewciw, L. and F. Barthelat, *Mechanical properties of striped bass fish skin: Evidence of an exotendon function of the stratum compactum.* J Mech Behav Biomed Mater, 2017. **73**: p. 28-37.
- 12. Vernerey, F.J., K. Musiket, and F. Barthelat, *Mechanics of fish skin: A computational approach for bio-inspired flexible composites*. International Journal of Solids and Structures, 2014. **51**(1): p. 274-283.
- 13. Vernerey, F.J. and F. Barthelat, *On the mechanics of fishscale structures*. International Journal of Solids and Structures, 2010. **47**(17): p. 2268-2275.
- 14. Ghosh, R., H. Ebrahimi, and A. Vaziri, *Contact kinematics of biomimetic scales*. Applied Physics Letters, 2014. **105**(23): p. 233701.
- 15. Ghosh, R., H. Ebrahimi, and A. Vaziri, *Frictional effects in biomimetic scales engagement*. EPL (Europhysics Letters), 2016. **113**(3): p. 34003.
- 16. Martini, R. and F. Barthelat, *Stretch-and-release fabrication, testing and optimization of a flexible ceramic armor inspired from fish scales.* Bioinspiration & Biomimetics, 2016. **11**(6): p. 066001.
- 17. Zhu, D.J., et al., *Puncture resistance of the scaled skin from striped bass: Collective mechanisms and inspiration for new flexible armor designs.* Journal of the Mechanical Behavior of Biomedical Materials, 2013. **24**: p. 30-40.
- 18. Browning, A., C. Ortiz, and M.C. Boyce, *Mechanics of composite elasmoid fish scale assemblies and their bioinspired analogues*. Journal of the Mechanical Behavior of Biomedical Materials, 2013. **19**: p. 75-86.

- 19. Tatari, M., et al., *Bending behavior of biomimetic scale covered beam with tunable stiffness scales.* Scientific Reports, 2020. **10**(1): p. 17083.
- 20. Funk, N., et al., *Bioinspired Fabrication and Characterization of a Synthetic Fish Skin for the Protection of Soft Materials*. ACS Applied Materials & Interfaces, 2015. **7**(10): p. 5972-5983.
- 21. Martini, R., Y. Balit, and F. Barthelat, *A comparative study of bio-inspired protective scales using 3D printing and mechanical testing*. Acta Biomaterialia, 2017. **55**: p. 360-372.
- 22. Rudykh, S., C. Ortiz, and M.C. Boyce, *Flexibility and protection by design: imbricated hybrid microstructures of bio-inspired armor*. Soft Matter, 2015. **11**(13): p. 2547-2554.
- 23. Shafiei, A., et al., *The very hard and the very soft: Modeling bio-inspired scaled skins using the discrete element method.* Journal of the Mechanics and Physics of Solids, 2020: p. 104176.
- 24. Martini, R. and F. Barthelat, *Stability of hard plates on soft substrates and application to the design of bioinspired segmented armor*. Journal of the Mechanics and Physics of Solids, 2016. **92**: p. 195-209.
- 25. Connors, M., et al., *Bioinspired design of flexible armor based on chiton scales*. Nature Communications, 2019. **10**(1): p. 5413.
- 26. Ghods, S., et al., *On the regeneration of fish scales: structure and mechanical behavior.* Journal of Experimental Biology, 2020. **223**(10).
- 27. Murcia, S., et al., *Temperature effects on the fracture resistance of scales from Cyprinus carpio*. Acta Biomaterialia, 2015. **14**: p. 154-163.
- 28. Ghods, S., et al., *Designed for resistance to puncture: The dynamic response of fish scales.* Journal of the Mechanical Behavior of Biomedical Materials, 2019. **90**: p. 451-459.
- 29. Dugué, M., et al., *Indentation of interlocked assemblies: 3D discrete simulations and experiments.* Computational Materials Science, 2013. **79**: p. 591-598.
- 30. Ghosh, R., H. Ebrahimi, and A. Vaziri, *Non-ideal effects in bending response of soft substrates covered with biomimetic scales*. Journal of the Mechanical Behavior of Biomedical Materials, 2017. **72**: p. 1-5.
- 31. Abid, N., M. Mirkhalaf, and F. Barthelat, *Discrete-element modeling of nacre-like materials: Effects of random microstructures on strain localization and mechanical performance*. Journal of the Mechanics and Physics of Solids, 2018. **112**: p. 385-402.
- 32. Abid, N., J.W. Pro, and F. Barthelat, *Fracture mechanics of nacre-like materials using discrete-element models: Effects of microstructure, interfaces and randomness.* Journal of the Mechanics and Physics of Solids, 2019. **124**: p. 350-365.
- 33. Pro, J.W. and F. Barthelat, *Discrete element models of fracture in tooth enamel: Failure mode competition and statistical effects.* Journal of the Mechanics and Physics of Solids, 2020. **137**: p. 103868.
- 34. Bolander, J.E. and S. Saito, *Fracture analyses using spring networks with random geometry*. Engineering Fracture Mechanics, 1998. **61**(5): p. 569-591.
- 35. Barber, J.R., Elasticity. 2002: Springer.
- 36. Okumura, I.A., *On the generalization of Cerruti's problem in an elastic half-space*. Doboku Gakkai Ronbunshu, 1995. **1995**(519): p. 1-10.

Chapter 5

Conclusions

Chapter 5: Conclusions

5.1 Summary of findings

In this thesis, we used the discrete element method (DEM) to study the mechanics of scale-covered protective systems. This method helped us vastly explore different combinations of scale geometries and arrangements to learn useful insights about the role of the scales in the mechanical performance of such systems. The main findings of this thesis are summarized below:

- Discrete element method (DEM) was successfully utilized to model fish-skin-like systems with two different configurations: hard scales on a soft substrate to study puncture resistance, and hard scales on a soft membrane to examine flexural compliance. The time efficiency of DEM enabled us to run 720 models (chapter 2) which cover a variety of scale geometries and arrangements. Our study shows that DEM can be an excellent alternative to finite element method (FEM) to numerically model fish-skin-like systems.
- The presence of scales has a significant effect on the puncture resistance of the system. The interaction of the neighboring scales through contact distributes the load over a larger area. By engaging the neighboring scales in the loading, the resistance of the punctured scale against tilting increases, which results in a higher puncture resistance. Slant angle helps the resistance against tilting by making the effect of the contact mechanism more pronounced. Too large slant angle however shows a negative effect on the puncture resistance.
- 3 In general, adding scales onto a soft membrane decreases the flexibility of the system. Optimizing the geometries and the arrangement of the scales therefore are important to reach a high puncture resistance and flexible system at the same time. Large gap distance is the best way to improve the flexural compliance, but it is obtained at the cost of low puncture resistance. Choosing scales with small aspect ratio is another way to increase the flexural compliance. The results also show that large slant angles have a negative effect on the flexibility of the system.
- Inducing wrinkles in the system is another way to increase the flexibility. Contact between the scales on the intrados side of the membrane stiffens the system, creates a high energy in it, and makes the mode-I intrados a less stable configuration than the mode I-extrados. Also, in some designs we observed "jamming" which can be used as a method to keep the system in a particular configuration. By adding scales on the both sides of the membrane we were able to

- impose a stable mode II configuration to the system, which is a requirement for forming wrinkles and increasing the overall flexural compliance.
- The base shape of the scale has a significant effect on the puncture resistance of the system. The dart and hexagon shapes show the highest resistance against tilting, where both shapes benefit from better interlocking mechanism compared to the other shapes that we examined. The interlocking mechanism improves the interaction between the scales through contact, therefore the punctured scale receives a better support from the neighboring scales. Giving a slant angle to the scales increases the effect of the interlocking mechanism, however, slant angles in different directions show different results.

5.2 Original thesis contributions and accomplishment

The following list summarizes the main original contributions and accomplishment achieved during the present study:

- Proposed DEM as a validated method to model scaled skins.
- A thorough exploration of scale-covered systems in both 2D and 3D with a various combination of scale architecture (aspect ratio, slant angle and base shape) and arrangement (gap distance and staggering scales) to optimize the system for a high puncture resistance and a high flexural compliance.
- Studied post-buckling behavior of scale-covered systems in mode I and II, which was, inspired of nature, taken as an approach to create wrinkles in the system and increase the flexural compliance.
- This study produced three journal papers, where one is published in the Journal of the Mechanics and Physics of Solids, one is accepted in Bioinspiration & Biomimetics, special issue and the last one is submitted to the International Journal of Solids and Structures.

5.3 Possible future directions

In this work, the main structural features of scale-covered protective systems were explored and discussed through numerical modeling based on the discrete element method (DEM). The

findings provide guidelines for the future design of synthetic high-performance fish-skin-like systems. The following points are proposed as a continuation of this work:

- For specific applications and boundary conditions, the model may be adjusted, and further simulations would be required.
- In this work we assumed a linear elastic substrate and membrane. For a better accuracy at large deformation, material nonlinearity can be considered, which will enrich the problem and bring new interactions between the scales and the substrate or membrane.
- Using scales is not the only way that nature uses to control buckling. Initial conditions
 such as imperfection in the system is another strategy to control buckling, which can
 be investigated in the future works.
- Aside from slant angles, using compliant tethers is another way in some natural armors
 to increase the stability of the scales under puncture loads. This matter can be explored
 in the future works.
- In each model, we used identical scales which were uniformly positioned (with equal gap distance). In further works, models with different scale sizes and gap distances could be considered. Also, it would be interesting to explore scales with more complex shapes and partial interface debonding.

5.4 Publications

- Shafiei, A., Pro, J. W., Martini, R. and Barthelat, F., "The very hard and the very soft: Modeling bio-inspired scaled skins using the discrete element method" *Journal of the Mechanics and Physics of Solids* 2021. 146:104176.
- 2. Shafiei, A., Pro, J. W. and Barthelat, F., "Bioinspired buckling of scaled skins" *Accepted* in **the journal of Bioinspiration & Biomimetics** 2021.
- 3. Shafiei, A. and Barthelat, F., "3D mechanics of scaled membranes" *Submitted*.
- 4. Shafiei, A., Pro, J. W. and Barthelat, F., "Bioinspired segmented armor: discrete element models, 3D printing and mechanical tests" *Presented* in **the TMS 14**th **annual meeting and exhibition**, USA, 2019.